THE GEOTECHNICAL DESIGN OF THE HIGHWALL MINING LAYOUT: A CASE STUDY AT THE 5 SEAM OPERATION OF GLENCORE COAL SA

Cassius Selai

A research report submitted to the Faculty of Engineering and the Built Environment, University of the Witwatersrand, in fulfilment of the requirements for the degree of Master of Science in Engineering.

Johannesburg, 2020

Declaration

I declare that this research report is my own unaided work. It is being submitted to the Degree of Master of Science to the University of the Witwatersrand, Johannesburg. It has not been submitted before for any degree or examination to any other University.

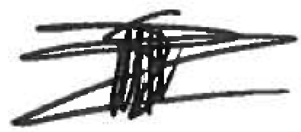

…………………………
(Signature of Candidate)

<u>17th</u> day of **<u>December 2020</u>** at **<u>Wits University</u>**

Abstract

The highwall mining method was adopted as an alternative method for extracting the remaining No.5 coal seam reserves at the 5 seam operation. There is currently a limited practical knowledge on the rockmass response to this mining method on various mining geometries. A great deal of experience has been derived and documented over the years in Australia and the USA, for instance and a number of empirical methods have been derived for pillar strength estimation. These require validation and verification against the local conditions and design geometries.

This research project is aimed at determining and validating the suitable pillar dimensions and spacing at various panel geometries. A hybrid methodology was adopted comprising of empirical and numerical modelling approaches. Pillar safety factor was determined using the Mark- Bieniawski pillar strength empirical formula and pillar stress obtained from UDEC numerical modelling software. For stability assessment, a threshold safety factor of 1.3 was adopted from the ARMPS-HWM minimum safety factor guidelines based on the panel span. Furthermore, the UDEC modelling outputs were closely monitored to ascertain the stress distribution and plastic (yielding) conditions as indication of potential instability. These results were validated by means of using the available instrumentation results that were obtained as the mining progresses using Geokon Stressmeter.

Based on the safety factor assessment, the minimum web pillar width at which the threshold safety factor of 1.3 is attained is 1.2m. This is achieved at a panel width of 28m (6 cuts / 5 pillars per panel) up to the maximum cover depth of 50m, which corresponds with the cover depth obtained from the geological information. The UDEC modelling assessment results depicted mainly potential shear failure mode, which is indicative of the presence of confinement. As a result, a 28m panel width comprising of 5 x 1.2m web pillars was selected for the initial pillar design layout and for instrumentation. The mining height of 1.8m was used based on the thickness of the coal seam and cover depth ranging from 40m to 45m. The available strain measurement results indicate the maximum web and barrier pillar stresses are less than 0.3xUCS (8.33MPa) and no failure or crack initiation was expected on the pillars. This was also confirmed during the actual mining activities, where no pillar fracturing occurred. These results present opportunities for layout optimization at various geometries.

Dedication

This work is dedicated to my wife Zandile Selai and our daughter Tshilidzi Selai, who have been a constant source of support and encouragement. I am truly thankful for having you in my life and love you stax!

Acknowledgements

First, I give glory to the Most High God for the gift of life and strength during this research work.

I am grateful to Glencore Coal South Africa, Development Committee and Executive Committee (EXCO) for the permission to use the information and database and for financing part of my studies. I would like to thank my Supervisor Prof. R. Mitra for his supported and untiring support and supervision. He consistently allowed this research to be my own work, but steered me in the right the direction whenever he thought I needed it.

I would also like to thank Middindi Consulting Pty (Ltd) who laid the foundation on which this research work was based. I am also thankful for the support and input provided by Mr. Kevin Le Bron of MLB Consulting particularly on the UDEC numerical modelling aspect of this research. Mr. Tony Ward of Seismogen Consulting is also acknowledged for his passionate participation and input on the stress monitoring and interpretation, without which the results validation could not have been successfully conducted.

I would also like to acknowledge Mr. Sandor Pethö as my Manager at Glencore Coal South Africa and as the second reader of this dissertation. I am gratefully indebted to his very valuable comments and editorial inputs on this report.

Finally, I must express my very profound gratitude to my parents and siblings, HRIM Ministries and its leadership for providing me with unfailing support and continuous encouragement throughout my years of study and through the process of researching and writing this dissertation. This accomplishment would not have been possible without them. Thank you.

Table of Contents

Contents **Page**

Declaration ..... **i**

Abstract ..... **ii**

Dedication ..... **iii**

Acknowledgements ..... **iv**

List of Figures ..... **vii**

List of Tables ..... **xiii**

Chapter 1 ..... **1**

Introduction **1**

1.1. Project Background 1

1.2. Study Area Background 1

1.3. Definition of the problem 4

1.4. Objectives and Scope of Research 5

1.5. Research Methodology 5

1.6. Content of the Report 6

Chapter 2 ..... **7**

Literature Review **7**

2.1. Overview of Highwall Mining Method 7

2.2. Geotechnical Highwall Mining Layout Design 9

2.2.1. Empirical Pillar Design 9

2.2.2. Numerical Modelling 25

2.3. Chapter Summary 37

Chapter 3 ..... **38**

Numerical Modelling Assessment **38**

3.1. Introduction 38

3.2. Model Input Parameters 38

3.2.1. Geological Sequence....38
3.2.2. Rockmass Classification....40
3.2.3. Laboratory Testing Results....43
3.2.4. UDEC Input Parameters....44
3.3. Model Geometry Construction....45
3.4. Model Boundary Conditions....46
3.5. Pillar Stress....47
3.6. Pillar Strength....49
3.7. Pillar Safety Factor....51
3.8. UDEC model output....51
3.9. Chapter Summary....52
Chapter 4....53
Results and Discussion....53
4.1. Introduction....53
4.2. Pillar Safety Factor....53
4.2.1. 0.8m Web Pillar....53
4.2.2. 1.2m Web Pillar....54
4.2.3. 1.6m Web Pillar....55
4.2.4. 2m Web Pillar....56
4.3. UDEC Output Simulation Results....58
4.3.1. 0.8m Web Pillar Width....58
4.3.2. 1.2m Web Pillar Width....67
4.3.3. 1.6m Web Pillar Width....76
4.3.4. 2m Web Pillar Width....79
4.4. Chapter Summary....81
Chapter 5....82
Pillar Stress Monitoring....82
5.1. Introduction....82

5.2. Sensor Layout 83
5.3. Drilling and Installation of Sensors 84
5.4. Data Collection 85
5.5. Data Interpretation 86
5.6. Stress Data and Analysis 89
5.7. Chapter Summary 91
Chapter 6 92
Conclusions and Recommendations 92
6.1. Conclusions 92
6.2. Recommendations 93
References 95

List of Figures

Figure 1-1: Geographical location of the study area (yellow dotted rectangle indicates mining area, which is zoomed in white infill insert) (Google Maps, 2018) 2

Figure 1-2: Coal Production for the three (3) year mining period (Glencore Coal SA Production report, 2010) 3

Figure 1-3: Plan showing two the pits that were chosen for the initial highwall mining method (*dotted lines depicting areas earmarked for highwall mining*) (Tweefontein Survey Department, 2010) 4

Figure 2-1: The cross-sectional view of the highwall mining layout (Luo, 2014) 7

Figure 2-2: ADDCAR Highwall Mining system during operation (ADDCAR Systems LLC, 2018) 8

Figure 2-3: Pressure arch concept applied in highwall mining method (Luo, 2014) ..14

Figure 2-4: Suggested web pillar width for safety factor of 1.6 and barrier pillar width for a safety factor of 1.0 at a 122m wide panel (Zipf, 2005)....................................17

Figure 2-5: Suggested web pillar width for a safety factor of 1.3 and barrier pillar width for a safety factor of 1.0 in a 61.0m wide panel (Zipf, 2005) 17

Figure 2-6: LSFM plots of maximum stable span and roof beam thickness at varying Young's modulus 19

Figure 2-7: Impact splitting test setup 20

Figure 2-8: Spatial distribution of unit ratings relative to the planned highwall mining outline (Middindi Consulting, 2012)..23

Figure 2-9: Unsupported span vs rockmass rating (Hutchinson and Diederichs, 1996) 24

Figure 2-10: Safety factor for unsupported Span vs Q-value (Houghton and Stacey, 1980) 24

Figure 2-11: Stability of the highwall mining layout using FLAC3D (Middindi Consulting, 2012) 26

Figure 2-12: Pillar stress change for varying pillar length to width ratio (Middindi Consulting, 2012) 27

Figure 2-13: FLAC3D stress-strain curves for a w/h of 1.25 for (a) long pillar and (b) equivalent square pillar (Porathur, *et al.,* 2013) 27
Figure 2-14: Long pillar-effective square pillar strength comparison (Porathur, *et al.,* 2013). 28
Figure 2-15: Cross sectional view of a web pillar in a highwall mining set up (Porathur, *et al.,* 2013) 29
Figure 2-16: Modelled and calculated vertical stresses before and after a web cut excavation (Porathur, *et al.,* 2013) 29
Figure 2-17: LAMODEL numerical assessment for (a) multiple seam mining interaction and (b) simulating a collapsed web pillar and monitoring of the CPF (Vandergrift and Garcia, 2005) 30
Figure 2-18: Typical calculation cycle used in the discrete element method (Itasca Consulting Group, 2014)..31
Figure 2-19: UDEC Model setup and execution process flowchart (Itasca Consulting Group, 2014)..32
Figure 2-20: Web pillar showing plastic yielding as predicted by UDEC (Shen and Duncan Fama, 2001)...33
Figure 2-21: Plots from the UDEC modelling results showing strength variation with varying w/h ratio and interface conditions (Duncan Fama, *et al.,* 1999) 34
Figure 2-22: Variations of pillar strength with pillar width for three different cases (Shen, 2014) 35
Figure 2-23: UDEC model vertical stress results for multiple seam workings (Vandergrift and Garcia, 2005) 36
Figure 3-1: Location of the geological boreholes at the East Pit Project area (indicated by the red triangles) (Tweefontein Survey Department, 2010) 39
Figure 3-2: Location of the geological boreholes at the West pit Project area (indicated by small black dots) (Tweefontein Survey Department, 2010) 39
Figure 3-3: A representative geological sequence for the two pits earmarked for highwall mining 40

Figure 3-4: Laboratory tests results of No.5 coal seam at varying confinement stresses 44
Figure 3-5: Simplified geological sequence and panel layout as modelled in UDEC modelling 45
Figure 3-6: Mesh set-up on various zones of the UDEC model 47
Figure 3-7: A schematic showing the pre-mining vertical stress contours in the UDEC model 47
Figure 3-8: Pillar stress for varying width to height ratio and cover depth 49
Figure 3-9: Conceptual stress profile showing yielding (red) and elastic (blue) zones across (a) larger and b) smaller pillar 52
Figure 4-1: Minimum safety factor for a 0.8m web pillar at varying depths and panel widths 54
Figure 4-2: Minimum safety factor for a 1.2m wide web pillar at varying depths and panel widths 55
Figure 4-3: Minimum safety factor for a 1.6m wide web pillar at varying depths and panel widths 56
Figure 4-4: Minimum safety factor for a 2m wide web pillar at varying depths and cuts per panel 57
Figure 4-5: Progression of stress distribution for decreasing w/h ratio at 30m cover depth 59
Figure 4-6: Progression of stress distribution for decreasing w/h ratio at a 40m cover depth 59
Figure 4-7: Vertical stress on (a) web pillars and (b) barrier pillar for a w/h ratio of 0.6 at a 50m cover depth 60
Figure 4-8: Progression of the yield zone on the barrier pillar side for a 50m cover depth and varying w/h ratio 61
Figure 4-9: Pillar stress for varying w/h ratios and cover depths for a 26m wide panel width 62
Figure 4-10: Progression of stress distribution for varying w/h ratio at a 30m cover depth 62

Figure 4-11: Progression of stress distribution for decreasing w/h ratio at a 40m cover depth.........63
Figure 4-12: Pillar stress for varying w/h ratios and cover depths for a 34m wide panel width.........64
Figure 4-13: Progression of stress distribution for decreasing w/h ratio at a 30m cover depth for a 43m panel width.........65
Figure 4-14: Progression of the stress distribution for decreasing w/h ratio at a 50m cover depth for a 43m panel width.........65
Figure 4-15: Plasticity state on the barrier pillar for various w/h ratios.........66
Figure 4-16: Pillar stress for varying w/h ratios and cover depths for a 43m wide panel width.........67
Figure 4-17: Progression of the stress distribution for a decreasing w/h ratio at a 30m cover depth for a 28m panel width.........68
Figure 4-18: Progression of the stress distribution for decreasing w/h ratio at 40m cover depth for a 28m panel width.........68
Figure 4-19: Progression of the stress distribution for a decreasing w/h ratio at a 50m cover depth for a 28m panel width.........69
Figure 4-20: Plasticity state on the barrier pillar for various w/h ratios.........70
Figure 4-21: Pillar stress for varying w/h ratios and cover depths for a 28m wide panel width.........71
Figure 4-22: Progression of the stress distribution for decreasing w/h ratio at a 30m cover depth for a 37m panel width.........71
Figure 4-23: Progression of the stress distribution for decreasing w/h ratio at a 40m cover depth for a 37m panel width.........72
Figure 4-24: Progression of the stress distribution for decreasing w/h ratio at a 50m cover depth for a 37m panel width.........72
Figure 4-25: Plasticity state on the barrier pillar for various w/h ratios.........73
Figure 4-26: Pillar stress for varying w/h ratios and cover depths for a 37m wide panel width.........73

Figure 4-27: Progression of the stress distribution for decreasing w/h ratio at a 30m cover depth for a 47m panel width 74
Figure 4-28: Progression of the stress distribution for decreasing w/h ratio at a 40m cover depth for a 47m panel width 74
Figure 4-29: Plasticity state on the barrier pillar for various w/h ratios 75
Figure 4-30: Pillar stress for varying w/h ratios and cover depths for a 47m wide panel width....76
Figure 4-31: Progression of the stress distribution for decreasing w/h ratio at varying cover depths and a 30m panel width 77
Figure 4-32: Progression of the stress distribution for decreasing w/h ratio at varying cover depths and a 40m panel width 78
Figure 4-33: Progression of the stress distribution for decreasing w/h ratio at varying cover depths and a 50m panel width 78
Figure 4-34: Progression of the stress distribution for decreasing w/h ratio at varying cover depths and a 32m panel width 79
Figure 4-35: Progression of the stress distribution for decreasing w/h ratio at varying cover depths and 43m panel width....80
Figure 4-36: Progression of the stress distribution for decreasing w/h ratio at varying cover depths and 54m panel width....80
Figure 5-1: Geokon model 4350 vibrating wire biaxial stressmeter (GEOKON, 2018) 82
Figure 5-2: Plan view showing the position of panel 21, where the sensors were installed 83
Figure 5-3: Section view of the array layout and sensor ID in panel 21 84
Figure 5-4: 15m length horizontal hole pre-drilling using a trailer mounted Atlas Copco Rotary drilling machine 84
Figure 5-5: Installation of the sensors and relative positions in panel 21 85
Figure 5-6: Geokon model GK-404 vibrating wire readout box (GEOKON, 2018)...85
Figure 5-7: Relative magnitude of measured change in diameter 86

Figure 5-8: Coefficient ‘A’ plotted against rockmass Poisson’s ratio (GEOKON, 2018) 87
Figure 5-9: Coefficient ‘B’ plotted against rockmass Poisson’s ratio (GEOKON, 2018) 88
Figure 5-10: Barrier pillar stress change distribution over time 89
Figure 5-11: Web pillar stress distribution over time 90
Figure 5-12: Pillar stress measurement plotted against the average UCS and crack initiation criterion 91

List of Tables

Table 2-1: Summary of coal pillar strength estimation formulae 10
Table 2-2: ARMPS-HWM Minimum safety factor guidelines (Mark, 2006) 16
Table 2-3: Laboratory tested rock properties (Glencore Coal Geotechnical Database, 2012) 18
Table 2-4: Unit and roof classification based on impact splitting test (Buddery and Oldroyd, 1992; Latilla, *et al.*, 2002) 21
Table 2-5: Summary of the impact splitting test results (Madden, 2002) 22
Table 3-1: Summary of Rock mass classification for various zones (Glencore Coal Geotechnical Database, 2012) 41
Table 3-2: Equivalent rock and joint properties as derived from the *RocData* software 44
Table 3-3: Pillar dimensions and corresponding panel dimensions 46
Table 3-4: Web pillar stress for varying pillar and panel dimensions 48
Table 3-5: Empirically determined web pillar strengths for a combination of pillar widths and mining heights 50
Table 5-1: Raw data (*in frequency*^{2}x10^{-3}) from the various sensors on various dates.88

Chapter 1
Introduction

1.1. Project Background

The initial underground mining of the No.5 coal seam at the 5 seam operation of Glencore Coal South Africa was ceased due to the operational and technical challenges, which include amongst others:

- Weak floor which in combination with water made it difficult for the equipment to manoeuvre and operate effectively;
- Low seam height which meant that some part of the overlying strata would be cut out to create an optimum working height for the personnel and equipment, thereby resulting in some quality issues; and
- Deteriorating roof conditions due to the exposure of weak mudstone layers at the immediate roof.

These challenges hampered both safety and coal production. For continued safe production, an alternative mining method was necessary in order to combat these challenges. A decision was made to adopt the highwall mining method based on the research conducted both locally and internationally. This decision was easy to make since the company also has mining operations in Australia which have been practicing this particular mining method.

1.2. Study Area Background

The 5 seam operation (*named after the coal seam being mined*) is a Glencore Coal South Africa operation and is operated under the Tweefontein Complex, situated approximately 40 km south of the city of eMalahleni (Figure 1-1). The opencast mining method was initially conducted between 2006 and 2007 using the dragline.

Figure 1-1: Geographical location of the study area (yellow dotted rectangle indicates mining area, which is zoomed in white infill insert) (Google Maps, 2018)

The underground bord and pillar mining method was employed by means of establishing the portals through the highwalls, using a continuous miner (CM) and continued from 2008 until 2010. The annual average production tonnes for this three year period was approximately 0.29Mt, with the maximum being 0.63Mt (Figure 1-2), between three (3) production sections (Glencore Coal SA Production report, 2010). This is short of the planned average annual target of 0.72Mt throughout the mining period.

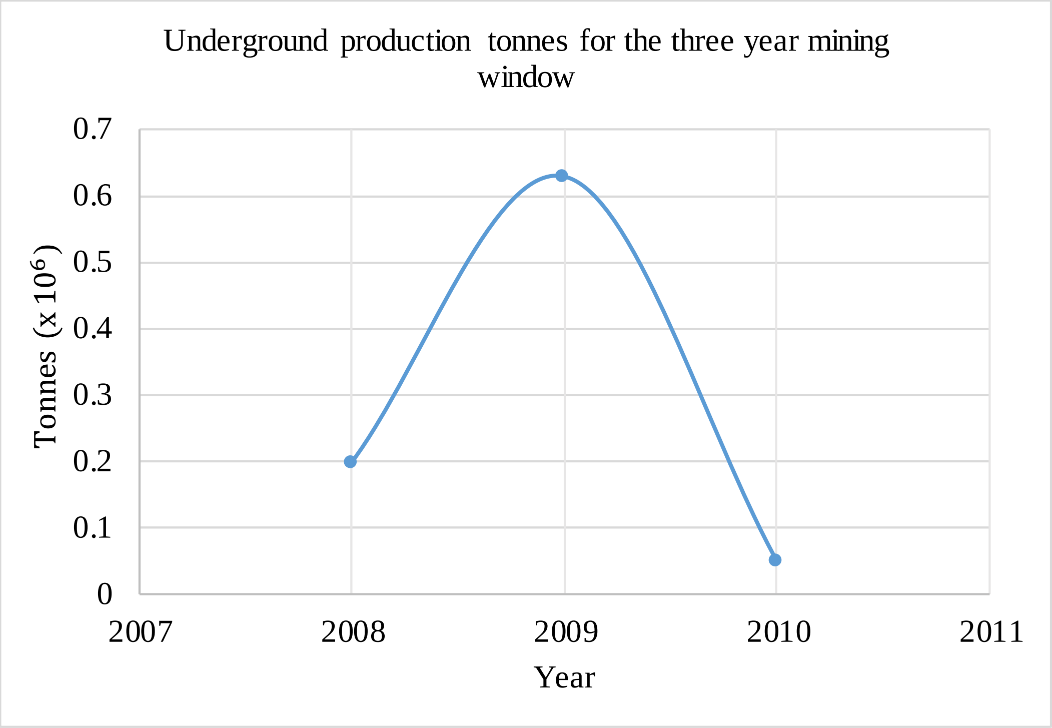

Figure 1-2: Coal Production for the three (3) year mining period (Glencore Coal SA Production report, 2010)

Following on from the pre-feasibility study conducted by Middindi Consulting (2012), two separate areas were earmarked for the highwall mining method on the West and East of the resource area (Figure 1-3). The Eastern portion would be the first pit where the implementation and experimentation would be conducted. This would then be rolled out to the rest of the earmarked areas. The Eastern portion is located adjacent to the old underground bord and pillar mining workings, which was also planned to be extracted as part of the highwall mining project, the details of which are outside the scope of this research.

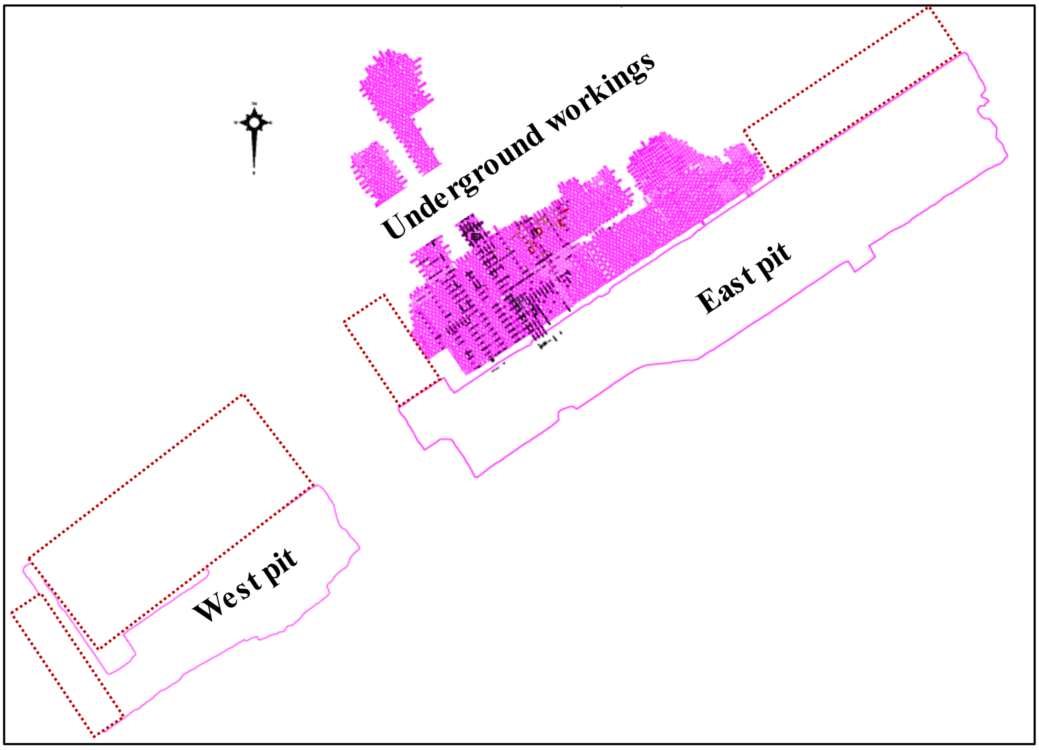

Figure 1-3: Plan showing two the pits that were chosen for the initial highwall mining method (*dotted lines depicting areas earmarked for highwall mining*) (Tweefontein Survey Department, 2010)

1.3. Definition of the problem

It is no doubt that a good understanding of the rock mass response to this mining method has been developed due to the number of considerable years that this had been consistently practiced in Australia and the USA, for instance. However, using the empirical methods derived in these countries without validation and verification in line with the local conditions can create unsafe mining conditions (Porathur, *et al*., 2013). Although similar mining method like Auger mining method was previously conducted in South Africa (Follington, *et al*., 2001), there is limited practical knowledge of this particular mining method.

The rock mass response varies in both local and regional scale owing to the differences in geological setting and conditions. It is imperative to understand these differences in rock mass responses and incorporate them in the design. An understanding of the rock mass response to this new mining method in the South African context will be of great benefit in the design of safe highwall mining layouts. This knowledge can be applied by extracting the coal reserves that are overlain by surface infrastructures and where the economics do not allow coal extraction using the conventional strip or underground mining methods.

1.4. Objectives of Research

The objectives of this research project are:

- To determine the required barrier pillar spacing and dimensions,
- To determine the stable web pillar dimensions, and
- To improve the design layout using the instrumentation results.

1.5. Research Methodology

This research project is mainly based on the combination of empirical and numerical modelling approaches. The 5 seam operation of Glencore Coal SA was used as a case study for this research, using the methodology summarized as follows:

- A combination of various web pillar dimensions and mining heights for varying overburden thicknesses was modelled, with a cut width fixed at 3.6m;
- The stresses acting on the pillars were measured from the models and compared with the empirically derived web pillar strength;
- A pillar safety factor was then calculated and compared with the chosen threshold;
- The UDEC modelling outputs were closely monitored to ascertain the stress distribution and plastic (yielding) conditions. These were used to estimate potential failure mechanism or stability of the pillars; and
- The numerical modelling results were validated by means of using the available instrumentation results that were obtained as the mining progresses.

1.6. Content of the Report

This chapter provided an insight of this project by outlining the introduction, background and the purpose of this project and the methodology followed. The remaining chapters of the report are presented below. A summary of the major findings and conclusions is provided at the end of each chapter.

- Chapter 2 contains the various components of literature review that was conducted for this research project. This mainly covered the review of the available web pillar strength estimation equations and the use of numerical modelling approach for pillar stability assessment,
- Chapter 3 provides the description of numerical modelling approach using UDEC software and application as used in this project,
- Chapter 4 contains the discussion of these results. This comprises of the web pillar safety factor results and numerical modelling results which focuses on the potential yielding,
- The available instrumentation results are presented and analysed in Chapter 5, and
- The major conclusions and recommendations for any additional future work are presented in Chapter 6.

Chapter 2

Literature Review

2.1. Overview of Highwall Mining Method

The highwall mining method is an adaptation of the auger mining method, which dates back to the early 1940's. It was introduced in the USA in the 1970's to address some of the limitations of auger mining and adopted in Australia in the 1990's (Porathur, *et al.*, 2017). Over the years, the highwall mining technology has evolved and more countries such as India, Russia, Colombia and New Zealand later adopted it (Mo, *et al.*, 2016). The extraction of coal reserves in the highwall mining method is done through rectangular entries remotely driven from the highwall thereby leaving a series of small pillars to prevent the strata from collapsing (Luo, 2014). A series of small pillars referred to as web pillars are separated by wide pillars referred to as barrier pillars with the web cut that is left unsupported and unventilated (Porathur, *et al.*, 2017) (Figure 2-1). This immediately alleviates the costs due to support and ventilation.

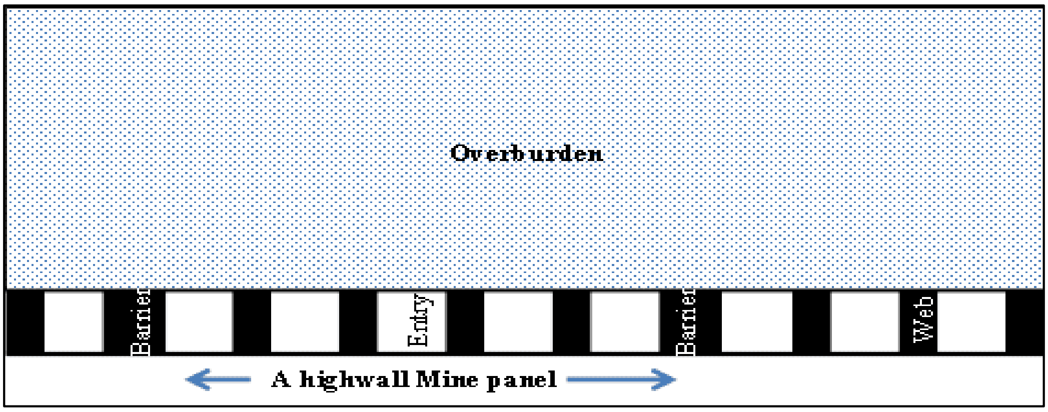

Figure 2-1: The cross-sectional view of the highwall mining layout (Luo, 2014)

The highwall mining method consists of a remotely operated continuous miner with a series of conveyor cars, which rely on the conveyor belts (Figure 2-2) for coal transportation up to a length of 350m (ADDCAR Systems LLC, 2018).

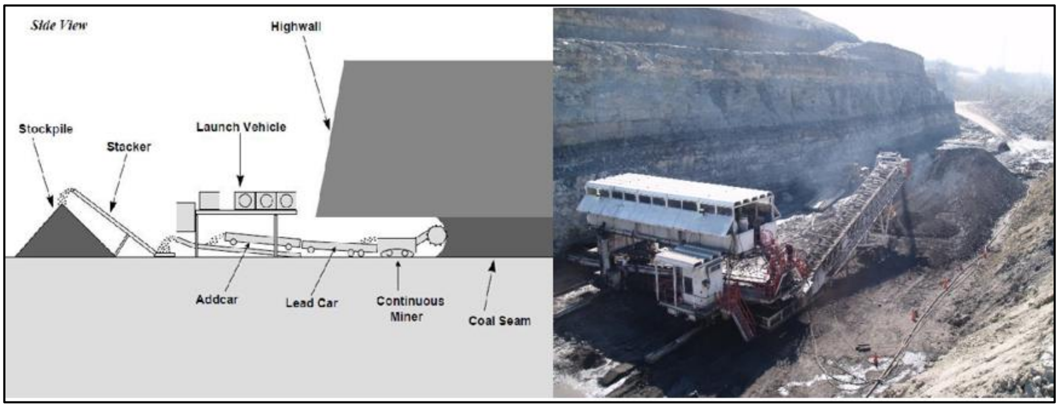

Figure 2-2: ADDCAR Highwall Mining system during operation (ADDCAR Systems LLC, 2018)

These capabilities waiver away the requirements for personnel to physically get exposed to the cutting face and increase the safety of personnel and equipment. The absence of personnel to directly navigate this equipment can result in offline mining and subsequent stability issues. In order to ameliorate this risk, the system is mounted with cameras and a gyroscopic guidance system (Zipf & Bhatt, 2004).

In addition to an increased safety benefit, the ADDCAR system is capable of extracting coal seams with thicknesses ranging from 0.97m to 5.2m, with dip angles up to 15° (Prakash, *et al.*, 2015). This is of great benefit in order to prevent cutting into the roof thereby causing dilution of the coal seam. In instances where the exposed roof comprises of weak layers susceptible to failure during the mining process, the ADDCAR system can tolerate roof falls up 0.3m without interrupting the mining process (Shen, 2014).

Significant improvement in production rates in excess of 1Mt/year have been achieved with highwall mining in Australia with low capital cost and lead times in contrast to the conventional underground operations (Adhikary, *et al.*, 2002). Despite few ongoing challenges, this indicates that the system is capable of improving the production rates at lower costs.

The overall highwall mining layout depends on the stability of the web, barrier and span of the entries. The pillars carry the full weight of the overburden in order to ensure a continued stability, whilst the span width plays a key role in ensuring that in the absence of artificial support, the rockmass around is self-supporting (Duncan

Fama, *et al.*, 1999). Owing to their width/height (w/h) ratio (<3) and length, the web pillars are considered to be slender pillars which needs to be considered in the design to avoid cascading pillar failure (Mark, 2006). Understanding the rockmass behaviour and the loading regime plays a fundamental role in ensuring that the layout is optimally designed for both the safety and economic viability.

2.2. Geotechnical Highwall Mining Layout Design

The geotechnical design in the context of the highwall mining method is necessary to determine the required mining parameters. This includes the span width, web pillar width, barrier pillar width and the number of entries between barrier pillars (Zipf, 2005). The layout design requires the application of an engineering judgement with the support of laboratory tests, experiments, numerical modelling and empirical methods (Porathur, *et al.*, 2017). Through this, the expected pillar load and the required pillar strength can be estimated. This is further used to determine the safety factor for stability criteria and to derive a good understanding of the pillar failure mechanism (Zipf, 2005). Two main layout design categories are identified as empirical techniques and numerical methods (Porathur, *et al.*, 2017), and are discussed below.

2.2.1 Empirical Pillar Design

Pillar design requires an understanding of the pillar strength and the load imposed on it. A pillar safety factor is then calculated as a ratio of pillar strength and load for stability assessment. These components of empirical pillar design are briefly described in the next few sections.

a. Pillar Strength

A myriad of empirical pillar strength estimation equations have been derived and proven successful over the years in different parts of the world by many authors (Porathur, *et al., 2017*). However, it is critical to note that the conditions in which these were originally derived differ from the local conditions and require to be calibrated (Porathur, *et al.*, 2013). Some of these were modified from those developed for square and rectangular pillars. Highwall mining pillars differ from these pillars with respect to their w/h ratio (Verma, *et al., 2014*). Table 2-1 provides a summary of some of the relevant pillar strength estimation equations as obtained from the literature.

Table 2-1: Summary of coal pillar strength estimation formulae

Name and Country	Equation	Source
Salamon and Munro (S&M) (South Africa)	$\sigma = 7.2 \frac{W^{0.46}}{h^{0.66}}$	(Salamon & Munro, 1967)
Van der Merwe linear (vdM_L) (South Africa)	$\sigma = 3.5 \frac{W}{h}$	(Van der Merwe, 2003)
van der Merwe and Mathey formula (vdM&M) (South Africa)	$\sigma\ (OR) = 5.47 \frac{W^{0.8}}{h}$	(van der Merwe & Mathey, 2013)
Mark-Bieniawski (M-B) (USA)	$\sigma = S_I[0.64 + 0.54\left(\frac{w}{h}\right)]$	(Mark, 1999)
CSIRO Pillar Strength (Australia)	$\sigma = 6 \times [0.64 + 0.36(0.69 + 0.44W/h)W/h]$	(Duncan Fama, *et al.*, 1999)
CSIR-CIMFR Pillar Strength (India)	$S = 0.27\sigma_c h^{-0.36} + \left(\frac{H}{250} + 1\right) \left(\frac{W_e}{h} - 1\right)$	(Sheorey, 1992)

Where: S and σ = Web pillar or barrier pillar strength (MPa)

h = Mining height (m)

w = Pillar width (m)

OR = Overlap Reduction Method

S_I = In situ coal strength (MPa)

H = Cover depth (m)

W_e = Equivalent pillar width (m) = $2W$ for long pillar

σ_c = Strength of a 25 mm cube coal sample (MPa)

The Salamon and Munro equation was derived in South Africa and was based on the database of failed and stable square pillars (Salamon & Munro, 1967). The length of pillar increases its strength and as such, the equations derived from the square pillars tend to underestimate the strength of long pillars such as the web pillars and barrier pillars in highwall mining method (Roberts, *et al.*, 2005). This is then not directly related to the highwall mining conditions of web and barrier pillar design.

van der Merwe (2003) back-analyzed the updated database from that used by Salamon and Munro (1967) using an overlap reduction technique and derived a linear equation. van der Merwe & Mathey (2013) further updated this database and established the link between the pillar safety factor and probability of pillar failure. Although this derivation presented a step forward with regards to the pillar stability assessment, the above limitation still applies based on the fact that the original derivation was purely based on the square pillars.

Sheorey (1992) derived the CSIR-CIMFR equation through a collaboration between the Indian Council of Scientific and Industrial Research (CSIR) and Central Institute of Mining and Fuel Research (CIMFR). This is an update of the original pillar strength by Sheorey, *et al.* (1987) which failed to match the actual field observations. This equation is widely used in the Indian coalfields where it was calibrated through consideration of the *in situ* stresses (Porathur, *et al.*, 2013). Both the original and the revised forms of this equation were derived from the square pillars. Through intensive comparative assessment of this equation and numerical modelling, Porathur, *et al.* (2013) concluded that this equation requires correction for it to be applicable for a highwall mining pillar design.

The Mark-Bieniawski equation was originally derived in South Africa through *in situ* testing of square coal pillars (van der Merwe and Madden, 2010). Mark (1999) modified it to take into consideration the pillar strength increase provided by its infinite length, typical of web and barrier pillars in the highwall mining layout. This modified version has been in use for many years as a basis for web and barrier pillar designs. The coal strength constant was found to be 4.3MPa for South African coalfields and 6.2MPa for the USA coalfields, where this equation is widely used (van der Merwe and Madden, 2010). Due to its subsequent modification and adaptation to suit the highwall mining conditions, this equation is preferred for this research.

In order to adapt the above square pillar strength equations to the highwall mining environment, Wagner (1974) introduced the concept of effective pillar width (W_{eff}) for irregular and rectangular shaped pillars of w/h ratio more than 1.0. The empirical equations above tend to underestimate the pillar strengths when directly employed (Porathur, *et al.*, 2017) without any adaptation to the local conditions.

For rectangular pillars,

$$W_{eff} = \frac{4A}{P} \tag{2-1}$$

For very long pillars, such as those in highwall mining (Porathur, *et al.*, 2017)

$$W_{eff} = 2W \tag{2-2}$$

Where: A = Area of the pillar

P = Perimeter of the pillar

W= Pillar width

Based on the experience garnered in the Australian highwall mining, Medhurst (1999) found that equation 2-3 is more appropriate at shallow depth with the mining height of 3.5m.

$$W_{eff} = 1.5W \tag{2-3}$$

b. Pillar Load

The discussion thus far focused on the pillar strength aspect of pillar design. The load acting on the pillars is generally estimated using the tributary area theory, which assumes that each individual pillar carries the load immediately above it. This is mathematically indicated in equation 2- 4.

$$P = \gamma H(W+W_C)/W \tag{2-4}$$

Where: P = load on the web pillar (MPa)

γ = unit weight (MPa/m)

H = depth of cover (m)

W = Width of web pillar (m)

W_C = Width of web cut (m)

Equation 2-4 can be written as indicated in equation 2-5 for barrier pillars assuming that the load acting on the web pillars is negligible and that the barrier pillars are carrying the entire load (Zipf, 2005).

$$S_{BP} = S_v(W_{PN}+W_{BP})/W_{BP} \tag{2-5}$$

Where: S_v = *in situ* vertical stress (MPa)

W_{PN} = panel width (m)

W_{BP} = barrier pillar width (m)

S_{BP} = barrier pillar load (MPa)

Panel width, W_{PN} can be calculated using equation 2-6, where the number of entries N, is known and W_{WP} represents the web pillar width.

$$W_{PN} = N(W_{WP}+W_C)+W_C \tag{2-6}$$

The load varies throughout the web and barrier pillar as a result of the factors such as depth and abutment stresses and this is not fully taken into consideration in the tributary area theory (Porathur, *et al.,* 2017). The weighted average approach can be used whereby both the minimum (D_{min}) and maximum (D_{max}) depths are taken into consideration in equation 2-7, in order to determine the design depth (Mark, *et al.,* 1995).

$$D_{design} = 0.75D_{max}+0.25D_{min} \tag{2-7}$$

The edge effects are also not taken into consideration and as a result, the vertical stresses on the pillars may not be entirely correct, due to the variation in cover depth (Luo, 2014). This is because the vertical stresses tend to decrease towards the end or edge of the mine boundary and increase at the entrance due to the presence of the highwall (Porathur, *et al.,* 2017). Therefore, using the design depth will also not provide the correct perspective with regards to the vertical stresses acting on the pillars.

In order to optimize the mining layout, Luo (2014) suggested that the concept of pressure arch is appropriate (Figure 2-3). This theory implies that with significant competent layers in the overburden, most of the load will be transferred to the barrier pillars and the web pillars will then be subjected to much less load. This allows for web pillars to be narrow and a lower safety factor can therefore be used.

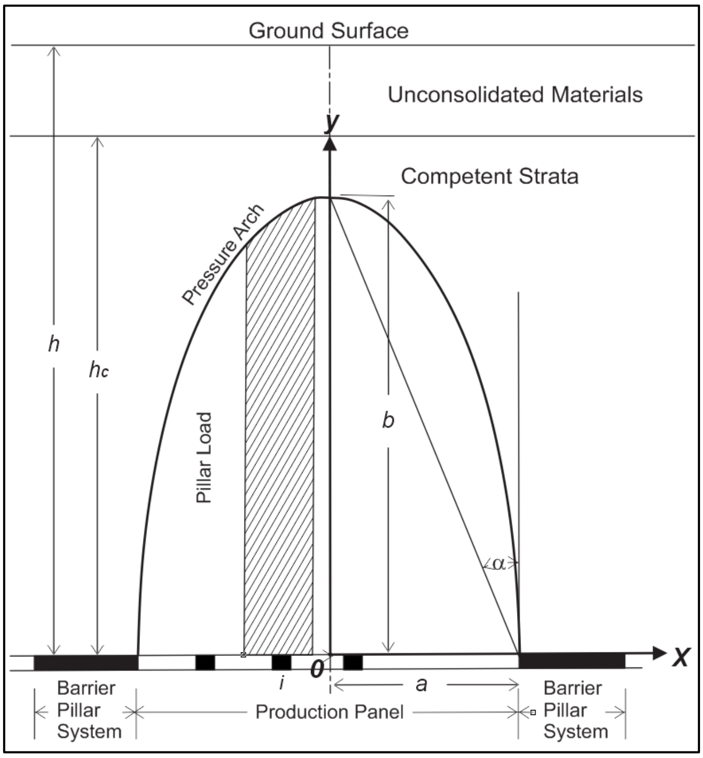

Figure 2-3: Pressure arch concept applied in highwall mining method (Luo, 2014)

c. Pillar Safety Factor

The pillar safety factor (SF) defines the ratio of the pillar strength to the load imposed on it, using the strength equations and pillar load calculation approaches described earlier. The following combined safety factor equations (2-8 and 2-9) can be used for both web and barrier pillar stability (Zipf, 2005), using the Mark-Bieniawski strength equation.

$$SF_{BP} = \frac{\text{Pillar Strength}}{\text{Pillar Load}} = \frac{S_I[0.64+0.54W_{BP}/H]}{[S_V(W_{PN}+W_{BP})/W_{BP}]} \tag{2-8}$$

$$SF_{WP} = \frac{S_I[0.64+0.54W_{WP}/H]}{[S_V(W_{WP}+W_E/W_{WP})]} \tag{2-9}$$

Where: SF_{BP} = Barrier pillar safety factor

SF_{WP} = Web pillar safety factor

In South Africa, the coal design safety factor threshold of 1.6 has generally been applied (van der Merwe and Madden, 2010). Based on the reviewed and updated database of failed and stable pillar database, van der Merwe and Mathey (2013) suggested a minimum safety factor of 1.3. However, in their research, they emphasised that this is simply taken as a path to obtaining the probability of pillar failure instead of it being solely applied. Ross, *et al.* (2017) provided the following safety factor and design criteria guidelines for a typical highwall mining excavation design:

- A highwall mining panel should not exceed 20 openings between barrier pillars
- Web pillar SF = 1.6 for normal operations
- Web pillar SF = 2.0 for protection of critical structures
- Minimum web pillar w/h ratio of 0.8
- Barrier pillar SF = 1.5 with w/h > 4; SF = 2.0 with w/h < 4
- Overall panel SF (webs and barriers) = 2.0

Mo, *et al.* (2016) provided the following safety factor guidelines:

- 1.6 in the absence of any reliable guidance system, for new operations
- 1.3 for a minimum web pillar w/h = 1.0
- The maximum critical panel width is restricted to the value that is equal to the shallowest depth of overburden
- A minimum pillar w/h = 4 is suggested for the barrier pillars

In an attempt to cater for the time dependency of pillar stability, Porathur, *et al.* (2017) suggested the following safety factors:

- Long term stability = 2.0
- Medium term stability = 1.5 – 2.0
- Short term stability = 1.0

Based on the back analyses of some of the failed cases using the Analysis of Retreat Mining Pillar Stability software for Highwall Mining (ARMPS-HWM), Mark (2006) came up with the following guidelines for safety factor requirements, as indicated in Table 2-2.

Table 2-2: ARMPS-HWM Minimum safety factor guidelines (Mark, 2006)

Web pillar SF	
1.6	When the panel width (excluding the barrier) exceeds approximately 60 m
1.3	When the panel width (excluding the barrier) is less than approximately 60 m
Barrier SF	
2.0	When the barrier's width-to-height ratio < 4.0
1.5	When the barrier's width-to-height ratio ≥ 4.0
Overall SF	
2.0	Applicable to all conditions

Zipf (2005) derived a number of design charts which can be used for guidance with the initial design of web and barrier pillar widths for various mining heights and cover depths. Figures 2-4 and 2-5 below are charts which were produced for a constant cut width of 3.66m and a safety factor of 1.3 and 1.6, respectively. The safety factor of 1.0 was used for barrier pillars, assuming that the web pillars have no carrying capacity. The Mark-Bieniawski coal pillar strength equation was used in the derivation of these charts, assuming an intact coal strength of 6.2MPa.

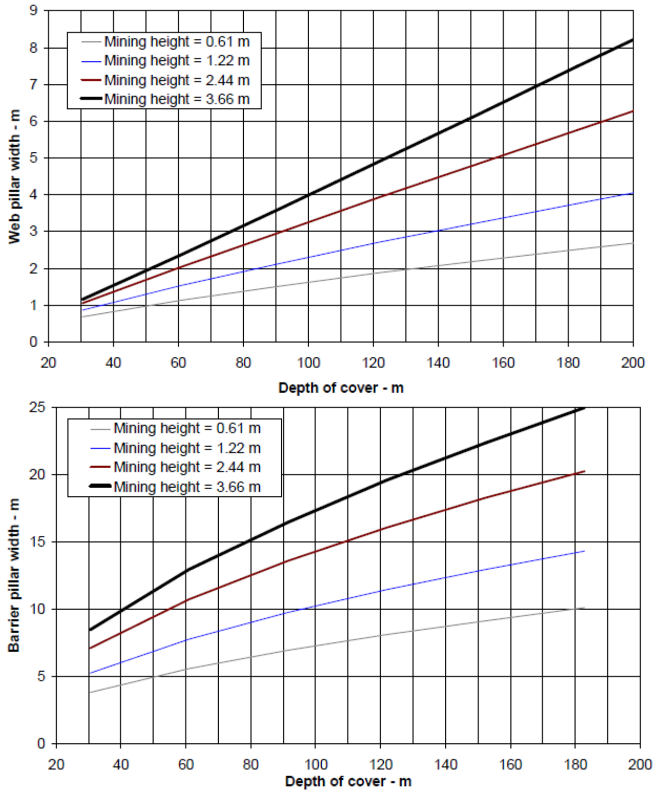

Figure 2-4: Suggested web pillar width for safety factor of 1.6 and barrier pillar width for a safety factor of 1.0 at a 122m wide panel (Zipf, 2005)

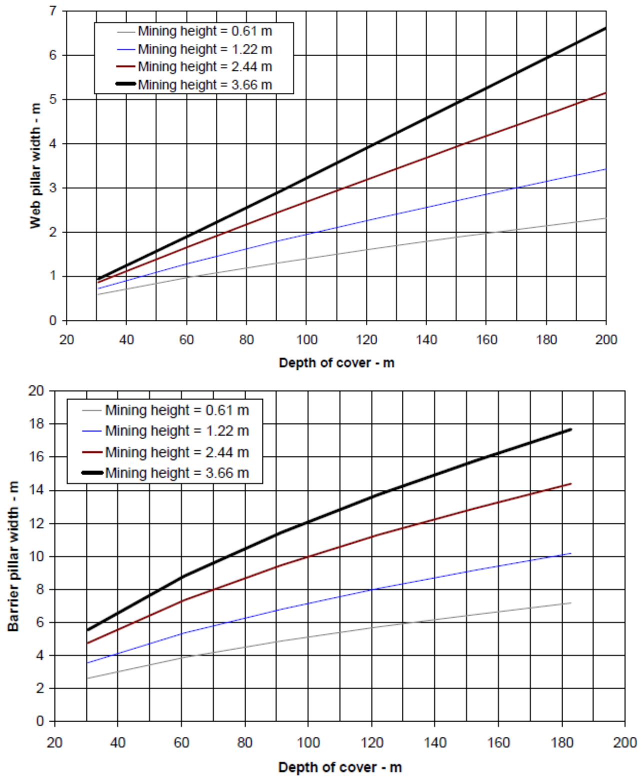

Figure 2-5: Suggested web pillar width for a safety factor of 1.3 and barrier pillar width for a safety factor of 1.0 in a 61.0m wide panel (Zipf, 2005)

d. Cut Width Design

The unsupported span stability is also of concern as much as the web pillars are, as it is required to be stable for the duration of the mining process (Shen, 2014). This is because once the excavation has been created; any inaccurate assumptions cannot be fully rectified (Hoelle, 2003). The cut width for this layout design in this research will be fixed to 3.6m in line with the CM cutter head. However, some of the available span stability assessment methodologies are briefly described below.

Shen and Duncan Fama (2001) obtained excellent agreement from the results obtained using the Laminated Span Failure Model (LSFM) mathematically presented in equation 2-10. They further refined this equation to incorporate possible crushing or yielding of rock during failure resulting in equation 2-11. Where no yielding or crushing is expected, equation 2-11 reverts back to equation 2-10.

$$S = 1.873t(E/p)^{1/4} \qquad (2\text{-}10)$$

$$S = 1.873t(E/p)^{1/4} x\, \delta\left(\frac{\sqrt{EP}}{\sigma_c}\right) \qquad (2\text{-}11)$$

Where: S = Span (m)

t = thickness (distance between beddings) (m)

E = Young's modulus of the roof rock (MPa)

p = Self-weight or distributed vertical load on the bedding (MPa)

δ = Rock Crushing Factor (≤ 1.0)

σ_c = Uniaxial Compressive Strength (MPa)

Using the mechanical properties of siltstone which forms part of the immediate roof in Table 2-3, plots were produced for varying Young modulus for the assessment of span stability (Figure 2-6).

Table 2-3: Laboratory tested rock properties (Glencore Coal Geotechnical Database, 2012)

Lithology	Parameter	UCS (MPa)	Young's Modulus (Tangent) (GPa)	Young's Modulus (Secant) (GPa)	Poisson's ratio (Tangent)	Poisson's ratio (Secant)
No. 1 Coal Seam	Average	20.22	8.25	5.44	0.33	0.2
	Standard deviation	8.16	5	4.18	0.12	0.03
	Minimum	11.65	4.28	2.43	0.2	0.16
	Maximum	35.95	18.9	14.9	0.59	0.23
No. 2 Coal Seam	Average	35.14	5.39	3.75	0.34	0.23
	Standard deviation	9.82	1.37	0.64	0.08	0.06
	Minimum	21.34	4.19	3.07	0.22	0.16
	Maximum	45.17	7.62	4.66	0.45	0.32
No. 4 Coal Seam	Average	38.28	7.88	5.72	0.25	0.17
	Standard deviation	8.96	0.45	1.42	0.11	0.09
	Minimum	31.96	7.56	4.71	0.18	0.11
	Maximum	44.61	8.19	6.72	0.33	0.24
Shale	Average	72.66	12.44	10.1	0.19	0.11
	Standard deviation	20.4	10.48	10.77	0.04	0.04
	Minimum	38.91	0.81	0.81	0.11	0.07
	Maximum	97.99	39.4	42	0.26	0.21
Sandstone	Average	85.48	22.01	15.99	0.38	0.18
	Standard deviation	24.72	9.92	8.32	0.13	0.05
	Minimum	40.94	9.6	5.9	0.14	0.06
	Maximum	140.16	47.7	38	0.63	0.29
Siltstone	Average	90.78	18.67	15.18	0.26	0.13
	Standard deviation	28.11	4.92	7.31	0.04	0.02
	Minimum	27.39	12.5	8.9	0.19	0.1
	Maximum	118.97	27.6	31.3	0.34	0.16
Mudstone	Average	18.74	1.16	0.87	0.31	0.21
	Standard deviation	11.08	0.68	0.42	0.09	0.08
	Minimum	9.33	0.36	0.33	0.21	0.14
	Maximum	41.39	2.13	1.44	0.5	0.32

The plots presented in Figure 2-6 indicate that the thicker the beam, the wider the span. For siltstone with E=15GPa and σ_c = 90MPa, at the design span of 3.6m, the required thickness is 0.4m. The average thickness obtained from the geological borehole logs is 0.64m, which therefore indicates no issues.

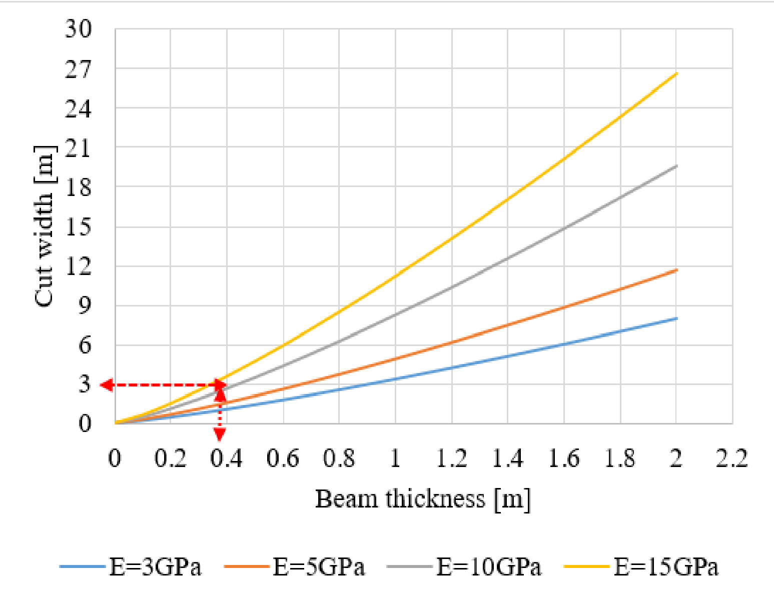

Figure 2-6: LSFM plots of maximum stable span and roof beam thickness at varying Young's modulus

The following fundamental fixed beam equations have also been used to estimate both the tensile strength and the amount of deformation as part of cut width designs.

$$\sigma_t = \frac{\gamma L^2}{2t} \tag{2-12}$$

$$\eta = \frac{\gamma L^4}{32Et} \tag{2-13}$$

$$\eta = \frac{\sigma_t L^2}{L16Et} \tag{2-14}$$

Where: σ_t = tensile stress (MPa)

L = length of the beam (m)

t = thickness of the beam (m)

E = modulus of Elasticity of the beam (GPa)

η = maximum deflection at centre of the beam (m)

Using the above fundamental tensile stress distribution on the fixed beam, Buddery & Oldroyd (1992) derived a system for testing and classifying the immediate 2m of roof and floor in the coal mines, using an impact splitter (Figure 2-7). In this test, a 1.5kg chisel is dropped from a pre-set height every 20mm on a drill core. The mean fracture spacing is then obtained due to the opening of weak bedding planes, indicative of the likely roof behaviour when subjected to *in situ* stresses.

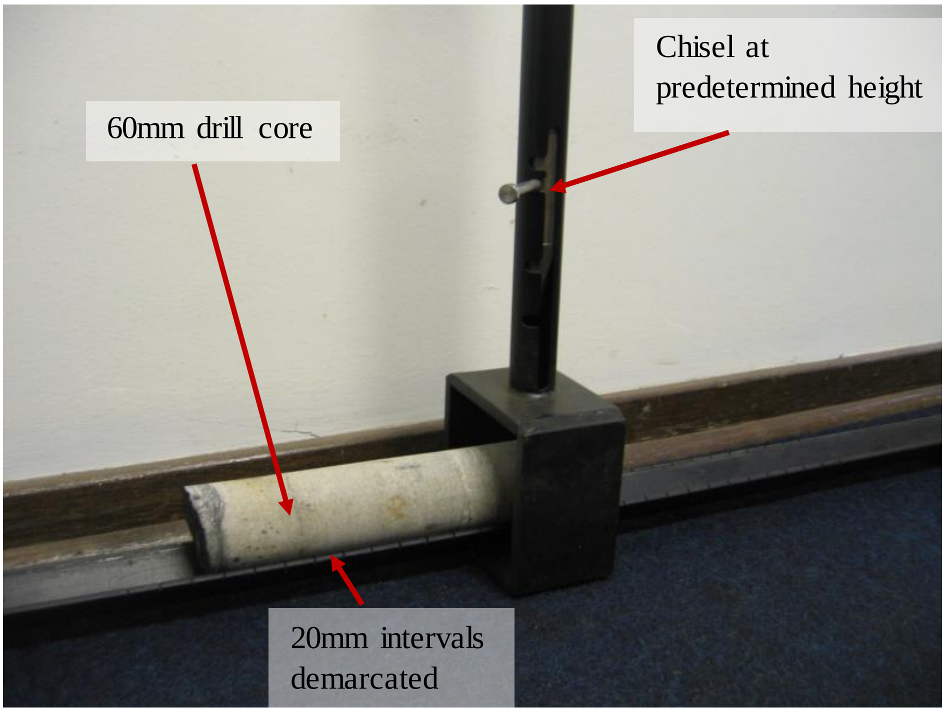

Figure 2-7: Impact splitting test setup

Each geological unit is then rated using either equation 2-15 or equation 2-16 based on the fracture spacing, F_s.

For $F_s < 5$: rating $= 4F_s$ (2-15)

For $F_s > 5$: rating $= 2F_s + 10$ (2-16)

The roof is classified by means of a weighted rating which is obtained by means of using equation 2-17. The final roof rating is obtained by summing up all the individual weighted ratings.

$$R_w = Rx2(2\text{-}h)t \tag{2-17}$$

Where: h = mean unit height above the roof (m)

R = individual roof rating

t = unit thickness (m)

Latilla, *et al.* (2002) reviewed the original classification based on the calibration of the actual conditions and the conditions predicted by impact splitting tests. These categories are also presented in Table 2-4 for comparison.

Table 2-4: Unit and roof classification based on impact splitting test (Buddery and Oldroyd, 1992; Latilla, *et al.*, 2002)

Unit rating		**Class**	**Roof rating**	
(Buddery and Oldroyd, 1992)	(Latilla, *et al.*, 2002)		(Buddery and Oldroyd, 1992)	(Latilla, *et al.*, 2002)
<10	<9	Very Poor	<39	<34
11-17	10-13	Poor	40-69	35-51
18-27	14-19	Moderate	70-99	52-75
28-32	20-28	Good	100-129	76-113
>32	29-42	Very Good	>130	114-167
	>42	Excellent		>167

Latilla, *et al.* (2002) reviewed the original procedure and provided the adjustments for coal roof and impacts of jointing on the final rating. In the instances where the immediate roof comprises of coal, the normal unit rating is simply multiplied by a factor of 1.56 (derived from the ratio of overlying rock to coal density). Although this procedure was originally derived to determine the appropriate support and not necessarily the requirements for support installation, the final rating can provide some overview with regards to the type of roof or floor response that can be encountered in the area of interest.

Madden (2002) conducted impact splitting tests on five (5) geological boreholes that were drilled to characterize the roof conditions as part of the feasibility study for the initial bord and pillar underground workings at the 5 seam operation. The roof rating results (Table 2-5) from Madden (2002) indicate a very good roof rating. However, moderate unit rating was found in the areas where siltstone is interlaminated with mudstone.

Table 2-5: Summary of the impact splitting test results (Madden, 2002)

Hole	Interlam. Siltstone-Mudstone			Marker Sandstone			Weighted Rating	Roof Rating
	Thickness (m)	Rating	Classification	Thickness (m)	Rating	Classification		
60	1.7	31.5	Good	0.3	130	Very Good	232	Very Good
61	1.7	27.5	Moderate	0.3	130	Very Good	221	Very Good
62	1.62	27.7	Moderate	0.38	86	Very Good	187	Very Good
63	1.87	41.6	Very Good	0.13	62	Very Good	176	Very Good
64	1.74	30.6	Good	0.3	70	Very Good	164	Very Good

An additional assessment was later conducted as part of the feasibility study for the areas earmarked for highwall mining (Middindi Consulting, 2012). The results indicated that the unit rating ranges from good (22) to very good (42) using the classification system from Latilla, *et al.* (2002). This indicates that the roof conditions associated with individual layers are expected to be stable. The spatial distribution of the results is indicated in Figure 2-8 relative to the planned mining layout.

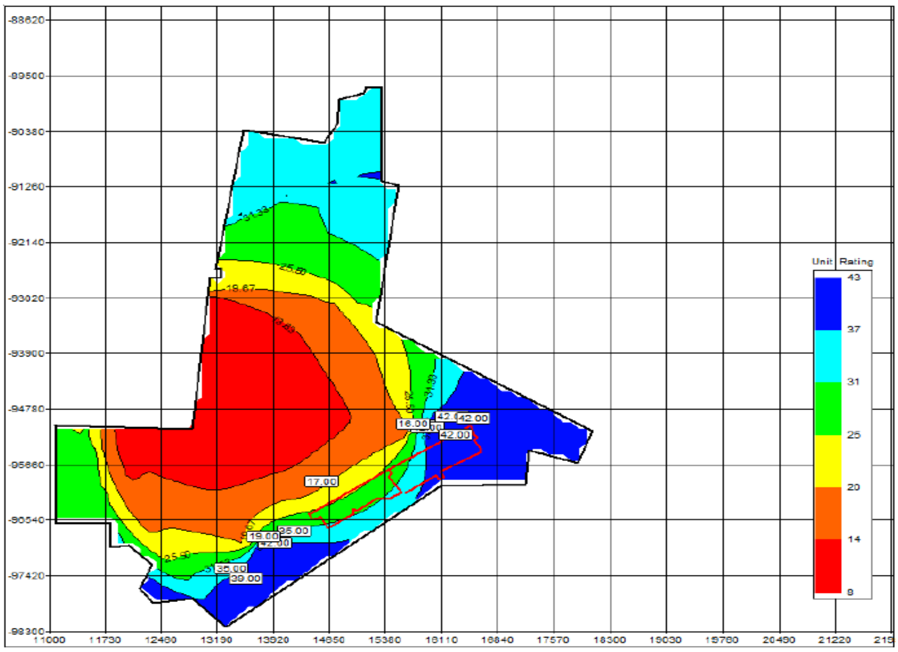

Figure 2-8: Spatial distribution of unit ratings relative to the planned highwall mining outline (Middindi Consulting, 2012)

A number of empirical standard charts exist which are based on several rockmass classification systems such as Bieniawski's (1989) Rock Mass Rating (RMR) and Barton, *et al.* (1974) Tunnel index (Q-system) and have been used for span stability assessment. Despite their limitations, particularly in the coal mining environment, these classification systems are valuable tools, which provide a first-hand indication of stability (Porathur, *et al.*, 2017). The No. 5 coal seam roof was found to have an average RMR of 59, with a minimum value of 42 and an average Q-value of 32 with a minimum of 0.01. A summary of the rockmass classification is provided in Table 3-1.

Hutchinson and Diederichs (1996) chart (Figure 2-9) which combines both the RMR and Q was used to determine the support requirements and to estimate the stand-up time. The average RMR line (orange) intersects the maximum span line (red line for 3.6m) below 10 years unsupported stand-up time line. This also defines a zone in which no support is required. The minimum RMR value intersects the span line at approximately 1 week unsupported span line. A web cut is generally required to stand-up for the duration of the cutting activity, which is generally a couple of days (Porathur, *et al.*, 2017).

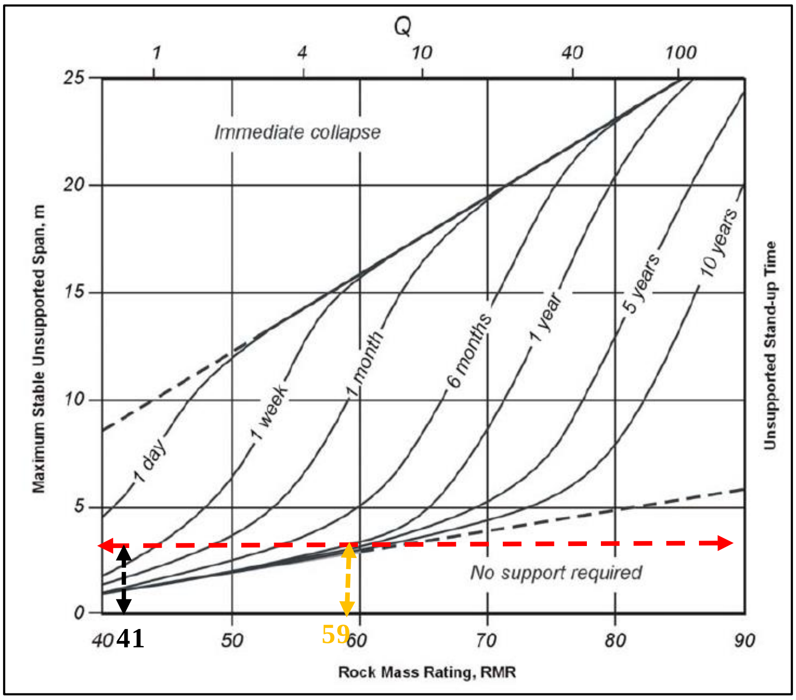

Figure 2-9: Unsupported span vs rockmass rating (Hutchinson and Diederichs, 1996)

To quantify the span stability, Houghton and Stacey (1980) chart (Figure 2-10) was utilized. The use of these charts indicates that using the average Q-value, the safety factor is greater than 1.3 and it plots on the stable zone. Using the minimum Q-value, the safety factor falls between 0.9 and 0.8. Combining the safety factor with the unsupported stand-up time obtained above, this safety factor should suffice for the planned cut width.

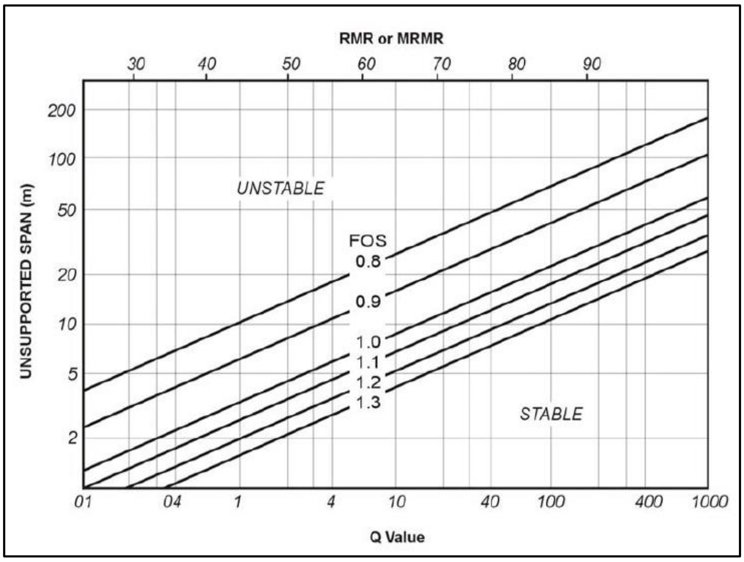

Figure 2-10: Safety factor for unsupported Span vs Q-value (Houghton and Stacey, 1980)

2.2.2 Numerical Modelling

Numerical modelling is used to determine the changes in stress distribution and the resulting rockmass response due to mining. It can be categorized as, either differential or integral method. This depends on whether the rockmass is modelled as a volume, which is curtailed by applying artificial boundaries or only concentrate on the boundary of the excavation with the stresses and displacement away from this excavation being assumed to be continuous (Lightfoot, 1999). The integral method comprises of Ficticious (FS), Discontinuity Displacement (DD) and Direct Boundary Integral method (Lightfoot, 1999). A number of modelling analysis methods exist which fit into the above main categories viz. Continuum method and Discontinuum method. Continuum method comprises of the Finite Difference Method (FDM) and the Finite Element Method (FEM). The numerical modelling codes in these categories are appropriate for modelling a continuous rockmass (massive, intact rock, soil-like or heavily jointed rockmass) (Itasca Consulting Group, 2014). Discontinuum methods comprise of Distinct Element Method (DEM) and Discrete Fracture Network (DFN). In this type of numerical method, the rockmass is modelled as a collection of discrete rock blocks, which interact through their boundaries (Lightfoot, 1999). Some of the most commonly used numerical methods in the highwall mining layout design are FDM: Fast Lagrangian Analysis of Continua (FLAC3D and FLAC2D), Boundary Element displacement discontinuity for laminated medium (LAMODEL) and DEM: Universal Distinct Element Code (UDEC) (Porathur, *et al.*, 2017).

a. Fast Lagrangian Analysis of Continua (FLAC3D)

FLAC3D is a three-dimensional program used for carrying out engineering mechanics computations. The materials are represented by polyhedral elements within a three-dimensional grid that is adjusted by the user to fit the shape of the object to be modelled. Each element behaves according to a prescribed linear or nonlinear stress / strain law in response to applied forces or boundary restraints (Itasca, 1996). It provides a 3D perspective of the stress distribution on the stability of the web pillars, barrier pillars, roof and floor of the excavations. Mohan, *et al.* (2001) summarized the procedure to be followed for numerical modelling using FLAC3D as discussed below:

- Grid generation
- Selection of an appropriate material behaviour model
- Incorporation of material properties
- In situ stresses and boundary conditions
- Solution to the equilibrium of the initial elastic model to generate the *in situ* stresses in the model
- Development of roadway excavations in the model and the application of a constant vertical velocity at the top of the model and continuous monitoring of the average vertical stress and strain in the pillar at each solution 'step'

Middindi Consulting (2012) used FLAC3D to mainly assess the influence of the pillar length on its stability, roof stability and floor stability (Figure 2-11).

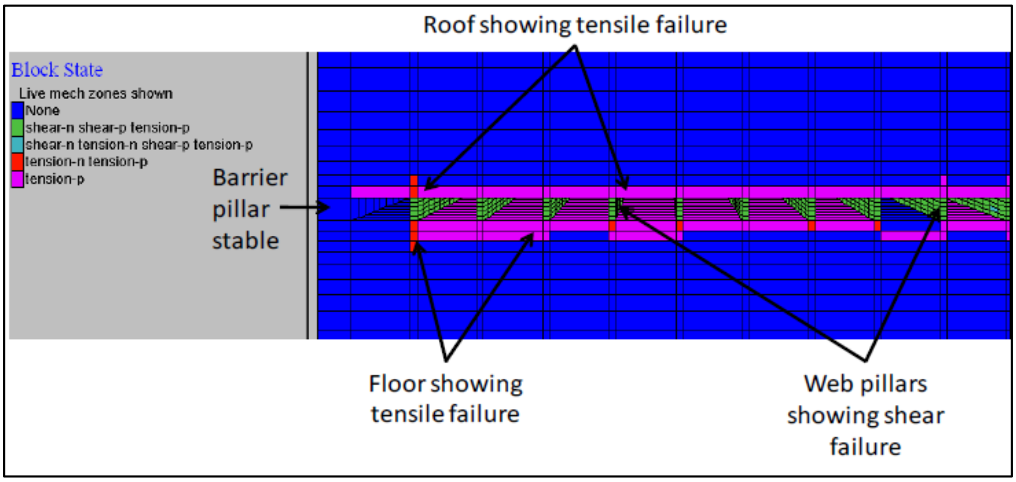

Figure 2-11: Stability of the highwall mining layout using FLAC3D (Middindi Consulting, 2012)

It was found that at the length to width ratios of 10 or less, a constant linear increase in stress occurs. It was further concluded that approximately 35% increase in pillar stres may be anticipated up to a length to width ratio of 16, after which it is expected to remain constant (Figure 2-12).

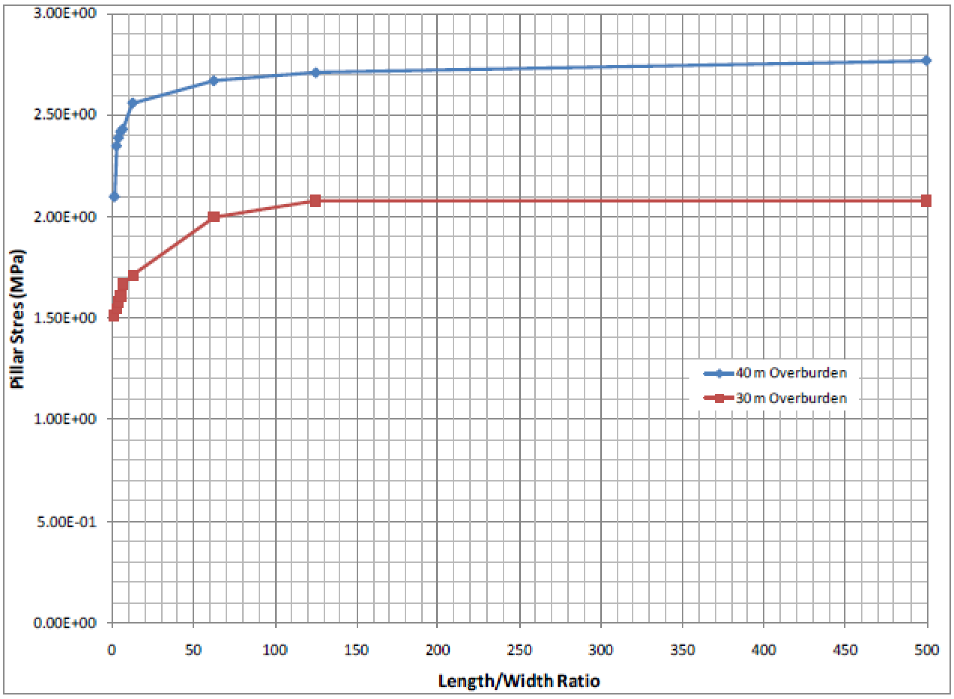

Figure 2-12: Pillar stress change for varying pillar length to width ratio (Middindi Consulting, 2012)

Porathur, *et al.* (2013) also used FLAC 3D for an assessment similar to the above for various slenderness ratios. The modelling assessment for this study was analogous to the laboratory uniaxial compressive strength test setup (Figure 2-13). The strength of a 5m wide and long pillar in the direction of mining i.e. continuous pillar with no interconnections, was compared to an equivalent 10m x 10m square pillar. The peak stresses were found to be comparative up to a w/h of 1.25.

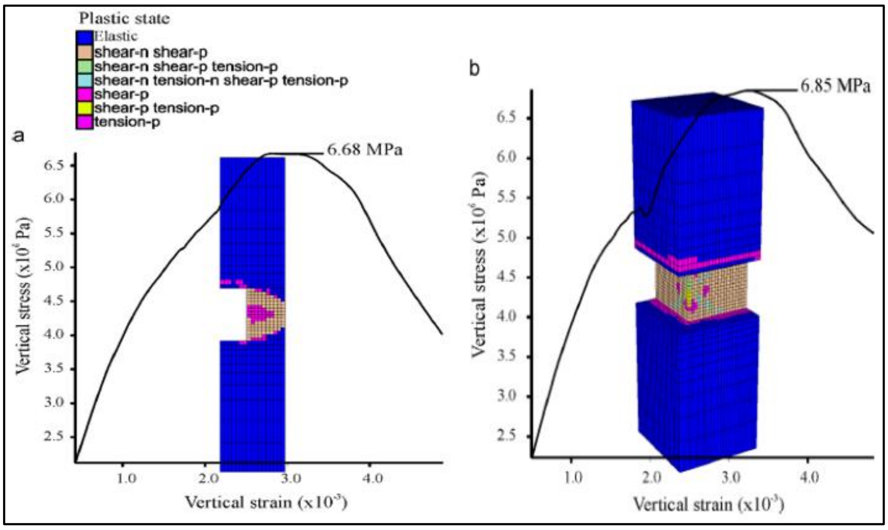

Figure 2-13: FLAC3D stress-strain curves for a w/h of 1.25 for (a) long pillar and (b) equivalent square pillar (Porathur, *et al.*, 2013)

From Figure 2-14, the following observations were made:

- The pillar strength generally increases with an increase in pillar w/h ratio
- The peak stresses are comparable up to the w/h of 1.25
- The adaptations were made to the empirical designs to account for the pillar slenderness

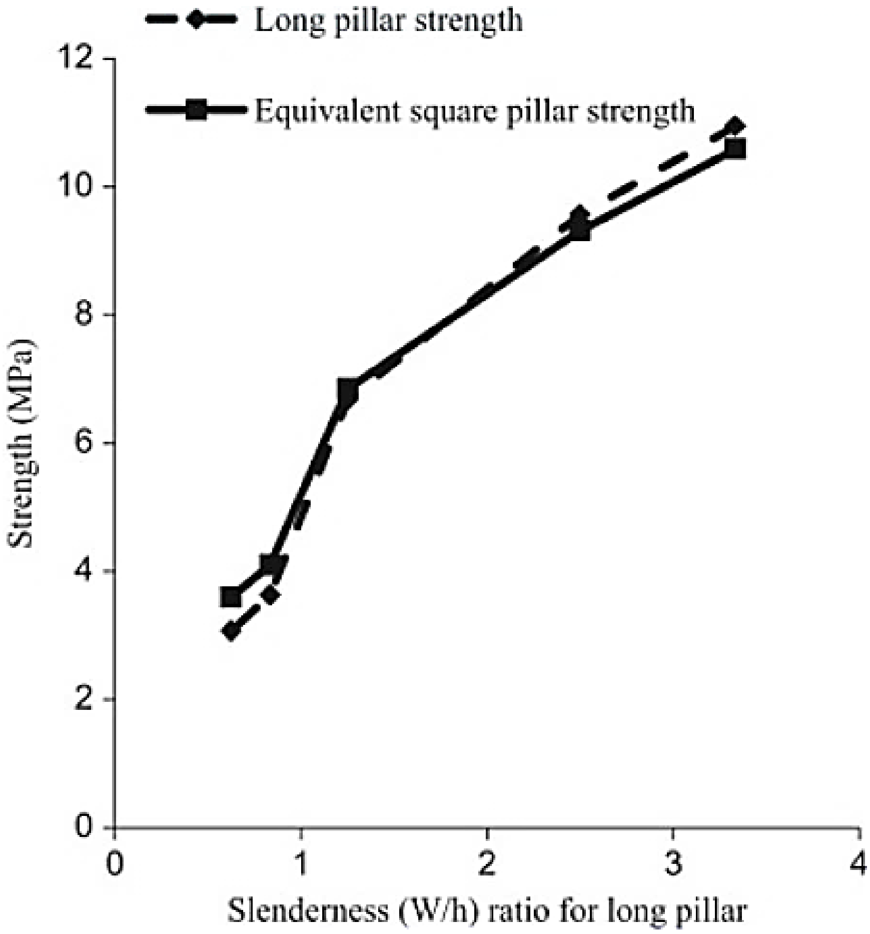

Figure 2-14: Long pillar-effective square pillar strength comparison (Porathur, *et al.*, 2013).

Furthermore, Porathur, *et al.* (2013) used FLAC3D to counteract the shortfall of an empirical assessment with regards to the vertical stress distribution along a web pillar dipping at -5° to +20° (Figure 2-15).

By comparing the modelled and calculated pillar stresses, Porathur, *et al.* (2013) were able to establish the trends as demonstrated in Figure 2-16. The virgin vertical stress profile calculated from the tributary area approach has a rising trend whilst the one obtained from the model is steep and has a subsequent drop near the toe of the slope.

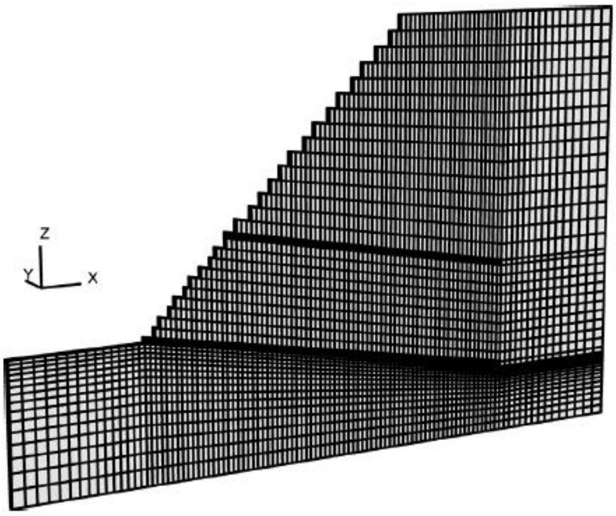

Figure 2-15: Cross sectional view of a web pillar in a highwall mining set up (Porathur, *et al.*, 2013)

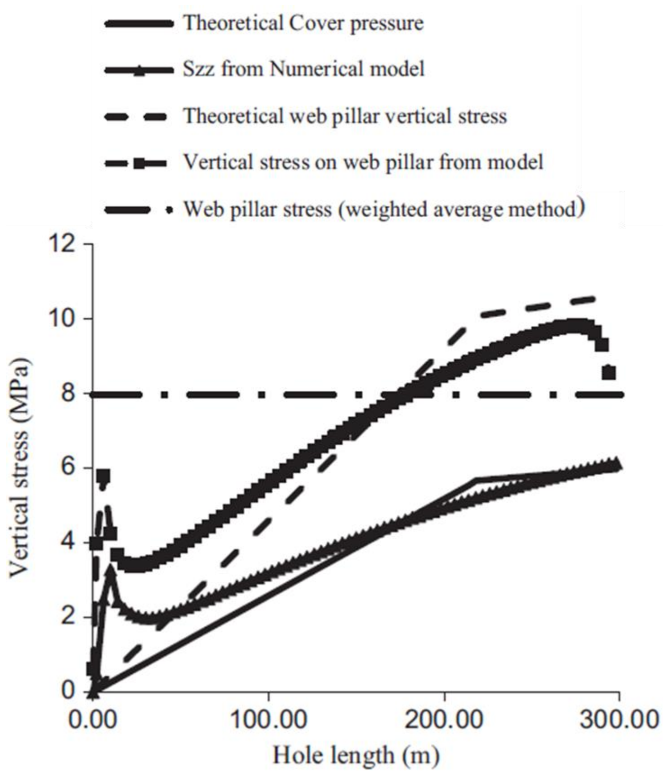

Figure 2-16: Modelled and calculated vertical stresses before and after a web cut excavation (Porathur, *et al.*, 2013)

b. Boundary Element Displacement Discontinuity for Laminated Medium (LAMODEL)

LAMODEL is a pseudo 3D software, Displacement-Discontinuity variation of the boundary element method and is used for calculating stress and displacement in thin-bedded deposits (NIOSH, 1998). LAMODEL is freely available. Vandergrift and Garcia (2005) used this modelling code to assess and verify the results obtained from the empirical equation with regard to the possibility of cascading pillar failure (CPF) and seam interactions. In this modelling, a web pillar failure was induced and the remaining pillars monitored to see if they could absorb the additional loading. Minimal stress transfer was observed in the model results showing a low probability of interburden failure as well as possible CPF (Figure 2-17).

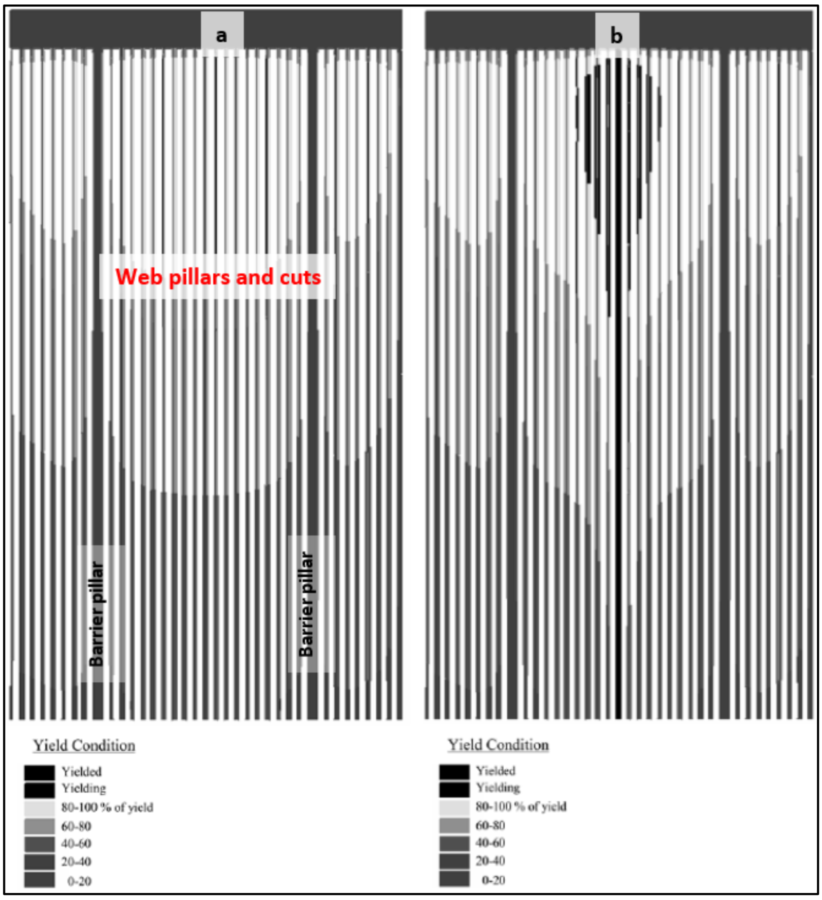

Figure 2-17: LAMODEL numerical assessment for (a) multiple seam mining interaction and (b) simulating a collapsed web pillar and monitoring of the CPF (Vandergrift and Garcia, 2005)

c. Universal Distinct Element Code (UDEC)

It is a two-dimensional numerical program, which is based on the distinct element method for discontinuum modeling (Itasca Consulting Group, 2014). The area is subdivided into smaller blocks whose boundaries represent both geologic features and engineered structures in the model (Itasca Consulting Group, 2014). These blocks can either be rigid or deformable material, the behavior of which is governed by a prescribed non-linear stress / strain relationship. This allows new stresses to be calculated within the elements as indicated in Figure 2-18.

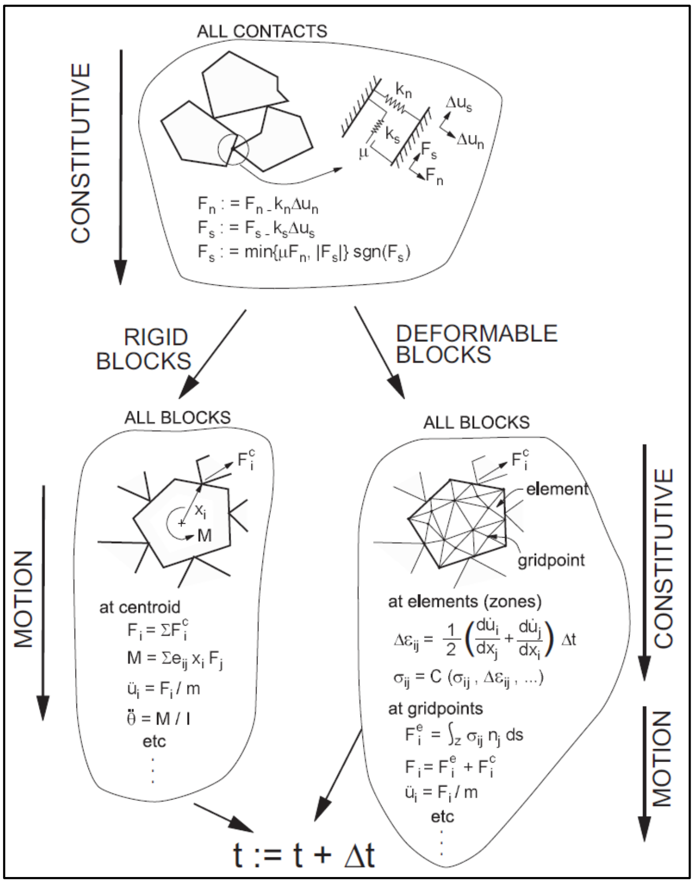

Figure 2-18: Typical calculation cycle used in the discrete element method (Itasca Consulting Group, 2014)

The program also has the ability to maintain numerical stability when many intersecting planes are modelled and has an automatic scheme for recognizing the formation of new contacts in the model. The process of model setup and execution is summarized in the flowchart in Figure 2-19, reproduced from Itasca Consulting Group (2014).

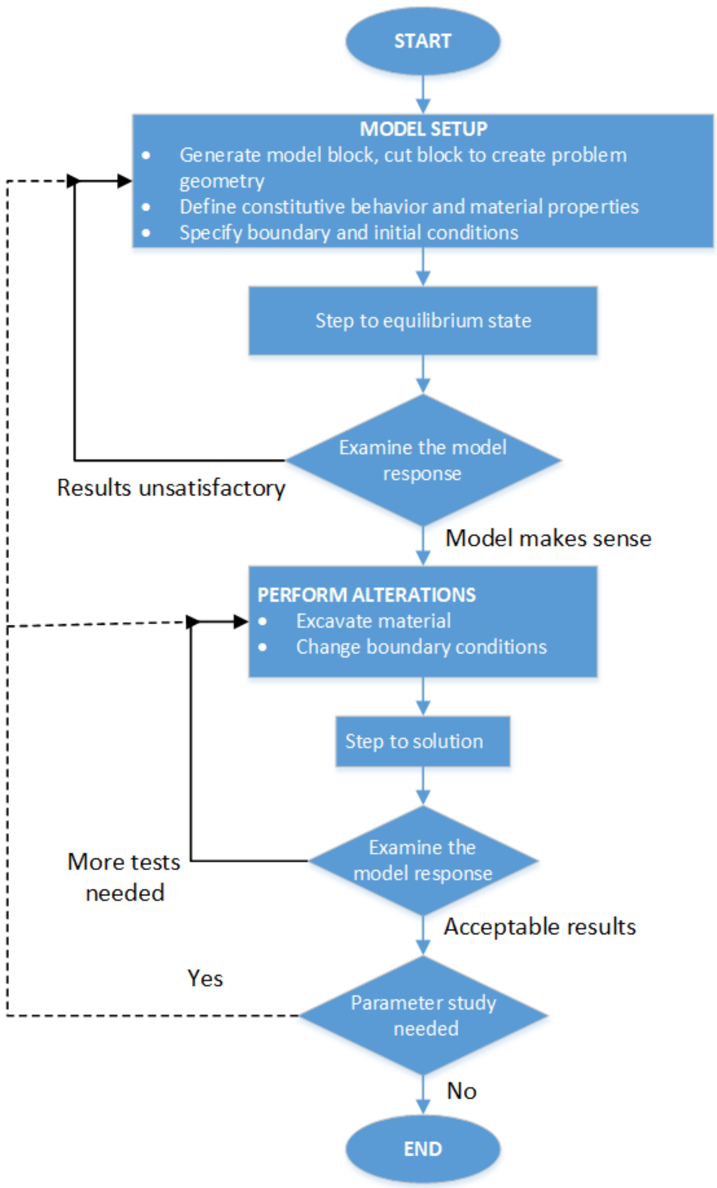

Figure 2-19: UDEC Model setup and execution process flowchart (Itasca Consulting Group, 2014)

UDEC has been used by various authors in the analyses and assessment of mining layout stability. Shen and Duncan Fama (2001) used UDEC for back analysis of severe roof failures, which frequently occurred during the highwall mining method, which resulted in a continuous miner being trapped. The model predicted a complete yielding and destressed web pillar, which implies failure (Figure 2-20). The failed web pillar was then completely removed from the model, assuming a web pillar failure and this resulted in a 3m thick roof fall being predicted by the model. This then indicated that the failure was as a result of an increased span caused by a collapsed web pillar that was narrowed as the penetration depth increases to 146m depth. This assessment indicates that even with its limitation as a 2D model, UDEC can still provide reasonable pillar stability assessment results.

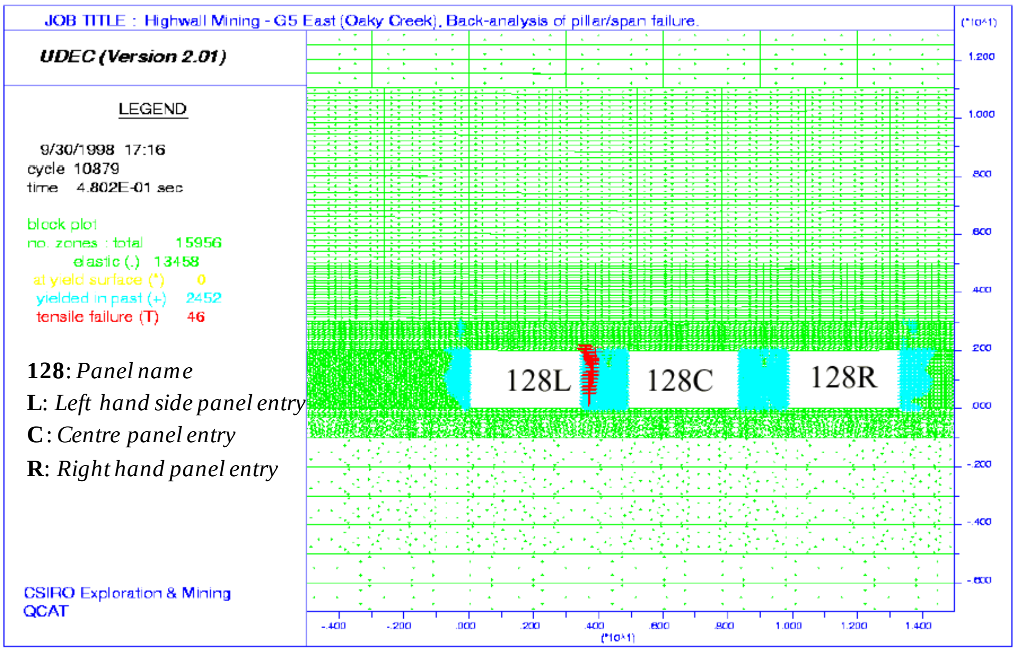

Figure 2-20: Web pillar showing plastic yielding as predicted by UDEC (Shen and Duncan Fama, 2001)

UDEC was also used to determine the effect of pillar cross-section shape, w:h ratio, *in situ* stress conditions, coal strength, and roof and floor interface conditions (Duncan Fama, *et al.*, 1999). An output from this modelling exercise was the relationship between pillar strength to w/h ratio for various materials for various interface conditions (Figure 2- 21).

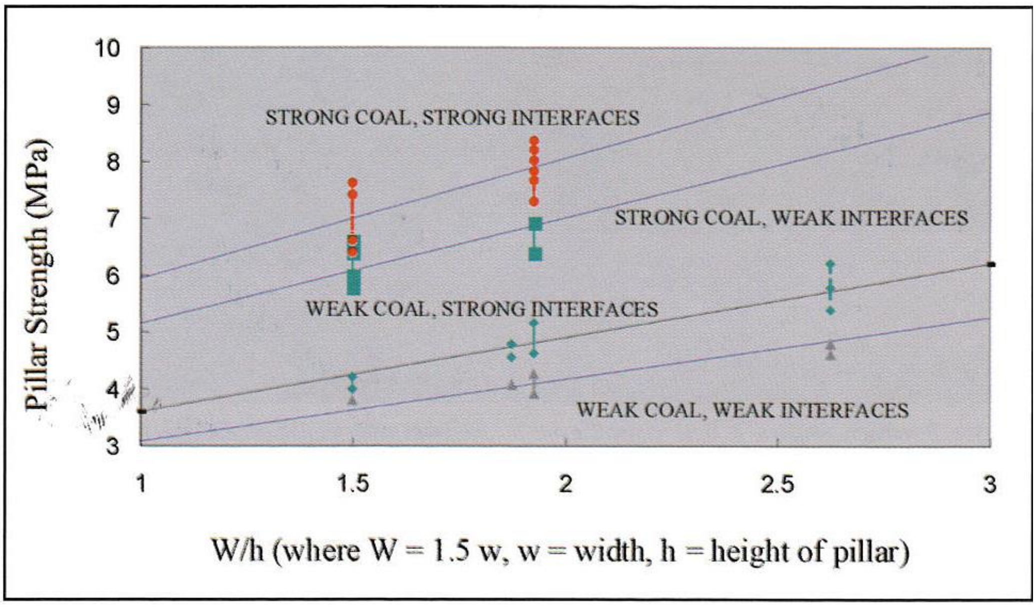

Figure 2-21: Plots from the UDEC modelling results showing strength variation with varying w/h ratio and interface conditions (Duncan Fama, *et al.*, 1999)

Shen (2014) also used UDEC to back analyse a rather strange subsidence that was observed on top of the barrier pillar. Three scenarios were modelled to establish the possible cause of this subsidence. In the first scenario, the entry geometry was modelled as per the design, assuming that this was achieved during the actual mining process. In the second scenario, 2m high roof falls were assumed thereby increasing the mining height to 4.8m and in addition, lower strength inclined joints were introduced in the third scenario, in order to assess its effects as well as the time dependency. The results of these three cases are indicated in Figure 2-22.

The simulation was used to investigate the stresses under the highwall, span stability and the various pillar width strengths, where there are inclined layering and joints. The following conclusions were then made with regards to the cause of the subsidence: The pillar strength was reduced by the roof falls which increased the pillar height, reduced joint strength due to the water infill as well as the progressive pillar weakening.

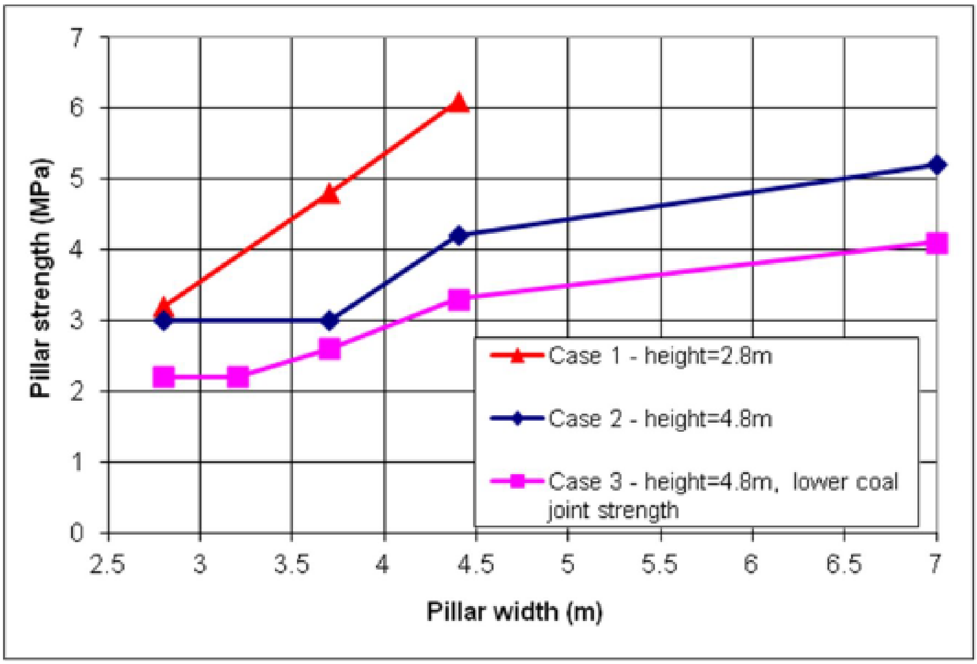

Figure 2-22: Variations of pillar strength with pillar width for three different cases (Shen, 2014)

The observed subsidence was successfully back analyzed by reducing the joint properties, which indicated the time effects as a result of the water inflow. Vandergrift and Garcia (2005) employed it to further confirm the empirical results and the modelling results from the LAMODEL software that was carried out as presented in Figure 2-17. The impact of the ground pressure from the continuous miner was also simulated where multiseam highwall mining was being conducted. The evidence of minor roof instabilities was observed in the areas where a weak mudstone layer was left on the immediate roof. The model further concluded that leaving a coal layer on the roof improves the stability. Figure 2-23 depicts the UDEC result output showing the vertical stress distribution between two coal seam workings (D2 and E2).

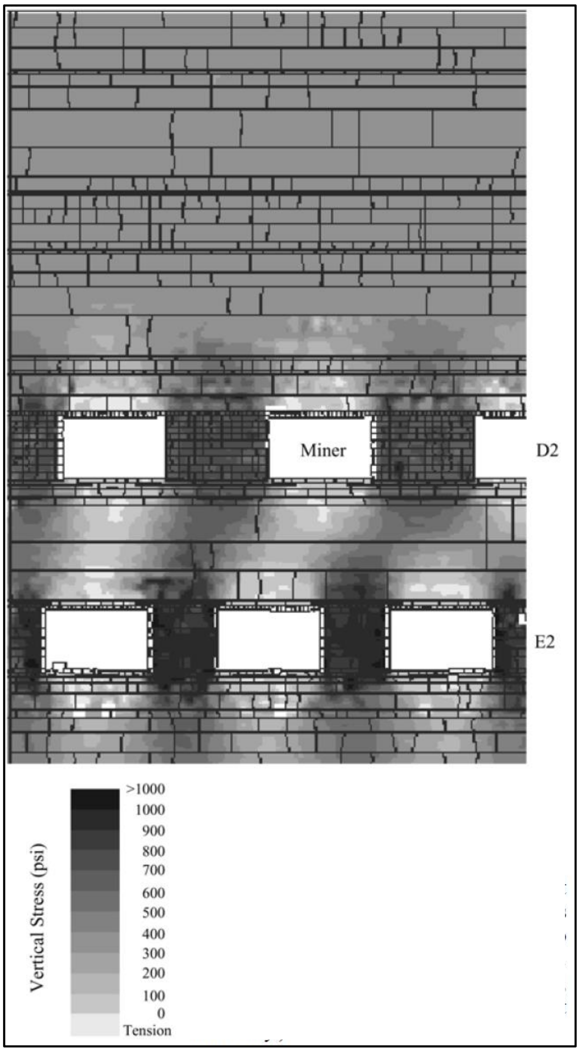

Figure 2-23: UDEC model vertical stress results for multiple seam workings (Vandergrift and Garcia, 2005)

Although the above mentioned case studies are mostly back analyses, it can be deduced that the web pillars that fail have undergone both shear and tensile failure, while it was observed that the roof and footwall undergo predominantly tensile failure. The importance of the pillar width to height ratio is also highlighted, as this determines the failure mechanism of these pillars. These need to be monitored closely during the modelling process in order to assess the pillar stability.

2.3. Chapter Summary

This chapter contains the relevant literature review that was conducted relating to the highwall mining layout design. A great deal of knowledge has been garnered and understanding of the rockmass behaviour derived over the decades of operating in countries such as the USA and Australia. This has attracted interest from other parts of the world where it is being adopted. A myriad of empirical pillar design equations were derived over the years. However, most of these were originally based on the data from the bord and pillar workings. Refinements are being made even to those that are directly related to the highwall mining conducted in various countries. This emphasizes the need to calibrate the empirical equations with the local conditions. Numerical modelling plays a pivotal role in the verification of the empirical techniques used in the design of the layouts. Various numerical codes are commercially available for this purpose, however, the choice of the code to be used must be in line with the conditions and geometric parameters for the results to be valid.

The hybrid design methodology, which is a combination of empirical techniques and numerical methods, will be adopted for this research project. The Mark-Bieniawski strength equation will be used for the empirical assessments with a coal strength of 4.3MPa as indicated for SA coalfields. Where required, the effective width concept $W_{eff} = 2w$ will be used to consider the possible impact of pillar length on the pillar strength. The results will then be verified by means of numerical modelling using UDEC. The choice of this modelling package is purely based on the time and availability.

Chapter 3

Numerical Modelling Assessment

3.1. Introduction

The numerical modelling assessment followed a well-defined process commencing with the derivation of modelling input parameters, through to model scenario construction to the analysis of the results. Numerical modelling was conducted using the UDEC modelling software. UDEC is a two-dimensional numerical program, which is based on the distinct element method for discontinuum modeling (Itasca Consulting Group, 2014). The area of interest is subdivided into smaller blocks whose boundaries represent both geological features and engineered structures in the model (Itasca Consulting Group, 2014). It has the ability to explicitly represent planes that subdivide the rock mass and represent failure using built-in industry accepted failure constitutive models. Individual blocks behave as either rigid or deformable materials that behave by some prescribed linear or non-linear stress/strain law. UDEC was used to determine the web and barrier pillar stress and behaviour at varying cover depths, panel widths and width-height ratios.

3.2. Model Input Parameters

3.2.1. Geological Sequence

In order to ensure that the assessment is in line with the actual conditions, the geological information of the project areas was derived from the geological borehole logs. A number of pre-existing geological borehole logs (Glencore Coal SA Southstock Geology department, 2012) were reviewed and relevant information extracted for analysis. A total of seven (7) pre-existing geological boreholes were analysed for the East Pit project area (Figure 3-1) and thirteen (13) geological borehole logs for the West Pit project area (Figure 3-2). Additional set of geological boreholes were drilled for the West pit project area since it was a new area, whilst for East pit the already existing boreholes were used together with the information that was collected during the initial underground mining.

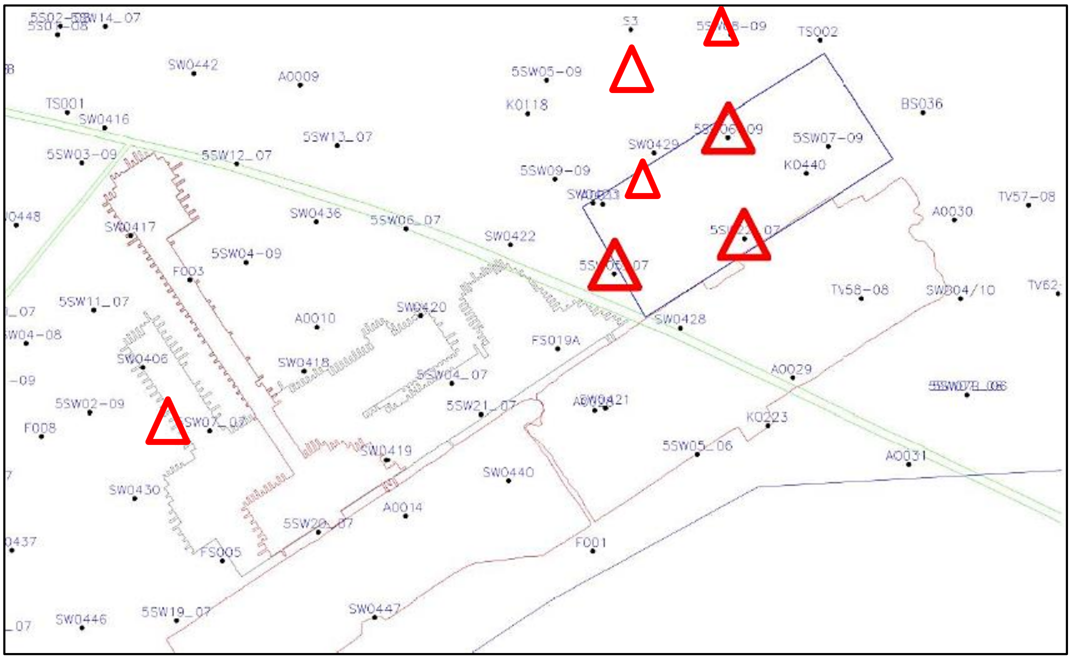

Figure 3-1: Location of the geological boreholes at the East Pit Project area (indicated by the red triangles) (Tweefontein Survey Department, 2010)

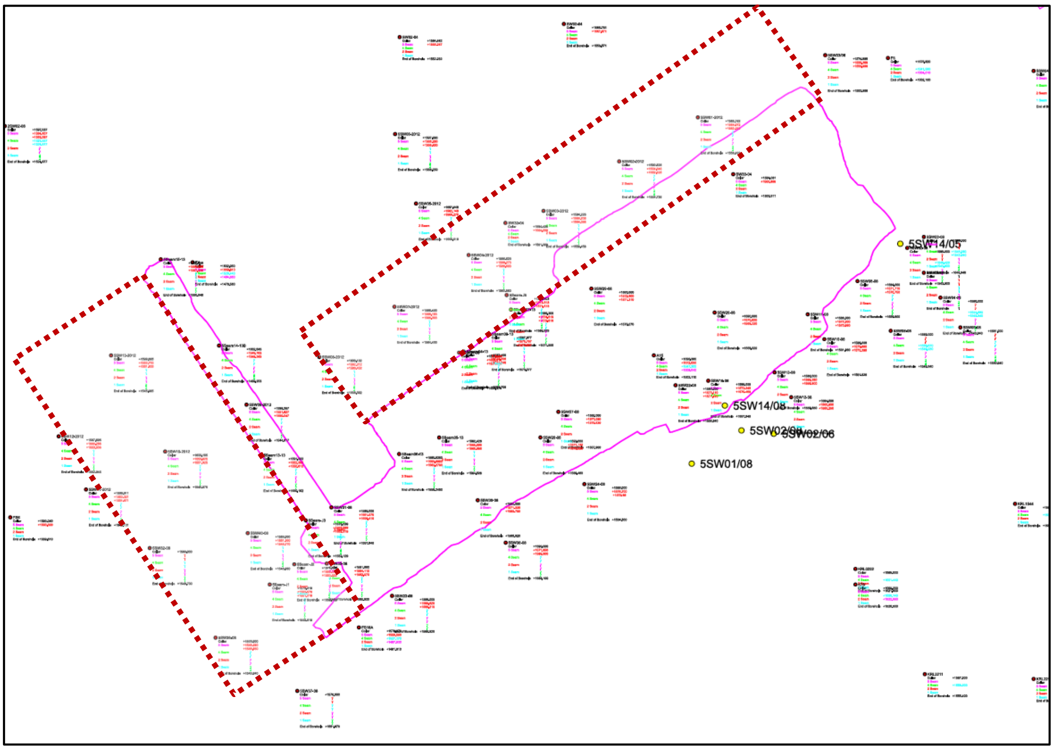

Figure 3-2: Location of the geological boreholes at the West pit Project area (indicated by small black dots) (Tweefontein Survey Department, 2010)

The general stratigraphy of the areas earmarked for highwall mining is depicted in Figure 3-3. The sequence generally comprises of a soil layer (SO), with alternating layers of sandstone (SST), siltstone (SLT) and inter-bedded siltstone and sandstone (ISS), with a moderately weathered sandstone (SSTW) appearing in some areas. The No. 5 coal seam thickness ranges from 1.44m to 1.88m for East Pit, with an average of 1.64m and ranges from 1.53m to 1.88m, with an average of 1.73m for West Pit. The immediate roof and floor vary between sandstone and siltstone/mudstone, but mainly comprises of siltstone/mudstone. The depth from surface to floor of the No. 5 coal seam ranges from 33.2m to 41.24m with an average of 37.10m for East Pit and ranges from 22.73m to 48.42m, with an average of 38.33m for West Pit.

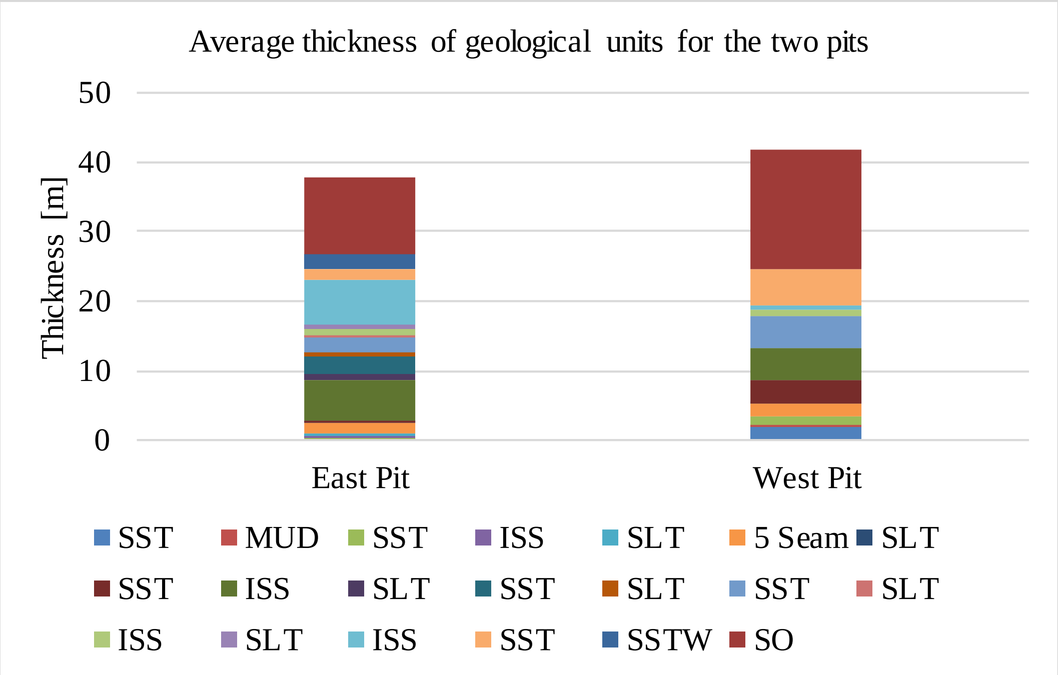

Figure 3-3: A representative geological sequence for the two pits earmarked for highwall mining

3.2.2. Rockmass Classification

The information pertaining to rockmass classification for this project was adopted from the existing database (Glencore Coal Geotechnical Database, 2012). The relevant information retrieved from the database is presented in Table 3-1 as obtained using various methods for comparison, for the various material zones. The main individual layers contained within each zone are described below, as:

- Seam 5 roof: Mudstone, sandstone and siltstone middling to the top weathered zone;
- Seam 5: Coal seam;
- Seam 4 roof: Siltstone, sandstone and siltstone middling to seam 5 footwall; and
- Seam 4: Coal seam.

Table 3-1: Summary of Rock mass classification for various zones (Glencore Coal Geotechnical Database, 2012)

Lithology	Parameter	GSI	RMR (Bieniaswki'89)	Adjusted RMR (Bieniaswki'89)	Q value
No.5 Coal Seam Roof	Average	51.8	58.65	55.32	32.13
	Minimum	34.8	41.81	36.81	0.01
	Maximum	72.4	70.29	67.01	122.21
	Standard deviation	11.3	9.94	9.57	37.16
No.5 Coal Seam	Average	45.4	53.26	50.29	29.27
	Minimum	26.8	36.81	34.81	0.01
	Maximum	64	70	63.83	131.22
	Standard deviation	12.7	10.81	9.95	36.3
No.4 Coal Seam roof	Average	53.3	61.65	58.53	43.73
	Minimum	32.7	39.7	29.7	0.62
	Maximum	74	79	74.27	240
	Standard deviation	8.71	8.66	9.05	57.24
No.4 Coal Seam	Average	46.5	56.06	53.04	21.78
	Minimum	30.8	41.03	39.03	0.03
	Maximum	72	77	72	118.05
	Standard deviation	8.51	8.71	8.31	27.63

The Geological Strength Index (GSI) is based upon an assessment of the lithology, structure and condition of discontinuity surfaces in the rock mass and it is estimated from visual examination of the rock mass exposed in surface excavations such as road cuts, in tunnel faces and in borehole core (Hoek, 2012). This was estimated using the chart by Marinos & Hoek (2000) during the core logging process. It was found to be ranging from 34.8 to 72.4 for the No.5 coal seam roof, with a standard deviation of 11.3 and a mean value of 51.8. For the No.5 coal seam itself, it was found to be ranging from 26.8 to 64, with a standard deviation of 13 and a mean value of 45.4.

The RMR classification system is a tool for characterising the rockmass by using the sum of the following six parameters which lies between 0 and 100 (Bieniawski, 1989):

- Uniaxial compressive strength of the rock material;
- Rock Quality Designation (RQD);
- Spacing of discontinuities;
- Condition of discontinuities;
- Groundwater conditions; and
- Orientation of discontinuities.

Alternatively, RMR can be derived from the value of GSI (Hoek & Brown, 1997) and Q-value (Bieniawski, 1979) using the equations 3-1 and 3-2, respectively.

$$RMR = GSI + 5 \qquad (3\text{-}1)$$

$$RMR = 9 \ln Q + 44 \qquad (3\text{-}2)$$

For the database used in this report, the RMR was obtained by summing up the abovementioned six parameters during the geotechnical logging process.

The average RMR of the roof zone and No. 5 coal seam is 58.7 and 53.3, respectively which classifies as a fair rock mass class for both zones. The standard deviation from these means was found to be 9.9 and 10.8, respectively. The roof zone has a minimum RMR of 41.8 (*Fair rockmass class*) and maximum of 70.3 (*Good rockmass class*) whilst the No. 5 coal seam has a minimum RMR of 36.8 (*Poor rockmass class*) and maximum of 70 (*Good rockmass class*).

The Q-System was derived by Barton, *et al.* (1974) for determination of rock mass characteristics and tunnel support requirements and has numerical values which vary on a logarithmic scale from 0.001 to a maximum of 1000 and is defined by equation 3-3.

$$Q = \frac{\mathrm{RQD}}{\mathrm{J_n}} \mathrm{x} \frac{\mathrm{J_r}}{\mathrm{J_a}} \mathrm{x} \frac{\mathrm{J_w}}{\mathrm{SRF}} \qquad (3\text{-}3)$$

Where: RQD = Rock Quality Designation,

J_n = Joint set number

J_r = Joint roughness number

J_a = Joint alteration number

J_w = Joint water reduction factor

SRF = Stress reduction factor

The No. 5 coal seam roof zone has an average Q-value of 32.13, with minimum and maximum values being 0.01 and 122, respectively. For the No. 5 coal seam, it ranges from 0.01 to 131.2 with an average of 29.3.

3.2.3. Laboratory Testing Results

Similar to the rockmass classification, the intact rock testing results were obtained from the Glencore Coal SA database. A suite of rock samples were selected from the drill core, using the International Society of Rock Mechanics (ISRM) guidelines for sample selection for different rock tests (Ulusay, 2015). Table 2-3 contains results of Uniaxial Compressive Strength (UCS), Uniaxial Compressive Strength with Moduli (UCM), and Triaxial Compressive Strength (TCS) for the different layers in the vicinity of the No.5 coal seam.

The UCS and TCS laboratory testing results of the No. 5 coal seam samples are presented in Figure 3-4. The UCS values are obtained along the compressive strength axis (Y-axis) at zero (0) confining stress. The average UCS is 26.4MPa with the minimum and maximum values of 14.05MPa and 60MPa, respectively. The TCS was conducted at six (6) confining stresses viz. 2.5MPa, 5.0MPa, 7.5MPa, 10MPa, 12.5MPa and 15MPa. The minimum and maximum TCS values within the dataset were found to be 52.4MPa and 139MPa, respectively.

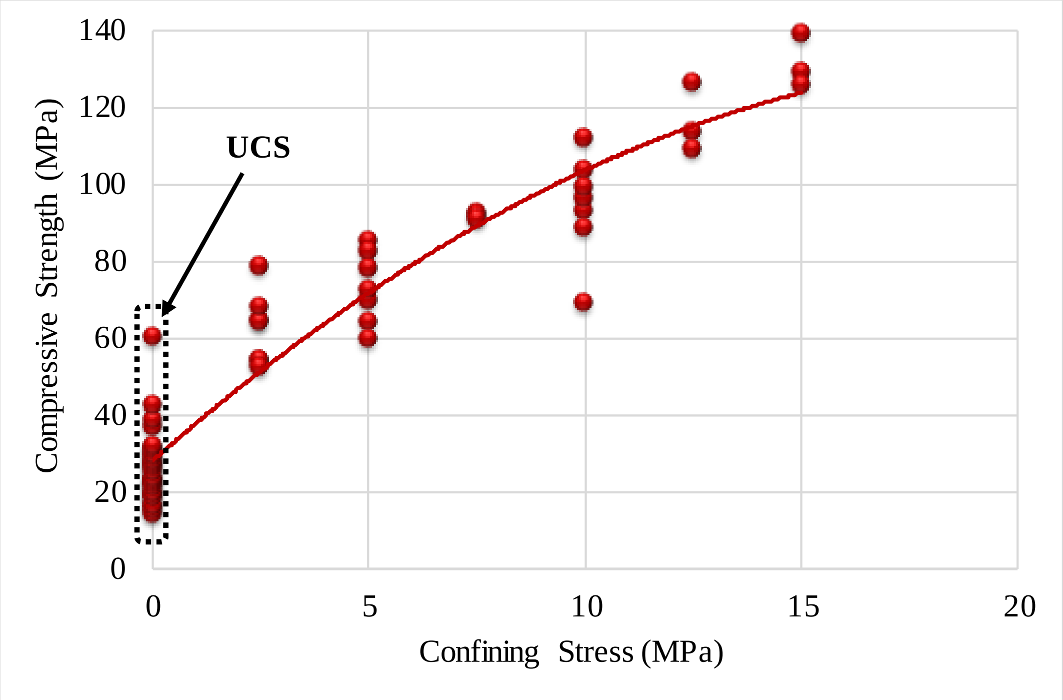

Figure 3-4: Laboratory tests results of No.5 coal seam at varying confinement stresses

3.2.4. UDEC Input Parameters

The relevant UDEC input rock and joint properties were derived from the *RocData* software program (Rocscience Inc., 2018). This was achieved by means of using the relevant laboratory rock tests and rockmass data obtained from the Rock Mass Classification, using a combination of Generalized Hoek-Brown criteria, Mohr-Coulomb and Barton-Bandis (Rocscience Inc., 2018). Equivalent rock properties derived as described above are presented in Table 3-2.

Table 3-2: Equivalent rock and joint properties as derived from the *RocData* software

Rock Type	Density (kg/m^3)	Poisson's ratio	Rock Mass Shear Modulus (GPa)	Rock Mass Bulk Modulus (GPa)	J_{kn} (GPa)	J_{ks} (GPa)	Cohesion (MPa)	Friction Angle (°)	Tensile Strength (MPa)
Sandstone	2480	0.3	2.04	4.42	4.64	3.44	5.32	36.89	0.078
Siltstone	2480	0.26	0.16	0.28	0.35	0.26	5.16	34.3	0.112
Shale	2480	0.19	0.50	0.65	0.68	0.55	2.97	25.28	0.264
Mudstone	2480	0.31	0.44	1.02	0.72	0.53	1.05	33.98	0.024
Coal 5 Seam	1500	0.3	1.15	2.50	3.89	2.88	0.80	24.54	0.039
Weathered Material	1880	0.2	0.01	0.01			0.05	36.89	0

* J_{kn} = *Joint normal stiffness* *J_{ks} = *Joint shear stiffness*

3.3. Model Geometry Construction

A base model was set up in UDEC to represent a simplified cross section of the main lithological units on the stratigraphy around the No.5 coal seam (Figure 3-5). The worst case scenario was modelled by including a weak siltstone and mudstone layer on the immediate roof and floor, respectively, in order to assess its full influence on the pillar and roof stability.

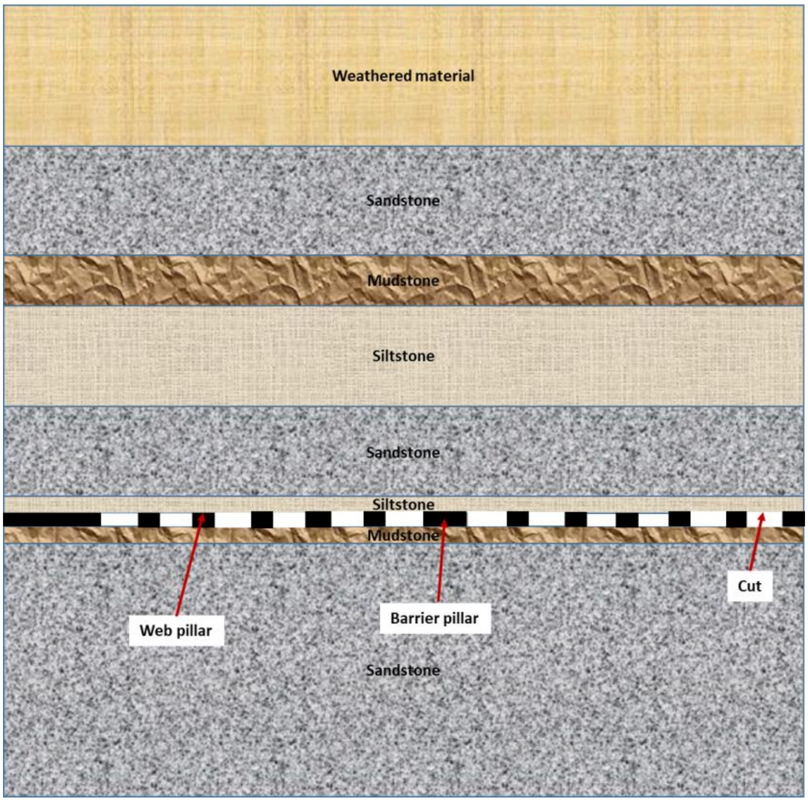

Figure 3-5: Simplified geological sequence and panel layout as modelled in UDEC modelling

The model comprised of varying web pillar dimensions, mining heights, panel widths and cover depths. The barrier pillar between the panels was kept constant at 4m, resulting in a minimum width to height ratio of 2. The cut width was also kept constant at 3.6m throughout the numerical modelling assessment. Additional information pertaining to the pillar dimensions and the corresponding panel widths (excluding barrier pillars) are presented in Table 3-3 together with the panel width (W) / cover depth (H) ratio. The panel width is dependent on the number of pillars per panel which is varied between 5, 7 and 9, as well as the pillar sizes.

Table 3-3: Pillar dimensions and corresponding panel dimensions

Pillar width [m]	Panel width (m) - Excluding barrier pillars		
	5 Pillars	7 Pillars	9 Pillars
0.8	26	34	43
1.2	28	37	47
1.6	30	40	50
2	32	43	54
W:H ratio			
30m Cover depth	0.87	1.13	1.43
	0.93	1.23	1.57
	1.00	1.33	1.67
	1.07	1.43	1.80
40m Cover depth	0.65	0.85	1.08
	0.70	0.93	1.18
	0.75	1.00	1.25
	0.80	1.08	1.35
50m Cover depth	0.52	0.68	0.86
	0.56	0.74	0.94
	0.60	0.80	1.00
	0.64	0.86	1.08

3.4. Model Boundary Conditions

A k-ratio of 2 (being the ratio of the horizontal to vertical stress) was applied in the model, and all vertical sides of the model simulated as symmetry lines. The upper boundary was simulated as a free surface and allowed to move in all the directions whilst the sides were fixed in the x-direction allowing them to move in the y-direction, with the bottom boundary fixed in both the directions. The Mohr Coulomb plasticity constitutive model in UDEC was then used in the analysis, using the input parameters described below. All the layers were modelled as deformable with the entire model meshed up. The fine mesh (0.3) was applied on the No.5 coal seam and coarser mesh (0.8) on the surrounding rockmass (Figure 3-6).

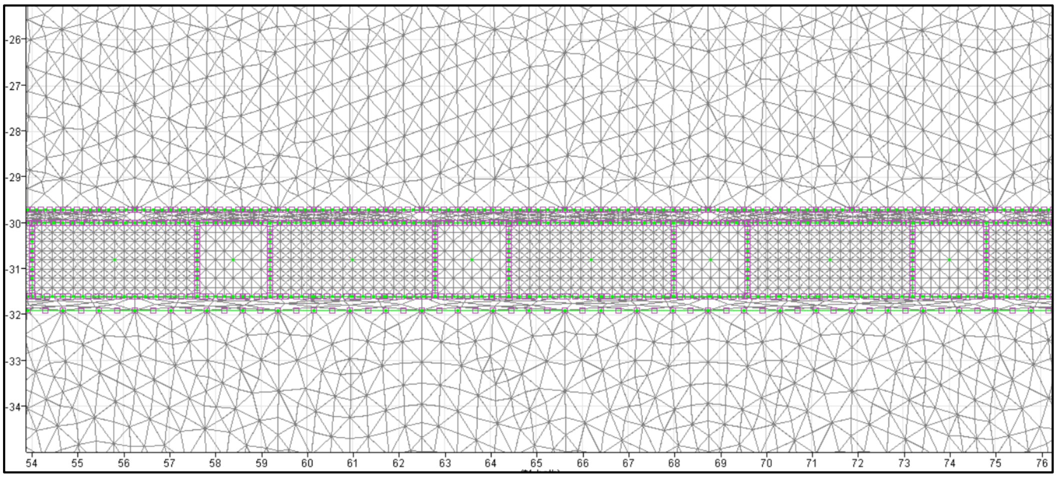

Figure 3-6: Mesh set-up on various zones of the UDEC model

3.5. Pillar Stress

The vertical stress distribution in the model was assessed as a check for the internal stress consistency and to ensure that the model reaches equilibrium prior to any simulation of the coal mining extraction (Figure 3-7). The modelled vertical virgin stresses were found to be in agreement with the theoretical value of vertical *in situ* stress (calculated as 0.023 x cover depth, MPa/m) levels expected based on the depth, density and gravitational acceleration values assigned in the models. The pre-mining vertical stresses were found to be 0.68MPa at a 30m cover depth, 0.916MPa at a 40m cover depth and 1.14MPa at a 50m cover depth.

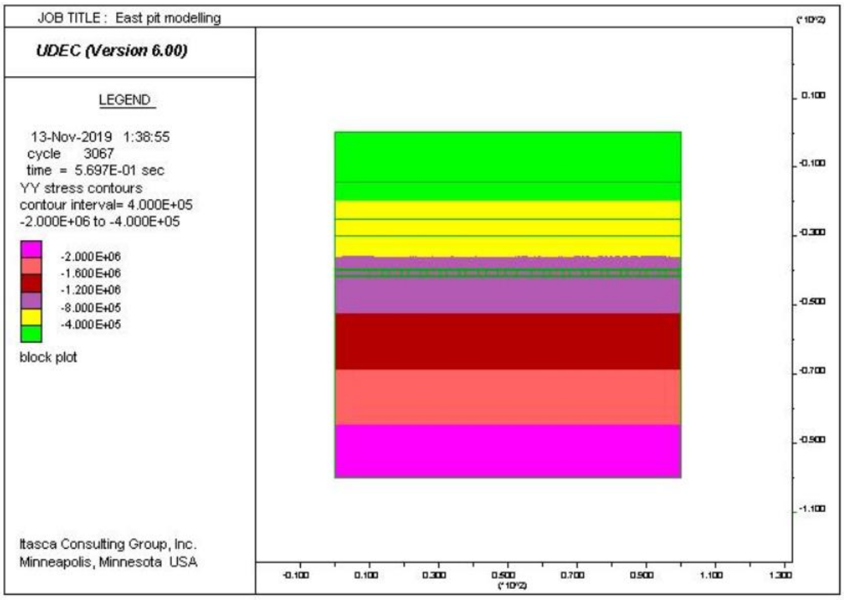

Figure 3-7: A schematic showing the pre-mining vertical stress contours in the UDEC model

Once the pre-mining vertical stress has been assessed and validated for consistency, the roadways were excavated in order for the model to reach a new state of equilibrium. The centre web pillar within the panel was used to monitor the vertical stresses as the parameters were varied. This is assumed to represent a reasonable pillar stress distribution due to its location away from the influence of any boundary conditions. History plots were generated on the pillar centre line and average pillar stress determined as an average of the zones along this line. This was repeated for a combination of web pillar widths, mining heights and cover depths. The panel width was then increased in order to assess the influence of this on the pillar stress. The peak vertical stresses on the centre pillar for a combination of mining geometries are presented in Table 3-4.

Table 3-4: Web pillar stress for varying pillar and panel dimensions

Mining height [m]	Pillar width [m]	No. of cuts per panel	6 Cuts			8 Cuts			10 Cuts		
		Cover depth [m]	30m	40m	50m	30m	40m	50m	30m	40m	50m
		w/h	Pillar vertical peak stress [MPa]								
1.2	0.8	0.7	2.6	3.2	3.8	3.1	3.5	3.9	3.4	3.6	4.0
	1.2	1.0	2.3	3.0	3.9	2.5	3.2	4.4	2.7	3.4	4.6
	1.6	1.3	2.0	2.5	3.3	2.2	2.7	3.6	2.3	2.8	3.8
	2.0	1.7	1.8	2.3	3.1	2.0	2.5	3.1	2.1	2.5	3.3
1.4	0.8	0.6	2.6	2.9	3.3	2.9	3.2	3.6	3.0	3.4	3.5
	1.2	0.9	2.2	2.9	3.6	2.5	3.1	4.0	2.7	3.3	4.1
	1.6	1.1	2.0	2.5	3.4	2.1	2.7	3.9	2.3	2.8	4.2
	2.0	1.4	1.8	2.4	3.1	2.0	2.5	3.2	2.1	2.6	3.4
1.6	0.8	0.5	2.5	2.6	2.5	2.6	2.6	2.6	2.5	2.7	2.5
	1.2	0.8	2.1	2.7	3.4	2.4	3.0	3.6	2.6	3.1	3.8
	1.6	1.0	2.0	2.5	3.5	2.1	2.6	3.8	2.3	2.8	4.1
	2.0	1.3	1.8	2.3	3.0	2.0	2.5	3.2	2.1	2.6	3.3
1.8	0.8	0.4	2.5	2.5	2.5	2.5	2.5	2.6	2.2	2.5	2.5
	1.2	0.7	2.1	2.6	3.3	2.4	2.9	3.4	2.5	3.0	3.6
	1.6	0.9	1.9	2.4	3.4	2.1	2.6	3.6	2.2	2.7	3.9
	2.0	1.1	1.8	2.3	3.0	2.0	2.5	3.2	2.0	2.5	3.3
2.0	0.8	0.4	2.5	2.5	2.6	2.5	2.5	2.6	2.2	2.5	2.6
	1.2	0.6	2.0	2.6	3.1	2.4	2.8	3.3	2.5	2.9	3.5
	1.6	0.8	1.9	2.4	3.2	2.1	2.6	3.5	2.2	2.7	3.7
	2.0	1.0	1.8	2.2	2.9	1.9	2.4	3.1	2.0	2.5	3.3

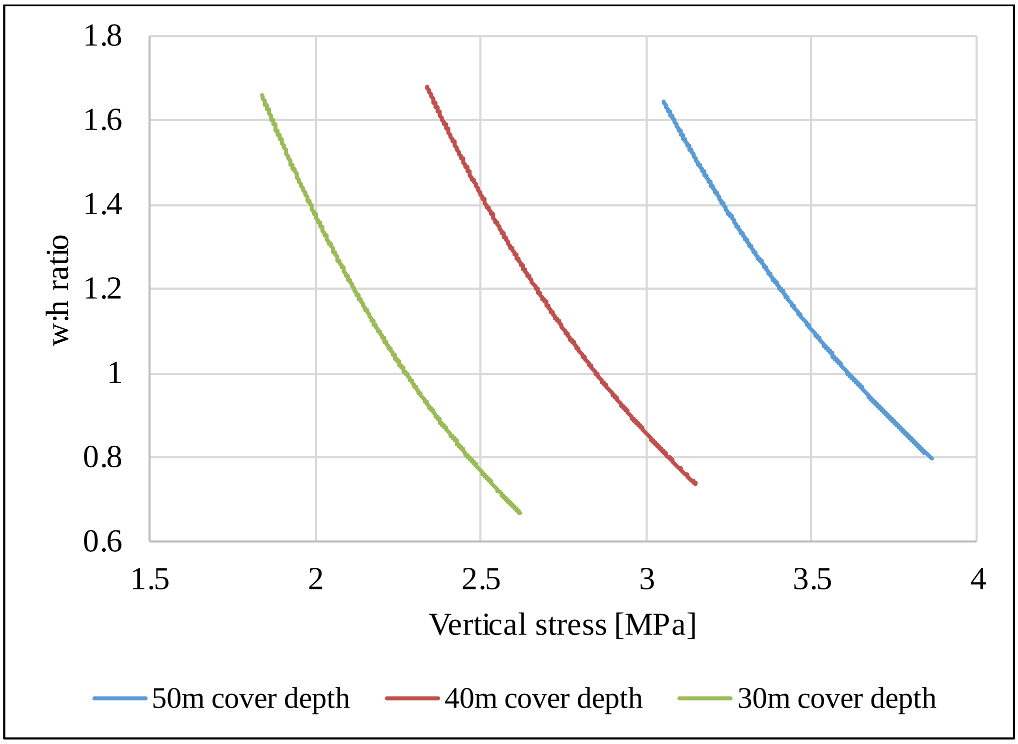

Figure 3-8: Pillar stress for varying width to height ratio and cover depth

Figure 3-8 indicates that for a constant mining height and panel width, the pillar stress decreases with an increase in pillar width to height ratio. Furthermore, pillar stress increases with an increase in cover depth. Further, from the pillar stress values in Table 3-4, it can be observed that pillar stresses also increase with an increase in panel width.

3.6. Pillar Strength

The web pillar strength was determined from Mark-Bieniawski empirical formula presented in equation 3-4 (Mark, 1999),

$$\sigma = S_I[0.64+0.54\left(\frac{w}{h}\right)] \qquad (3\text{-}4)$$

Where: S_I = In situ coal strength (4.3MPa)

w = Pillar width (m)

h = Mining height (m)

The strength was assessed for a combination of mining heights and pillar widths, which will be later compared to the pillar stress from the numerical modelling analysis. The calculated pillar strengths are shown in Table 3-5 for various dimensions including varying w/h ratios. Linear increase in web pillar strength with an increase in w/h ratio is evident from this data, in line with the strength formula utilized.

Table 3-5: Empirically determined web pillar strengths for a combination of pillar widths and mining heights

Mining height [m]	Pillar width [m]	w/h	Pillar Strength [MPa]
1.2	0.8	0.67	4.3
	1.2	1.00	5.1
	1.6	1.33	5.8
	2	1.67	6.6
1.4	0.8	0.57	4.1
	1.2	0.86	4.7
	1.6	1.14	5.4
	2	1.43	6.1
1.6	0.8	0.50	3.9
	1.2	0.75	4.5
	1.6	1.00	5.1
	2	1.25	5.7
1.8	0.8	0.44	3.8
	1.2	0.67	4.3
	1.6	0.89	4.8
	2	1.11	5.3
2	0.8	0.40	3.7
	1.2	0.60	4.1
	1.6	0.80	4.6
	2	1.00	5.1

3.7. Pillar Safety Factor

As a form of pillar stability assessment, the pillar safety factor was determined as a ratio of the empirically derived pillar strength (Table 3-5) and pillar stresses (Table 3-4). The range of safety factors obtained for a range of mining geometries will be plotted and compared with the threshold safety factor. The threshold safety factor was adopted from ARMPS-HWM minimum safety factor guidelines (Mark, 2006) which is 1.3 for web pillars and 2.0 for barrier pillar, for a panel width of less than 60m. The final panel layout (pillar size, spacing and panel width) is based on this threshold.

3.8. UDEC model output

The pillar behaviour will be assessed from the stress distribution for plasticity (yielding) zone, in order to establish potential failure zones based on the concept presented in Figure 3-9. It indicates (a) higher stresses on the edges and lower stress level on the core of the pillar for a relatively large pillar and (b) failure of edges thereby transferring stress on the core of the pillar. The presence of high compressive stresses on the pillars results in yielding on the pillar edges. With further increase in compressive stress, the yield zones extend into the core of the pillar, particularly in relatively smaller pillars. The pillar loses its load carrying capability once the yield zones intersect. As long as the core of the pillar maintains its elasticity, the pillar will remain stable (Porathur, *et al.*, 2017).

In an inelastic modelling code, yielding is characterized by a drop in stress level, which is then transferred into elastic core and the abutments. This will be monitored from the pillar stress distribution from the UDEC output files. The tensile failure and shear failure zones will also be monitored on the web pillars, roof and footwall, in order to ascertain the potential failure mechanism.

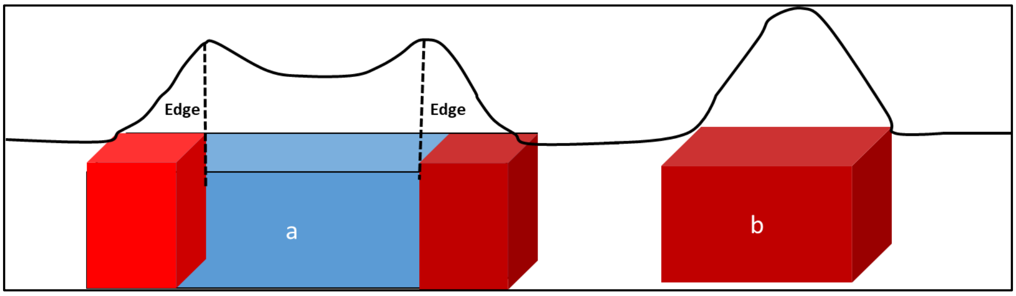

Figure 3-9: Conceptual stress profile showing yielding (red) and elastic (blue) zones across (a) larger and b) smaller pillar

3.9. Chapter Summary

This chapter provided an overview on the numerical modelling assessment as applied in this project. UDEC and its applicability was introduced as a numerical modelling code. The modelling input parameters were explained as sourced from the Glencore Coal SA geotechnical database of rockmass classification and characterization. The modelled geometrical parameters and their combinations i.e. web pillar sizes, panel widths and cover depth were also presented as described in conjunction with the representative geological sequence around the No.5 coal seam. In order to ensure consistency in stress distribution, vertical stress before mining was assessed from which changes were monitored after excavations have been created. The use of pillar stress and empirically derived pillar strength to determine the pillar safety factor was also explained and the preferred threshold indicated. In addition, the model output interpretation approach was outlined which will focus on the identification of potential yielding zones and their extent.

Chapter 4

Results and Discussion

4.1. Introduction

This chapter presents the results of the analyses conducted as described in Chapter 3. The following aspects of pillar stability assessment will be presented and analysed:

- Pillar safety factor
- Stress distribution and yielding zones

The results are presented in separate sections and sub-sections below and will be summarised at the end of the chapter.

4.2. Pillar Safety Factor

Pillar safety factor was determined as a ratio of the empirically derived pillar strength and pillar stress obtained from UDEC simulations. The pillar safety factor was calculated for various combinations of cover depths, mining heights and panel widths. As a result, each pillar size produced a number of safety factors for each of these variables. For the ease of plotting and interpretation of the results, the minimum pillar safety factor was chosen and plotted for each pillar size at varying cover depths and panel widths. This implies that the only mining height or width/height (w/h) ratio considered is the one that produces the lowest safety factor instead of plotting all five (mining heights). The web pillar safety factors assessment results are presented and described in the following sections for various pillar sizes and are plotted together with the threshold safety factor line (green horizontal line).

4.2.1. 0.8m Web Pillar

The safety factor for a 0.8m wide web pillar for varying cover depths and panel width is indicated in Figure 4-1. A general decrease in safety factor with an increase in cover depth and panel width is observed. As the cover depth increases beyond 45m, the difference in pillar safety factor decreases between 34m and 43m panel widths. At the panel width of 26m, the maximum pillar safety factor is 1.5 at cover depth of 30m and decreases to 1.11 at 50m cover depth. With an increase in panel width to 34m, the safety factor decreases to 1.4 and 1.1, respectively and further decreases to 1.21 and 1.07 at 43m panel width.

The cover depth at which the threshold safety factor is attained decreases with an increase in panel width. At 26m panel width the threshold safety factor is attained at the cover depth of 41.5m. With an increase in panel width to 34m, the threshold safety factor is achieved at the cover depth of 36m while for the panel width of 43m, the safety factor is below the threshold across all the cover depths.

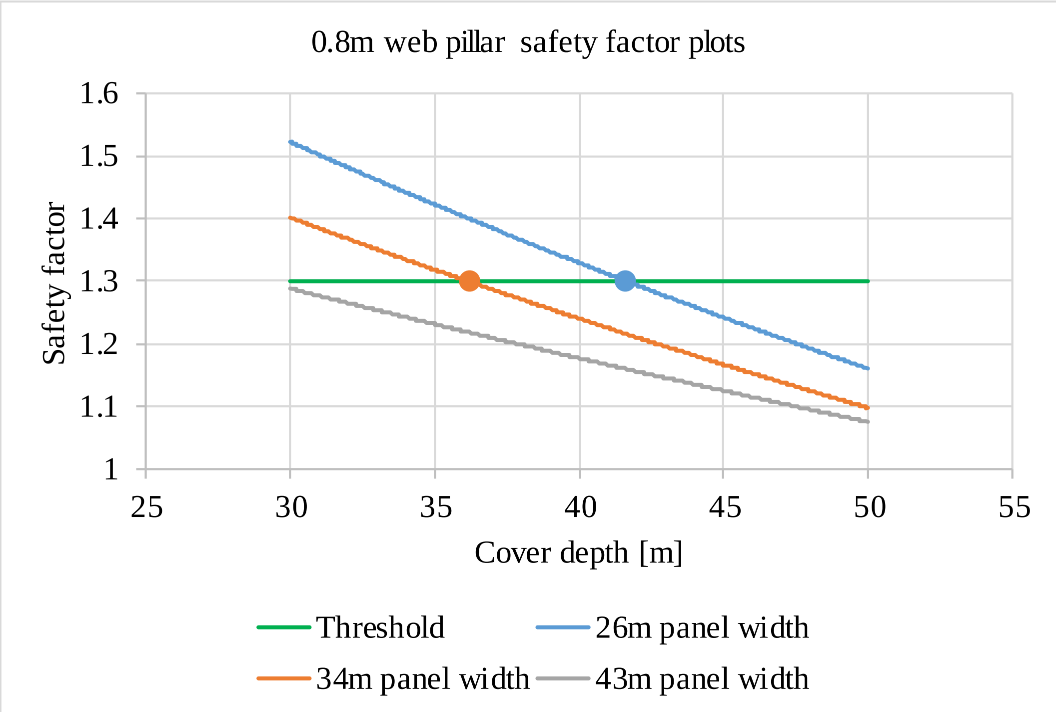

Figure 4-1: Minimum safety factor for a 0.8m web pillar at varying depths and panel widths

4.2.2. 1.2m Web Pillar

Figure 4-2 depicts the safety factor for a 1.2m wide web pillar at varying cover depths and panel widths. At the panel width of 28m and cover depth of 30m, the pillar safety factor is 2.06, which decreases to 1.31 at the maximum cover depth of 50m. At the panel width of 37m, the above safety factors decrease to 1.75 and 1.15, respectively while at the panel width of 47m the safety factors further decrease to 1.21 and 1.07.

The cover depth at which the threshold safety factor is attained decreases with an increase in panel width. At the panel width of 28m, the threshold safety factor is attained at 50m cover depth. With an increase in panel width to 37m, the cover depth corresponding with the threshold safety factor decreases to 45m and further decreases to 43m with an increase in panel width to 47m.

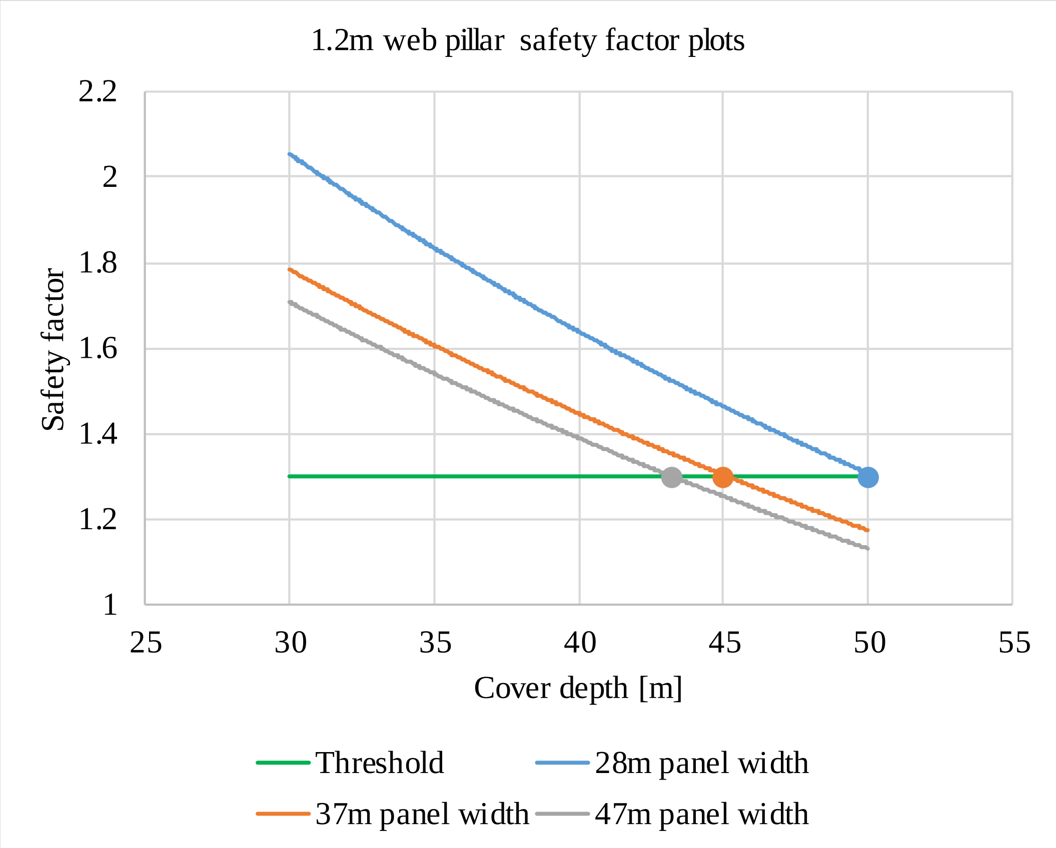

Figure 4-2: Minimum safety factor for a 1.2m wide web pillar at varying depths and panel widths

4.2.3. 1.6m Web Pillar

At a panel width of 30m and cover depth of 30m, a 1.6m web pillar has a safety factor of 2.44. This decreases to 1.43 with an increase in cover depth to 50m (Figure 4-3). With an increase in panel width to 40m, the safety factor decreases to 2.20 at the cover depth of 30m and 1.34 at the cover depth of 50m. With a further increase in panel width to 50m, the above safety factor further decreases to 2.10 and 1.25, respectively. The safety factors are well above the threshold value for the panel width of 30m and 40m. At panel width of 50m, the threshold safety factor is achieved at a 49m cover depth.

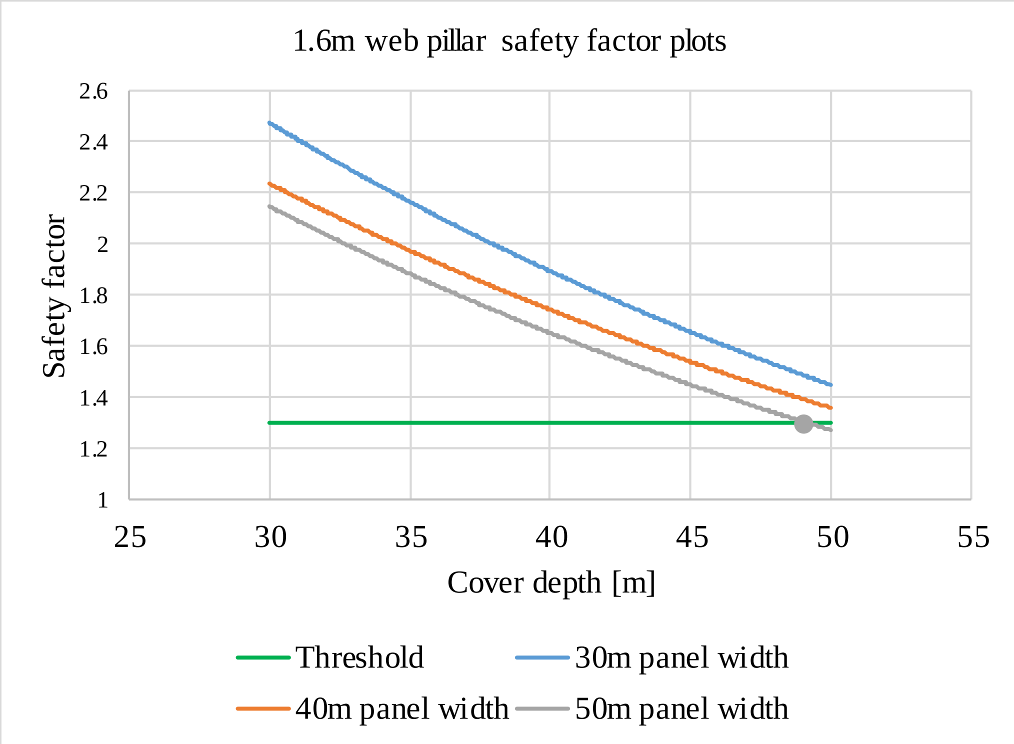

Figure 4-3: Minimum safety factor for a 1.6m wide web pillar at varying depths and panel widths

4.2.4. 2m Web Pillar

A 2m wide web pillar has a safety factor of 2.88 at the cover depth of 30m and panel width of 32m. This safety factor decreases to 1.73 as the cover depth increases to 50m at a constant panel width of 32m (Figure 4-4). With an increase in panel width to 43m, the safety factor decreases to 2.61 at 30m cover depth and 1.61 at 50m cover depth. At the panel width of 54m, the above safety factors further decreases to 2.53 and 1.55, respectively. The pillar safety factors are well above the threshold line across all the panel width and cover depths.

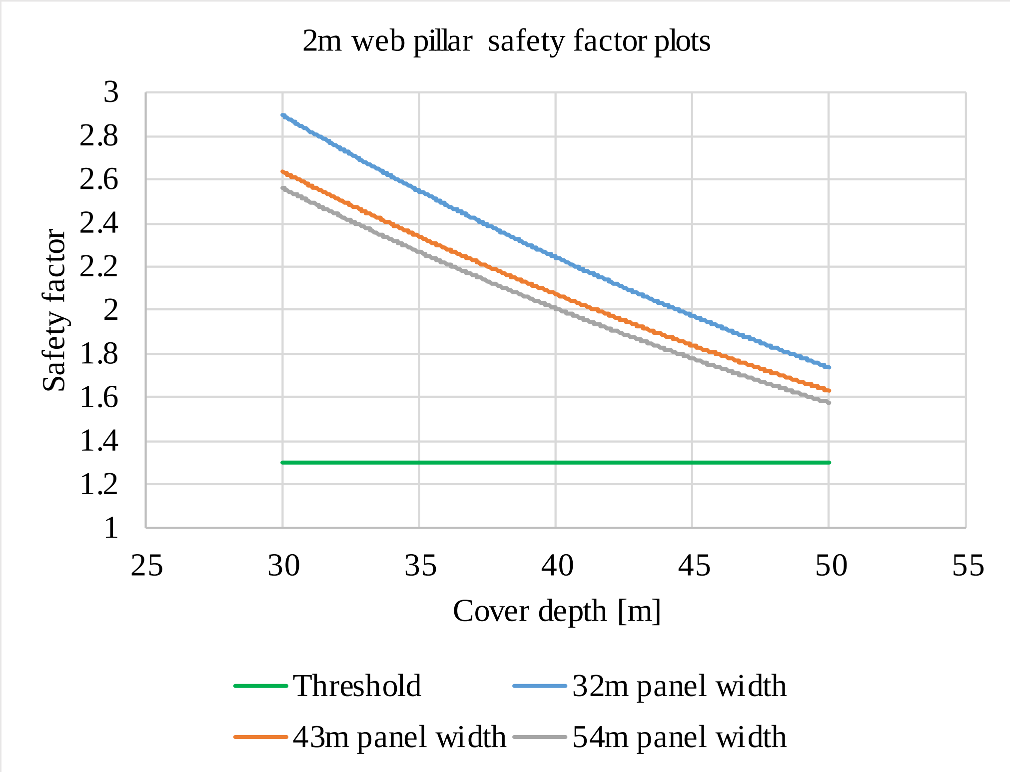

Figure 4-4: Minimum safety factor for a 2m wide web pillar at varying depths and cuts per panel

4.2.5. Summary

The above pillar stability assessment was conducted using a safety factor threshold of 1.3. It was observed that a 0.8m web pillar safety factor is above the threshold value with the panel widths of 34m and 43m. These intersect with the threshold value at cover depths of 36m and 41.5m, respectively. A 1.2m web pillar attains the threshold safety factor at the cover depths of 45m and 43m, which correspond with 37m and 47m panel widths, respectively. At the panel width of 28m, a 1.2m web pillar safety factor is above the threshold safety factor across all the cover depths. Increasing the web pillar size to 1.6m results in a threshold safety factor being attained across all the panel widths up to the cover depth of 40m. A 2m web pillar safety factor is higher than the threshold value for all the cover depths and panel widths. Based on the above safety factor assessment, the web pillar width at which the threshold safety factor of 1.3 is attained is 1.2m. This is achieved at a panel width of 28m (6 cuts / 5 pillars per panel) up to the maximum cover depth of 50m, which correspond with the cover depth obtained from the geological information.

4.3. UDEC Output Simulation Results

In order to assess the potential instability or stability of the pillars, the stress distribution was monitored for various widths, cover depths and w/h ratios. This was conducted for the identification of yielding zones and their extent within a pillar, paying particular attention to tensile failure, shear failure or a combination of both. In UDEC, compressive stresses are indicated by negative values whilst positive values indicate tension (Itasca Consulting Group, 2014). The findings will be discussed below for each web pillar size and a combination of other variables.

4.3.1. 0.8m Web Pillar Width

The pillar stress monitoring was carried out for varying geometrical parameters relating to the cover depth, w/h ratio and panel widths. Various modelling results and the analysis thereof are presented under varying panel widths in the sections that follow.

a. 26m Panel Width

A 26m wide panel comprises of six (6) excavations and five (5) web pillars and is measured between barrier pillars. The UDEC model outputs for a 26m panel width are presented in Figures 4-5 to 4-8 for varying w/h ratios and cover depths. These are graphically represented in Figure 4-9 to cover all the w/h ratios covered in this project.

Figure 4-5 depicts the distribution of stress contours within web pillars at various w/h ratios and a 30m depth of cover. The results of three (3) values of w/h ratios which represent minimum, maximum and median values at a 30m cover depth are presented in this analysis. The stress on the web pillar ranges from 2MPa to 3MPa based on the location within the pillar. The sidewalls generally experience lower stresses (up to 2MPa) compared to the core of the pillar (up to 3MPa). At the minimum w/h ratio of 0.4, the low stress zone (red contour) extends deeper into the pillar and covers a significant portion of the web pillar. However, the high stress contour is still visible on the corners and the core of the pillar. This demonstrates the ability of these parts of the pillar to retain and sustain the increased stress. Where the stress exceeds the pillar strength, it is expected that web pillars with w/h ratio less than 0.5, will fail in tension / splitting whilst those beyond this will fail in shear.

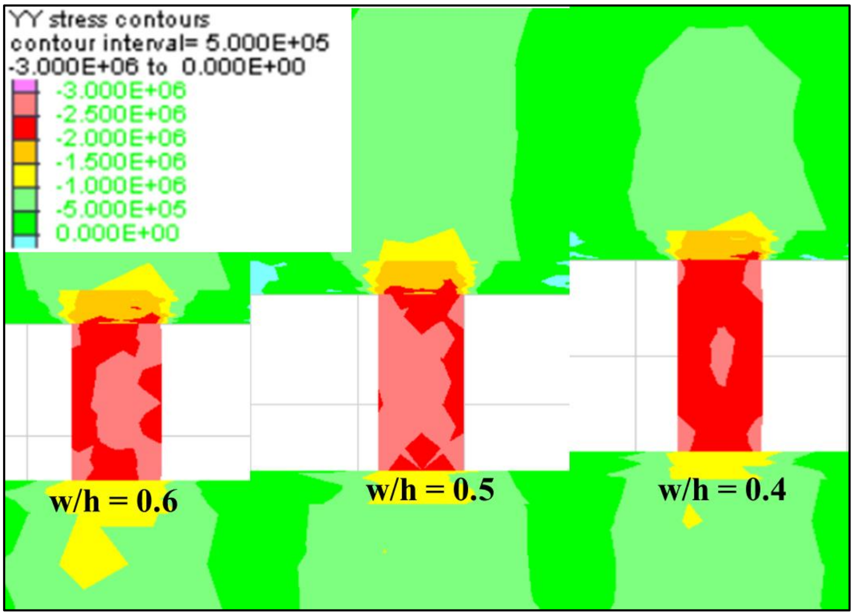

Figure 4-5: Progression of stress distribution for decreasing w/h ratio at 30m cover depth

The progression of stress distribution at a cover depth of 40m is depicted in Figure 4-6 for varying w/h ratios. A similar trend for a 30m depth is observed, with the slightly higher stress magnitude. However, at the w/h ratio of 0.4, the yield zone covers the entire pillar width with the corners sustaining higher stresses. This is possibly due to the confinement at the contacts with the surrounding roof and floor.

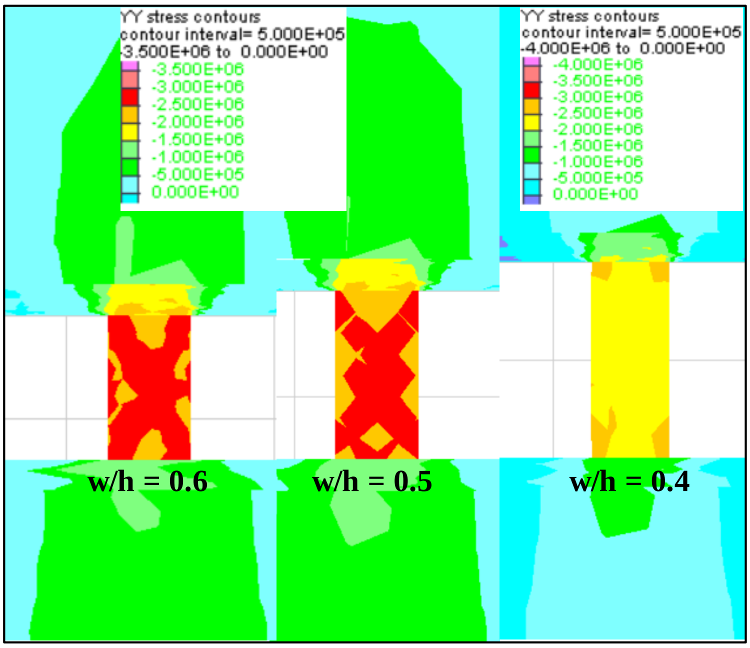

Figure 4-6: Progression of stress distribution for decreasing w/h ratio at a 40m cover depth

The stress at a cover depth of 50m remains constant across the web pillar in comparison with that observed at the cover depth of 40m throughout the various w/h ratios. This is indicated in Figure 4-7 (a) which demonstrates this phenomenon at the w/h ratio of 0.6 and was observed to be the same in other w/h ratios. Although the web pillar stress is constant, Figure 4-7 (b) indicates the stress increase on the barrier pillar up to 5MPa in places.

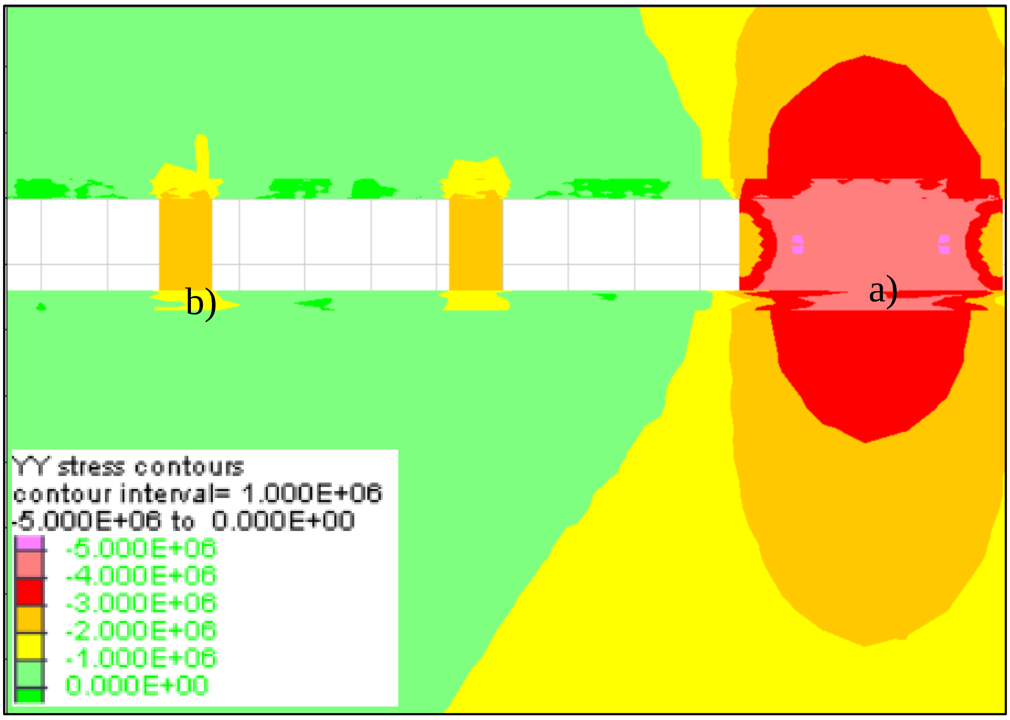

Figure 4-7: Vertical stress on (a) web pillars and (b) barrier pillar for a w/h ratio of 0.6 at a 50m cover depth

The above increase in stress on the barrier pillar results in the development of yield zone into the barrier pillar sides measured to be 0.7m, 0.9m and 1.07m for w/h ratios of 0.6, 0.5 and 0.4, respectively (Figure 4-8). Despite this extended yield zone into the barrier sides, the barrier pillar still possesses a significant elastic zone.

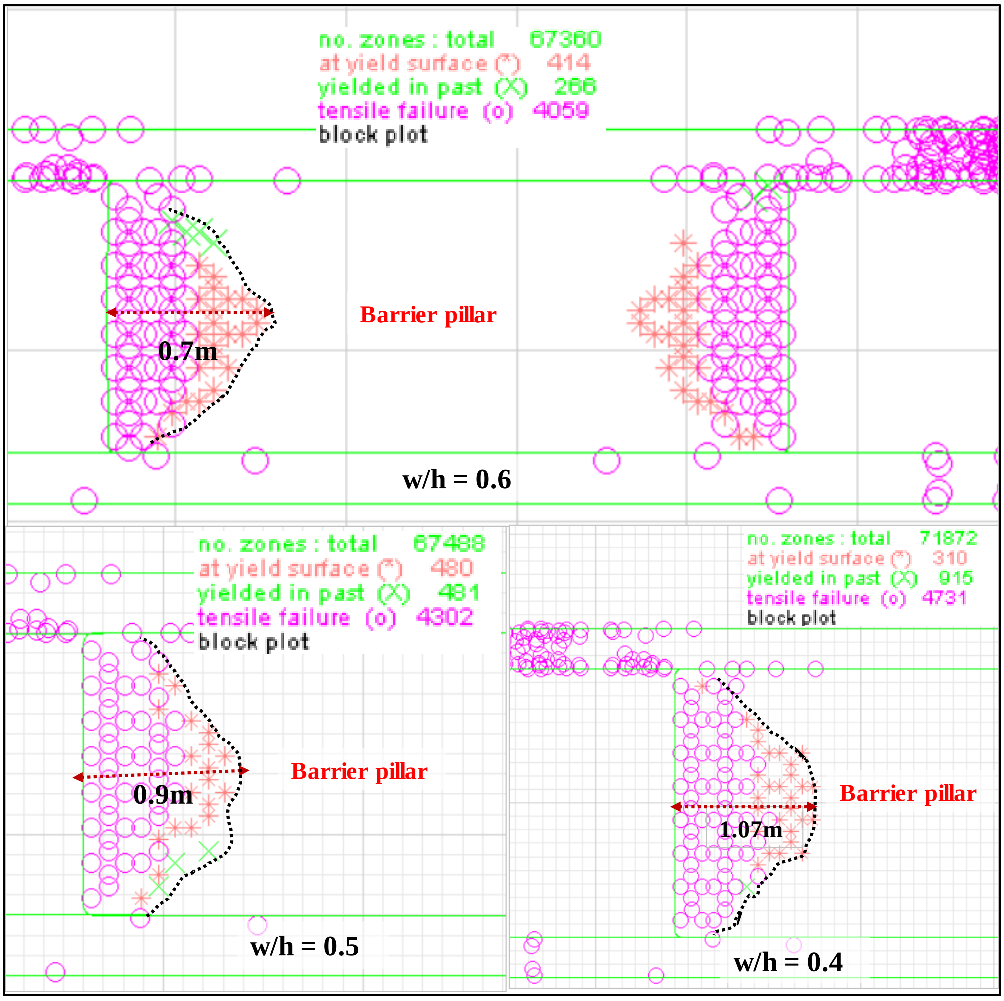

Figure 4-8: Progression of the yield zone on the barrier pillar side for a 50m cover depth and varying w/h ratio

Figure 4-9 depicts the general behaviour of web pillars in a 26m wide panel width, for varying w/h ratios and cover depths. The graphs indicate a general approximation of an "S" shape, with a linear portion corresponding with low w/h ratio between 0.4 and 0.5. The change in behaviour is observed at the w/h ratio of 0.5, wherein the pillar stress increases with an increase in w/h ratio. This behaviour becomes clearer with an increase in cover depth from 30m to 50m. This indicates that the potential failure mechanism below the w/h ratio 0.5 is tensile / splitting. Beyond the w/h ratio of 0.5, the web pillar seem to develop confinement, which changes the failure mechanism to shear.

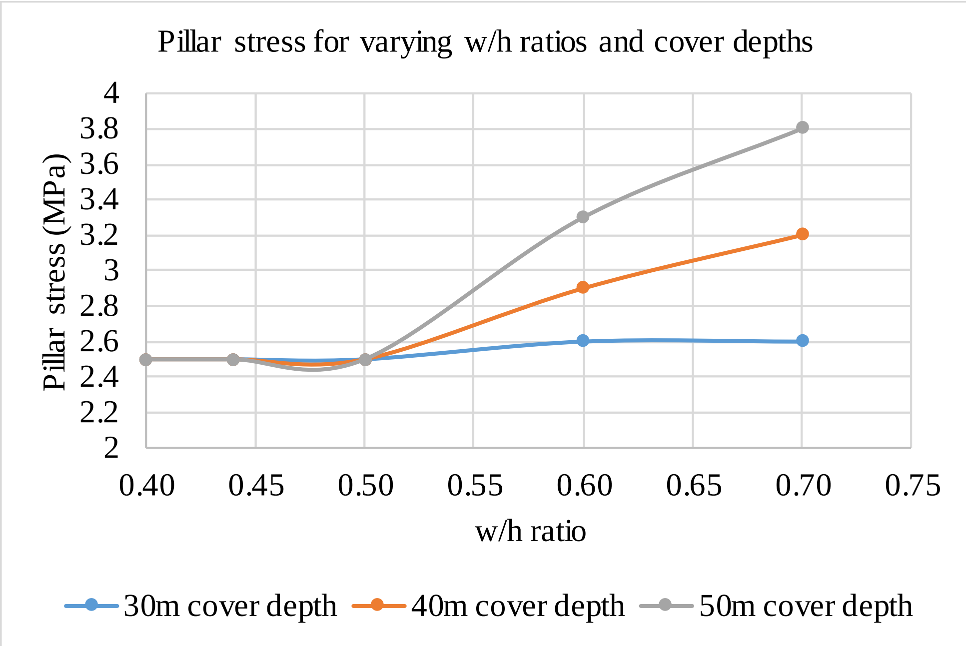

Figure 4-9: Pillar stress for varying w/h ratios and cover depths for a 26m wide panel width

b. 34m Width Panel

A 34m wide panel comprises of eight (8) 3.6m wide excavations and seven (7) 0.8m wide web pillars. The progression of vertical stress distribution on the web pillars for various w/h ratios at a 30m cover depth is presented in Figure 4-10. Although the general trends are similar to those observed in the preceding discussion, graphical representation of pillar stress and w/h ratio (Figure 4-12) indicates that the change in pillar stress behaviour is observed at a w/h ratio of 0.4. However, the pillar corners retain some stresses whilst the rest exhibit potential shear failure.

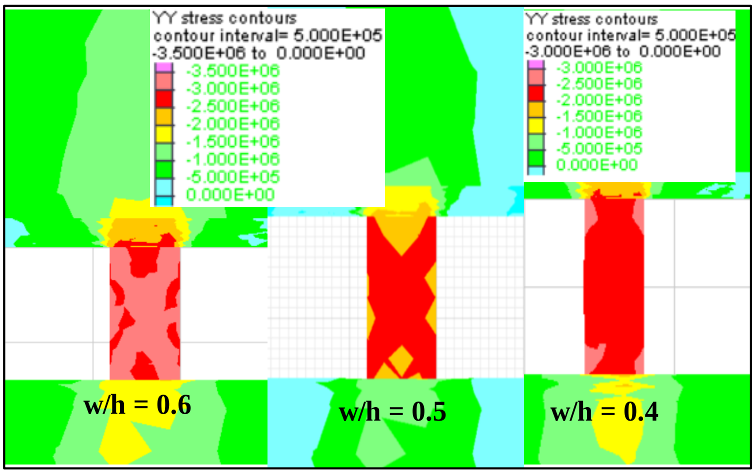

Figure 4-10: Progression of stress distribution for varying w/h ratio at a 30m cover depth

Figure 4-11 depicts vertical pillar stress progression for a cover depth of 40m across varying width to height ratios. At the w/h ratio of 0.4, the pillar behaviour is similar to that observed in a 28m panel width, where stress is higher at the pillar corners than on the core. However, this maximum stress at the corners reduces to between 2.5MPa and 3MPa as compared to 3.0MPa and 3.5MPa observed in a panel width of 28m. This drop in maximum stress is attributed to further yielding as a result of an increased cover depth. At the w/h ratio of 0.5, the maximum stress zone develops through the core of the pillar, which increases the probability of pillar splitting when the stress exceeds the pillar strength.

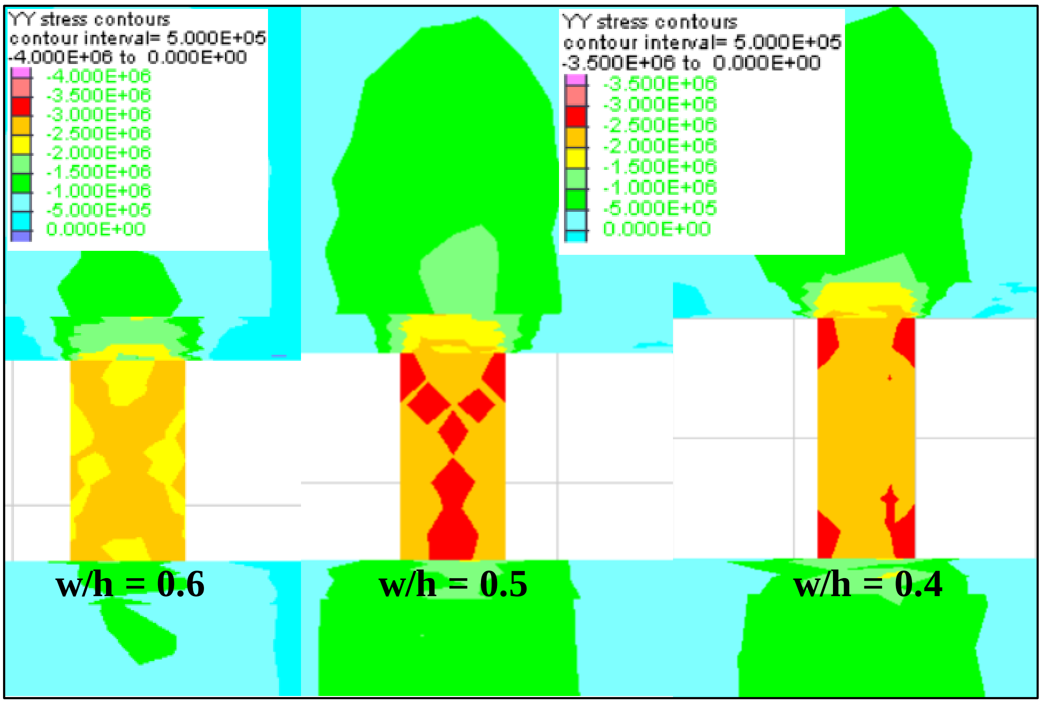

Figure 4-11: Progression of stress distribution for decreasing w/h ratio at a 40m cover depth

Figure 4-12 summarizes the general behaviour of web pillars with various w/h ratios and cover depths at a constant panel width of 34m. Despite the general increase in pillar stresses, the behaviour of web pillars is akin to that observed in panel width of 26m, with the change in behaviour at the w/h ratio of 0.5. Similarly, the potential failure mechanism comprises of tensile/splitting and shear at w/h ratio of 0.5 and beyond, respectively.

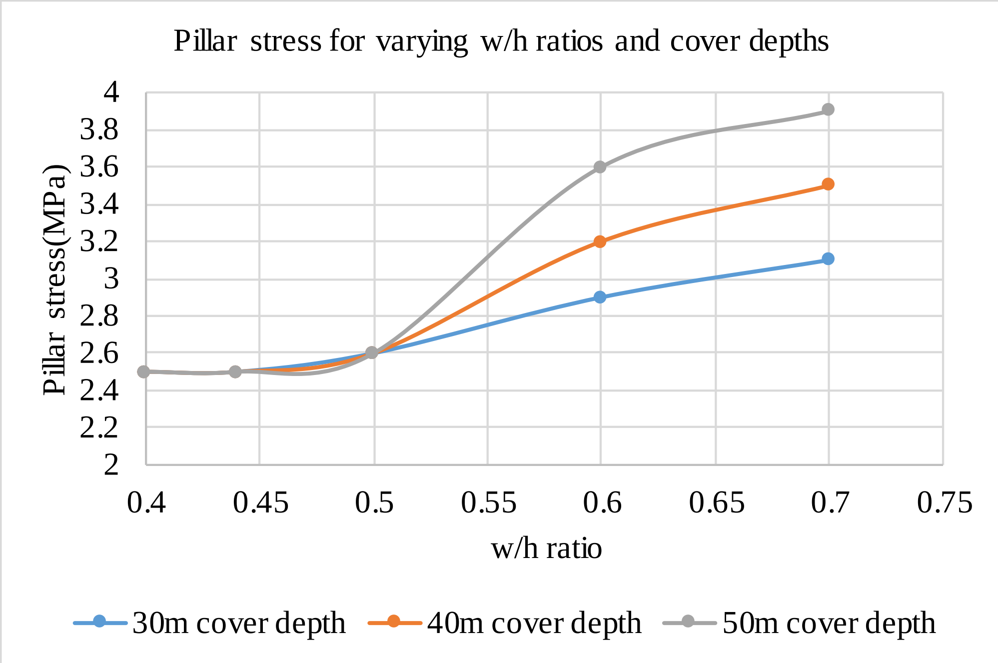

Figure 4-12: Pillar stress for varying w/h ratios and cover depths for a 34m wide panel width

c. 43m Width Panel

A 43m wide panel comprises of ten (10) 3.6m wide excavations and nine (9) 0.8m wide web pillars and is also measured to exclude the barrier pillars. The progression of the vertical stress distribution on the web pillars for various w/h ratios for 30m cover depth is presented in Figure 4-13. At the w/h ratio of 0.6, the pillar sides have already yielded at mid-height resulting in stress being transferred onto the core of the pillar. This high stress at the core forms a potential shear failure plane. A decrease in the w/h ratio to 0.5 results in further yielding at the pillar mid-height and potential total yielding at w/h ratio of 0.4. Although stress drop is evident at the core of the pillar at w/h of 0.4, the pillar corners are experiencing high stresses. This is due to the presence of confinement at the pillar-roof/floor contact.

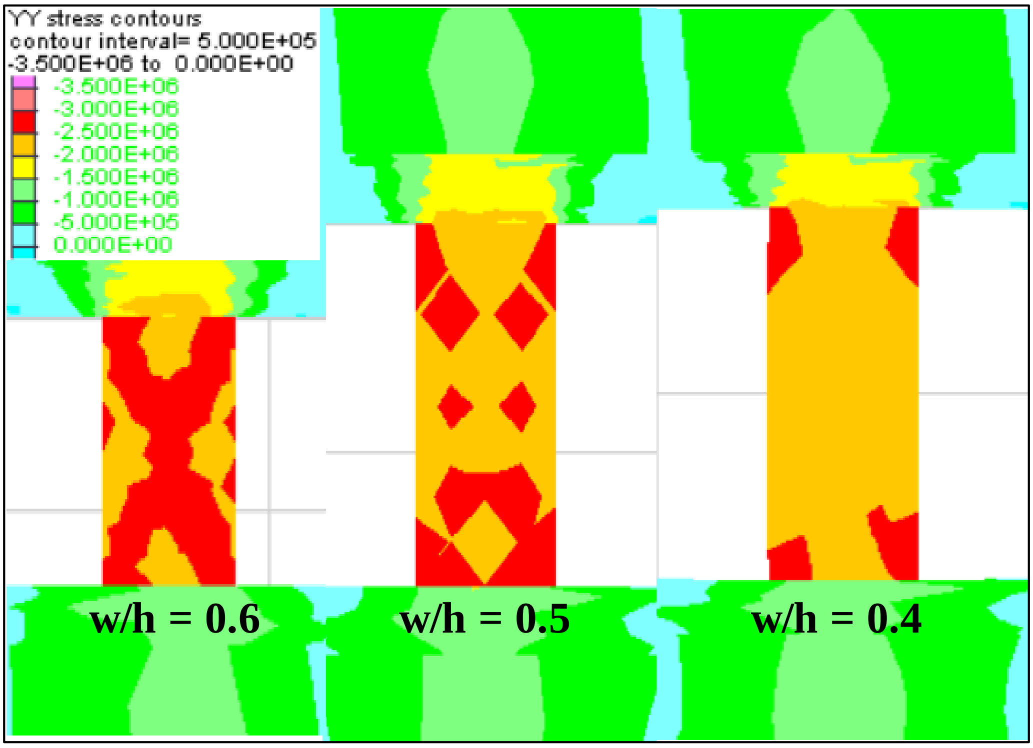

Figure 4-13: Progression of stress distribution for decreasing w/h ratio at a 30m cover depth for a 43m panel width

At the cover depth of 40m, the vertical stress is evenly distributed throughout the web pillar (Figure 4-14). This trend is also evident across the various w/h ratios at the cover depth of 50m. For further analysis, the maximum shear strain (Figure 4-15) and plasticity behaviour (Figure 4-16) results are also presented and analysed.

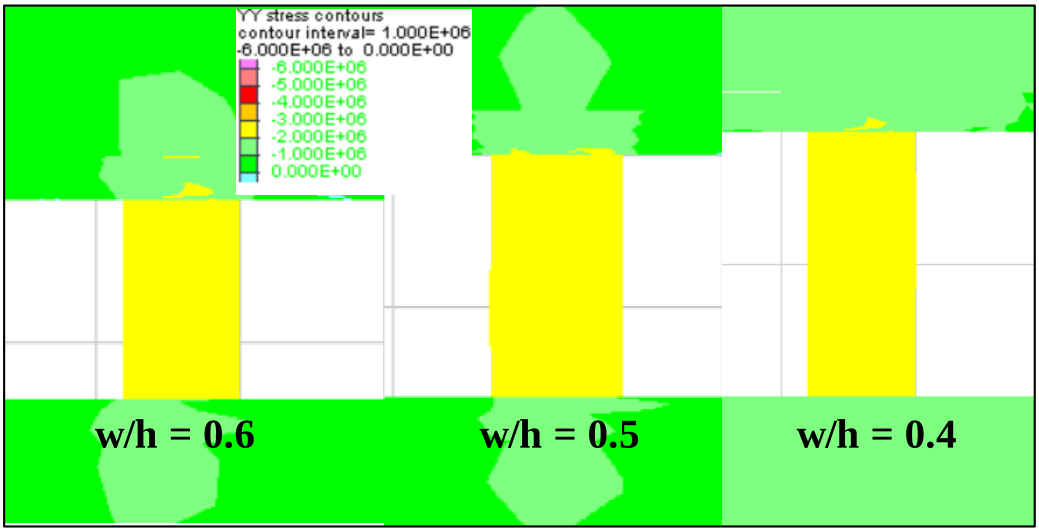

Figure 4-14: Progression of the stress distribution for decreasing w/h ratio at a 50m cover depth for a 43m panel width

Due to the yielding of the in-panel web pillars, the load is transferred to the barrier pillars. This results in yielding on the edges of the barrier pillar (Figure 4-15). The yielding zone increases with a decrease in w/h ratio as 0.87m, 0.96m and 1.21m at the w/h ratio of 0.6, 0.5 and 0.4, respectively.

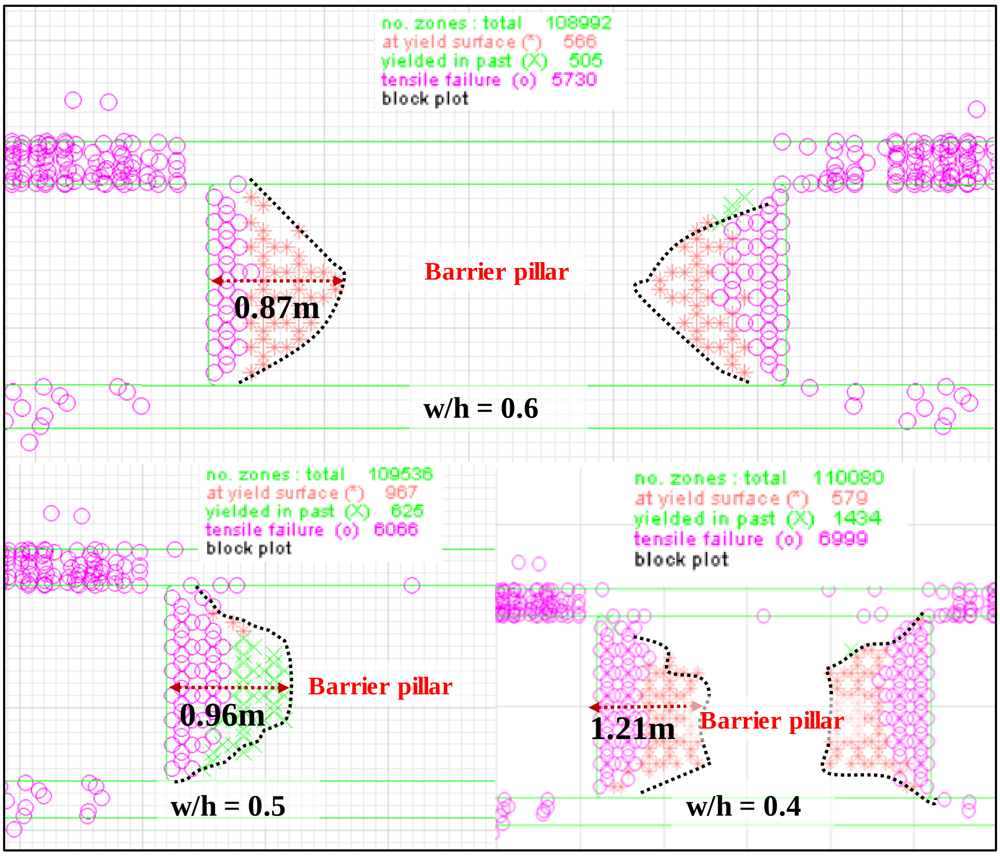

Figure 4-15: Plasticity state on the barrier pillar for various w/h ratios

Figure 4-16 summarizes the general behaviour of web pillars with various w/h ratios and cover depths at a constant panel width of 43m. Despite the general increase in pillar stresses, the behaviour of web pillars is akin to that observed for a panel width of 26m, with the change in behaviour at the w/h ratio of 0.5. Similarly, the potential failure mechanism comprises of tensile/splitting and shear at w/h ratio of 0.5 and beyond.

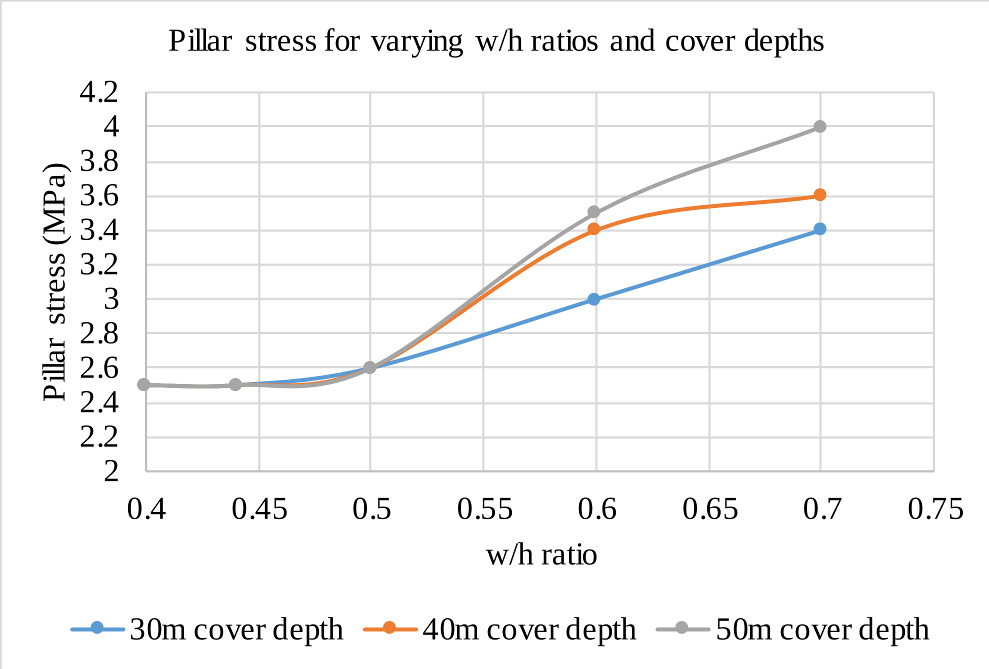

Figure 4-16: Pillar stress for varying w/h ratios and cover depths for a 43m wide panel width

The analysis of stress distribution on a 0.8m wide web pillar indicates an increase in pillar stress with an increase in panel width and cover depth. Furthermore, the change in behaviour occurs at the w/h ratio of 0.5. This indicates that the potential failure mechanism below 0.5 will be tensile/splitting and shear failure beyond width

4.3.2. 1.2m Web Pillar Width

Three (3) panel widths were analysed comprising of six (6) roadways or five (5) web pillars, eight (8) roadways or seven (7) web pillars and ten (10) roadways or nine (9) web pillars. A combination of these parameters results in 28m, 37m and 47m panel widths. The pillar stability assessment is conducted under each of these panel widths for varying w/h ratios. Three (3) w/h ratios are considered for this assessment which represent the maximum, median and minimum values (0.85, 0.75 and 0.60).

a. 28m Panel Width

Figure 4-17 depicts the vertical stress distribution for the three (3) w/h ratios at the cover depth of 30m. The high stress contour zone consistently traverses through the pillar core, with the sidewalls of the pillar experiencing low stress at the mid-height throughout all of the three w/h ratios. This indicates yielding of the sidewalls, particularly at the mid-height which then transfers the load onto the core. The same trend is observed at a 40m cover depth with the difference being an increased stress magnitude (Figure 4-18). Where the stress exceeds the pillar strength, failure of the pillar may be through sidewall splitting and then shear failure through the core.

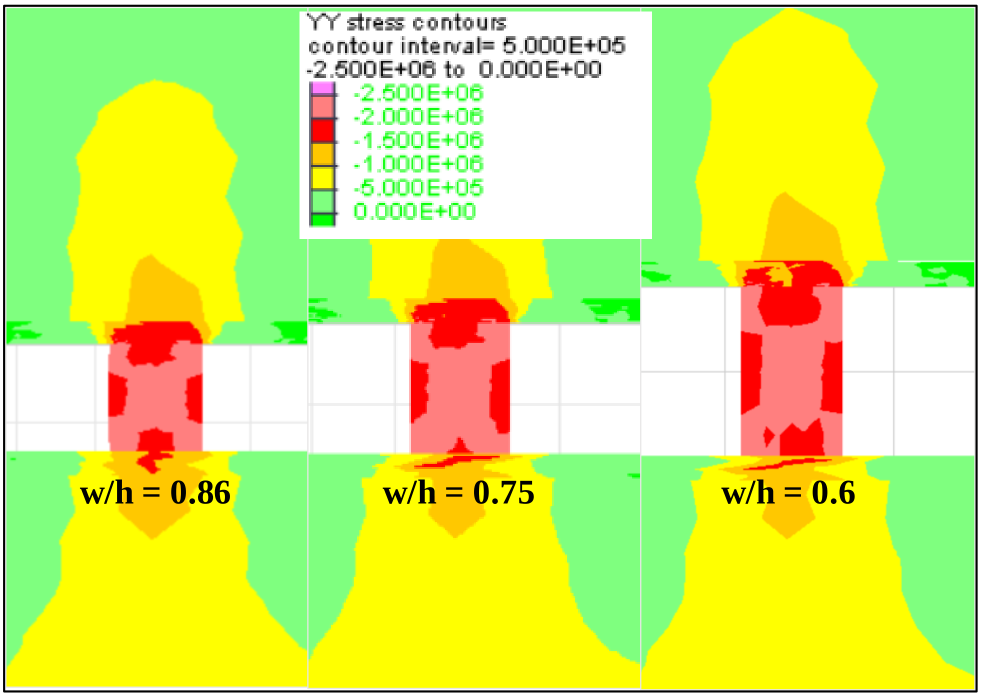

Figure 4-17: Progression of the stress distribution for a decreasing w/h ratio at a 30m cover depth for a 28m panel width

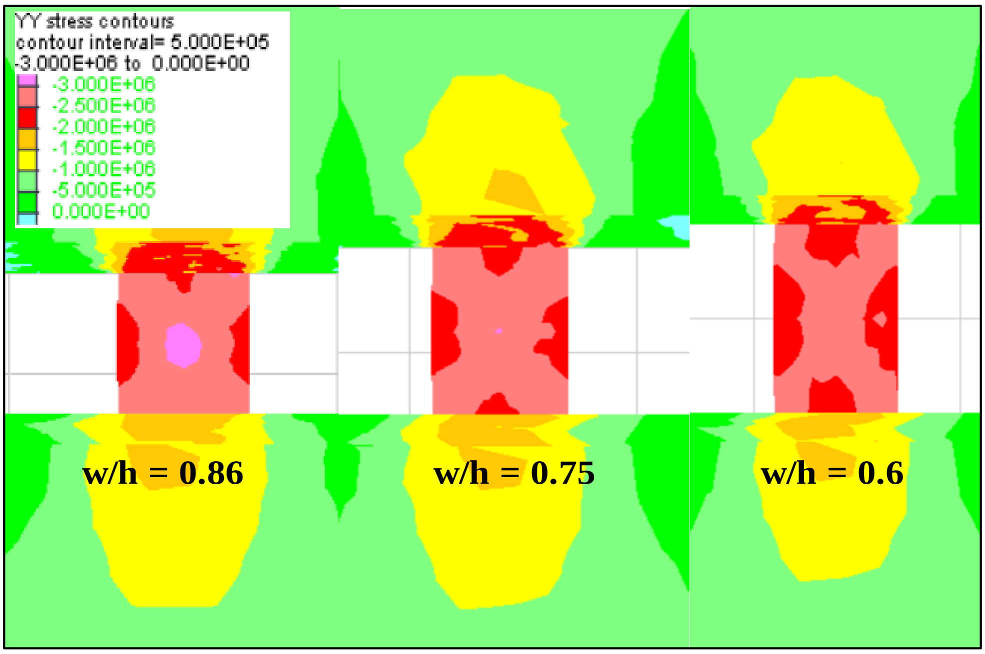

Figure 4-18: Progression of the stress distribution for decreasing w/h ratio at 40m cover depth for a 28m panel width

The stress distribution at a 50m cover depth is presented in Figure 4-19. At a w/h ratio of 0.86, the sidewalls experience lower stress compared to the core of the pillar. Whilst the stress is up to 4MPa at the core, this ranges from 2-3MPa on the sidewalls and extends up to approximately 0.68m into the pillar. Where the stress acting on the pillar is higher than the pillar strength, failure is expected to be in shear, based on the stress distribution. At the w/h ratio of 0.75, the stress drop extends wider inside the web pillar, at which stage the core and parts of the corners still sustain high stress. However, the stress at the core has dropped relative to the web pillar at a w/h ratio of 0.75. With a further decrease in the w/h ratio to 0.6, the low stress zone is spread throughout most parts of the pillar, with the high stress occurring on the pillar corners.

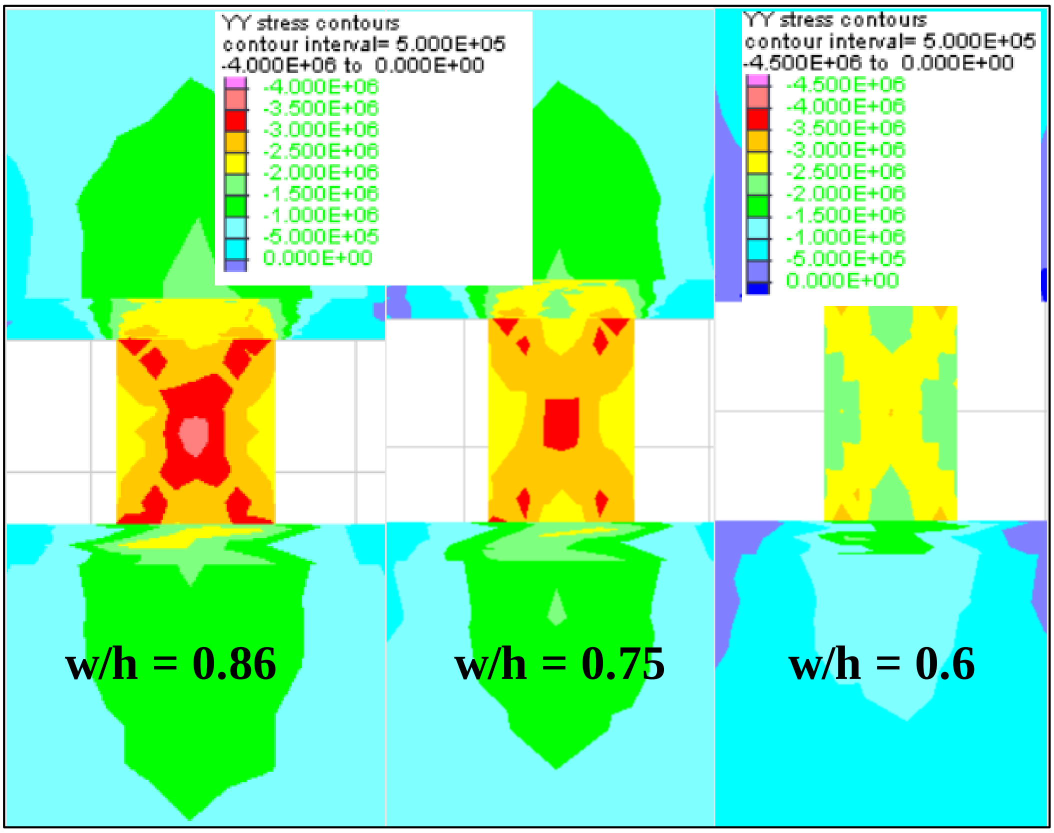

Figure 4-19: Progression of the stress distribution for a decreasing w/h ratio at a 50m cover depth for a 28m panel width

Due to the stress drop discussed above, the web pillar sheds stress onto the barrier pillar. Figure 4-20 indicates the width of the yielding zone caused by the stress transfer from the web pillars. The yielding zone increases with a decrease in w/h ratio, however, this does not affect the core of the pillar. This further indicates that should the web pillars in the panel collapse, this failure will not cascade.

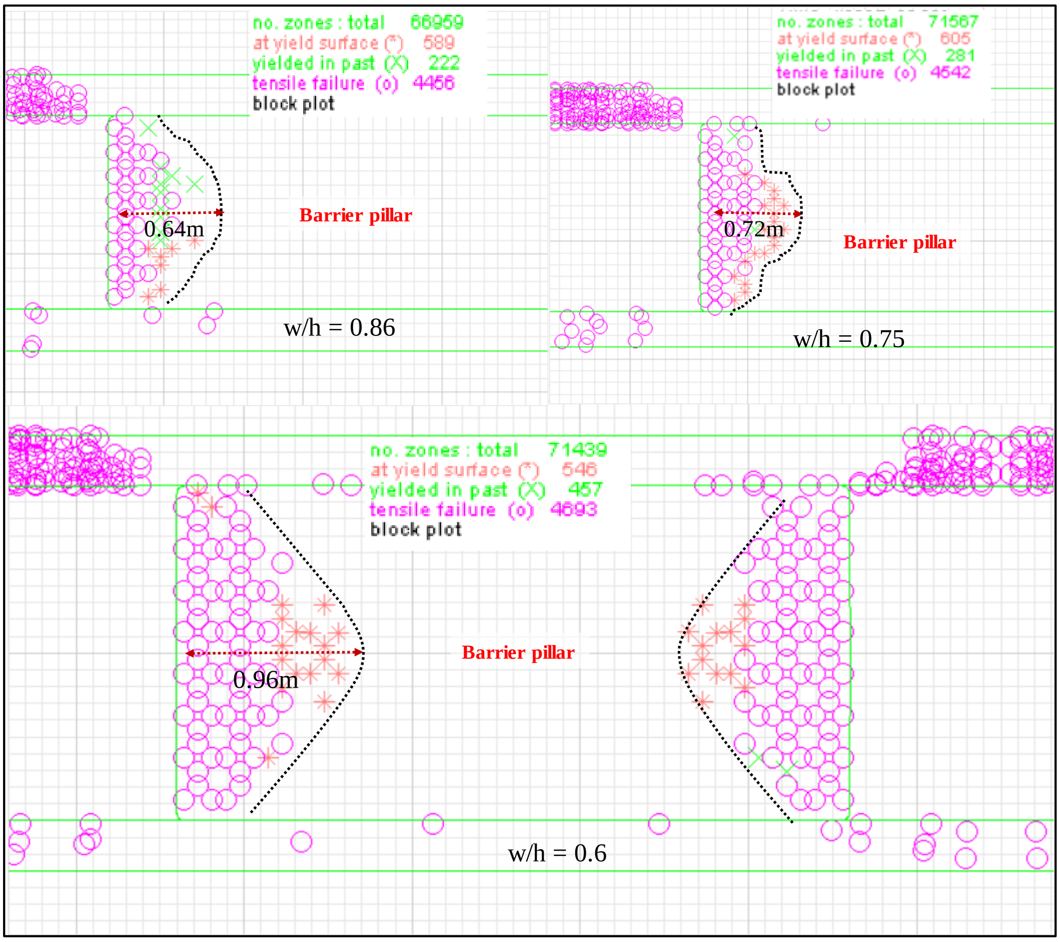

Figure 4-20: Plasticity state on the barrier pillar for various w/h ratios

The general behaviour of a 1.2m wide web pillar in 28m wide panel width at various w/h ratios and cover depths is depicted in Figure 4-21. General increase in pillar stress is observed at various cover depths. There is a change in behaviour at the w/h ratio of 0.75 at the cover depth of 50m. However, the stress increase and behaviour indicate the presence of confinement sufficient to result in a shear failure.

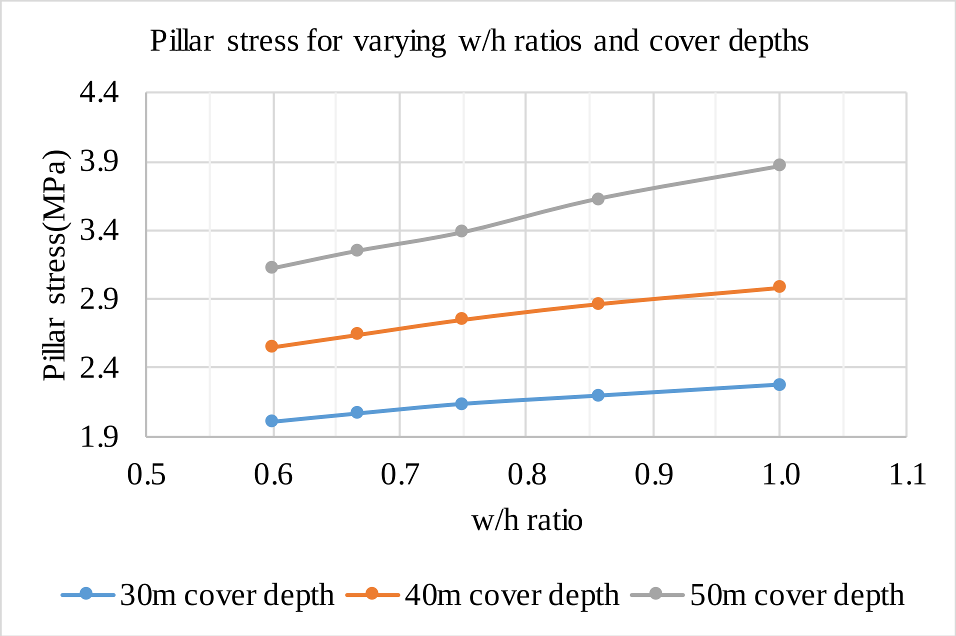

Figure 4-21: Pillar stress for varying w/h ratios and cover depths for a 28m wide panel width

b. 37m Panel Width

Figure 4-22 depicts the vertical stress distribution for various w/h ratios at a cover depth of 30m. The pillar stress is consistently distributed within the web pillar, with some indication of a stress drop on the top and bottom contacts at the w/h ratio of 0.6, indicative of localized yielding. At the cover depth of 40m (Figure 4-23), the sides of the pillar yield resulting in the stress being transferred onto the core of the pillar. Should the pillar stress exceed the pillar strength, the pillar failure is likely to be in shear.

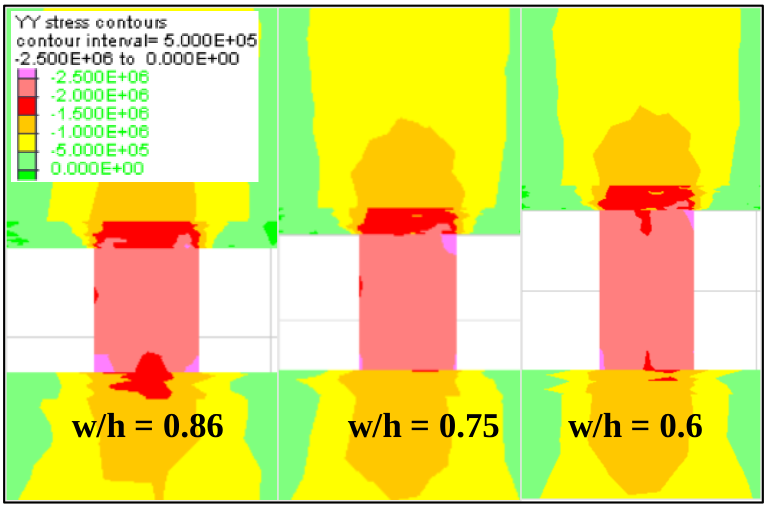

Figure 4-22: Progression of the stress distribution for decreasing w/h ratio at a 30m cover depth for a 37m panel width

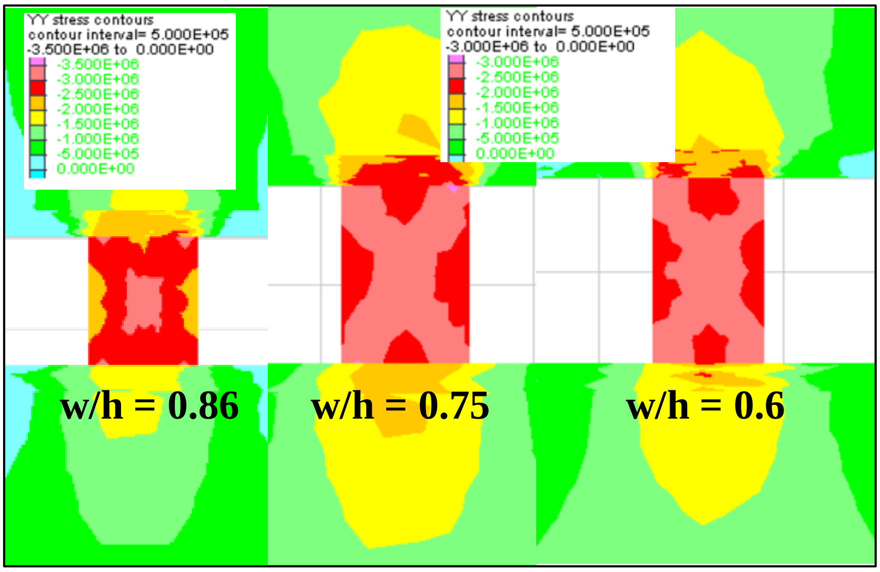

Figure 4-23: Progression of the stress distribution for decreasing w/h ratio at a 40m cover depth for a 37m panel width

Figure 4-24 indicates a further stress drop deeper into the core of the web pillar with an increase in cover depth to 50m. The elastic portion of the web pillar diminishes with a decrease in the w/h ratio. At the w/h ratio of 0.6, the stress is concentrated at the corners. Whilst the web pillars yield, the stress is transferred onto the barrier pillar sides where it results in a yield zone of varying widths as the w/h ratio decreases (Figure 4-25).

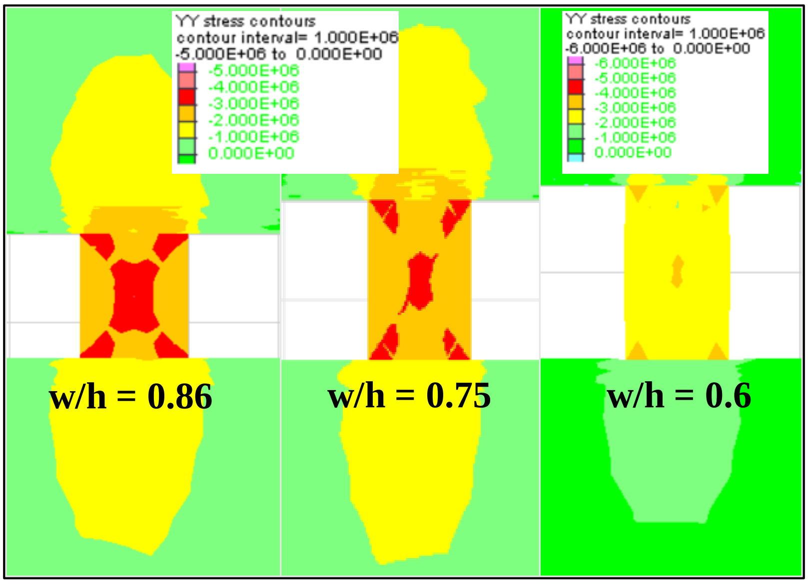

Figure 4-24: Progression of the stress distribution for decreasing w/h ratio at a 50m cover depth for a 37m panel width

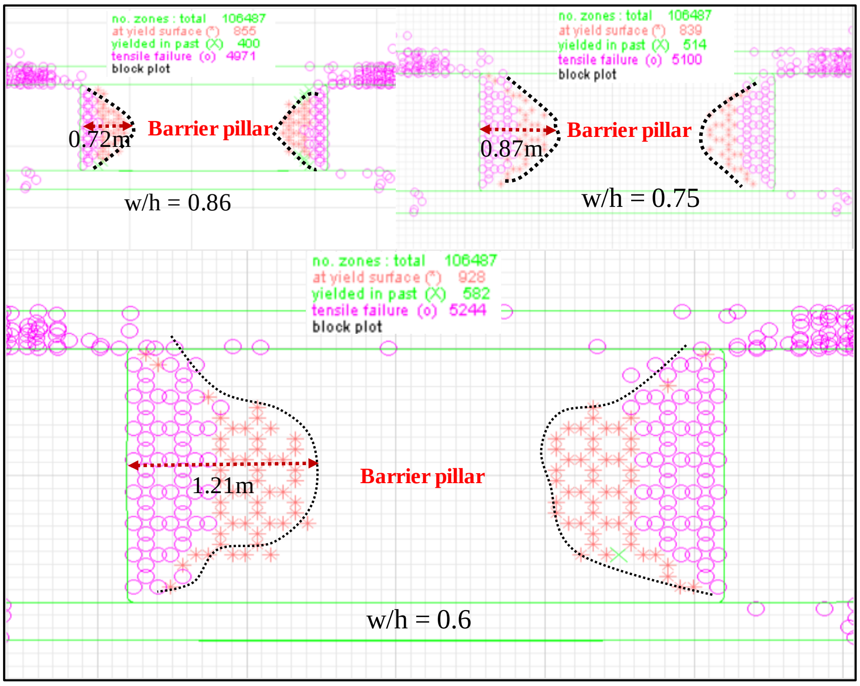

Figure 4-25: Plasticity state on the barrier pillar for various w/h ratios

The behaviour of the web pillars in a 37m wide panel is summarized in Figure 4-26 for various w/h ratios and cover depths. It indicates a general change in behaviour at a w/h ratio of 0.67. This is more pronounced at the cover depth of 50m, where the failure mechanism is likely to be in tension or splitting and beyond this w/h, the failure mechanism will be in shear.

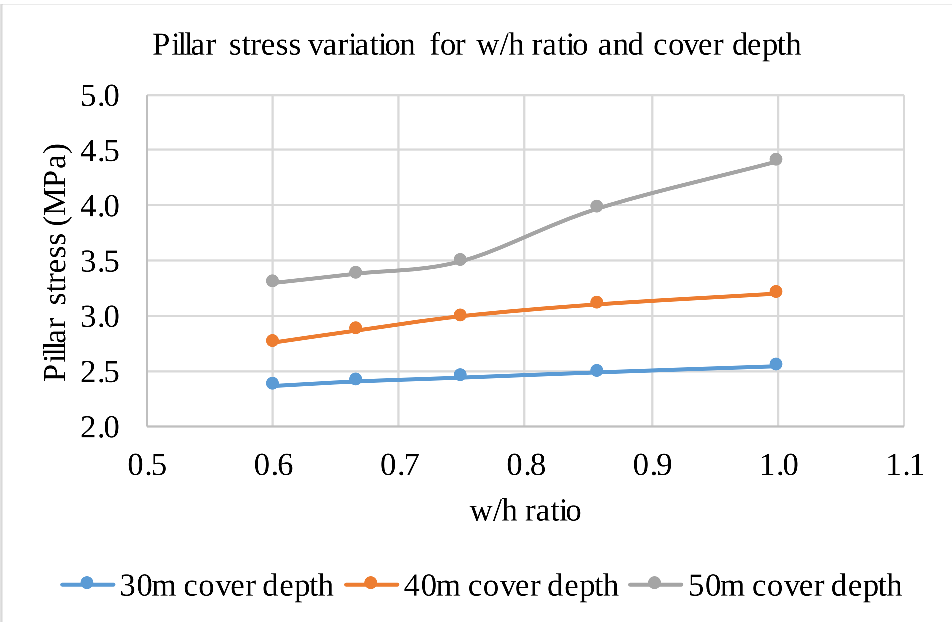

Figure 4-26: Pillar stress for varying w/h ratios and cover depths for a 37m wide panel width

c.   47m Panel Width

The stress distribution on the web pillars is presented in Figure 4-27 and Figure 4-28 for 30m and 40m cover depths, respectively. The vertical stress is consistently distributed at the centre and core of the pillars throughout the w/h ratios at the cover depth of 30m. The sides of the pillars are experiencing lower stress relative to the core of the pillar. At the cover depth of 40m, further yielding is observed which results in a reduced load carrying capacity at the w/h ratio of 0.6.

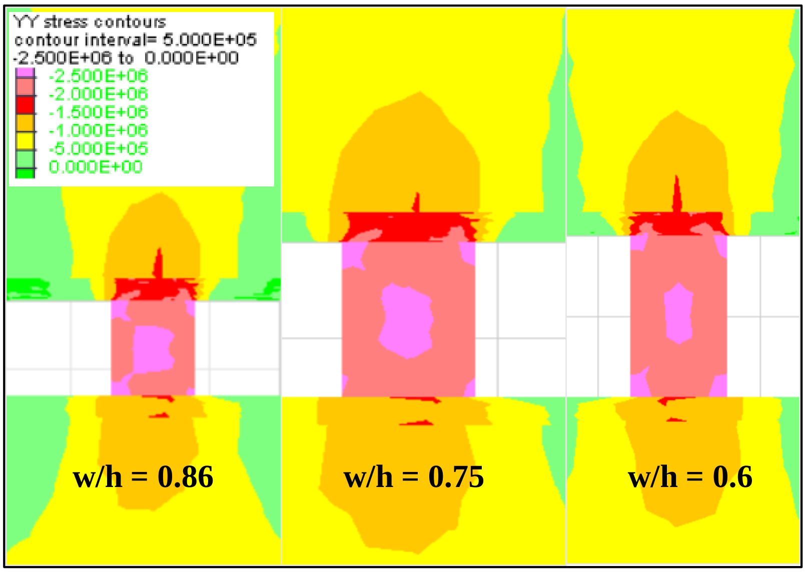

Figure 4-27: Progression of the stress distribution for decreasing w/h ratio at a 30m cover depth for a 47m panel width

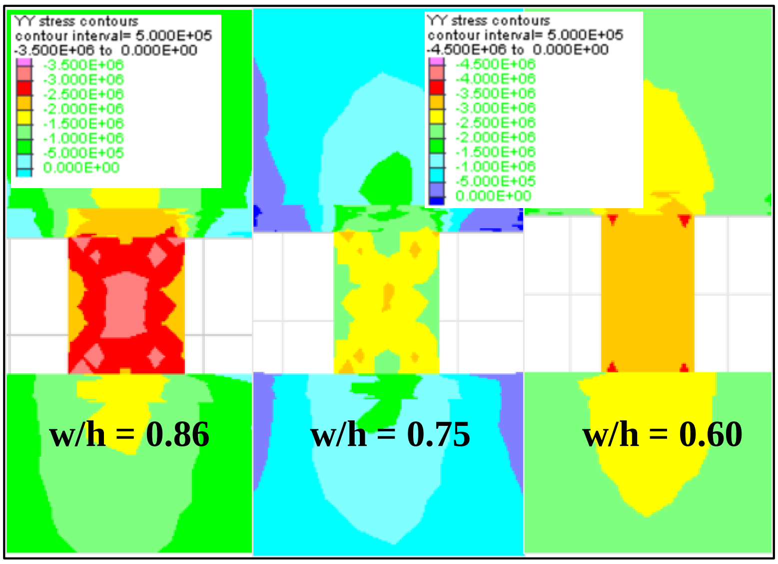

Figure 4-28: Progression of the stress distribution for decreasing w/h ratio at a 40m cover depth for a 47m panel width

Further yielding of web pillars results in stress shedding onto the barrier pillar as the cover depth increases to 50m (Figure 4-29). The width of the yield zones on the sidewall of the barrier pillar increases as the w/h ratio decreases. At the w/h ratio of 0.6, the yield zone extends deeper resulting in a 1.1m elastic zone.

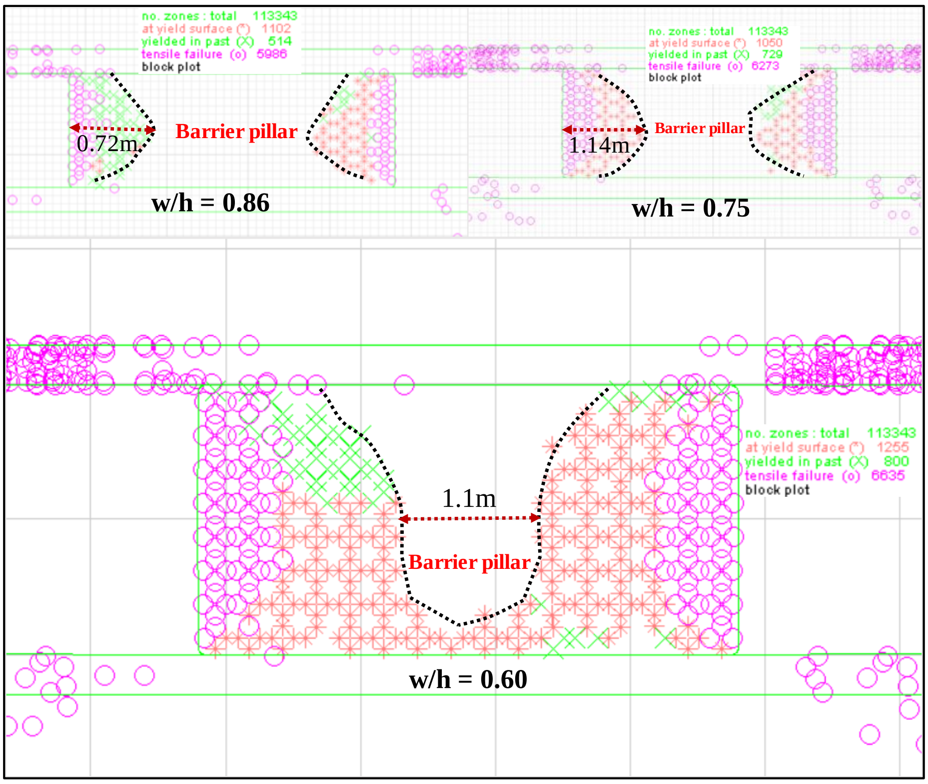

Figure 4-29: Plasticity state on the barrier pillar for various w/h ratios

The behaviour of the web pillars in a 47m wide panel is summarized in Figure 4-30 for various w/h ratios and cover depths. It indicates a general change in behaviour at a w/h ratio of 0.75. This is more pronounced at the cover depth of 50m, where the failure mechanism is likely to be in tension or splitting and beyond this w/h, the failure mechanism will be in shear.

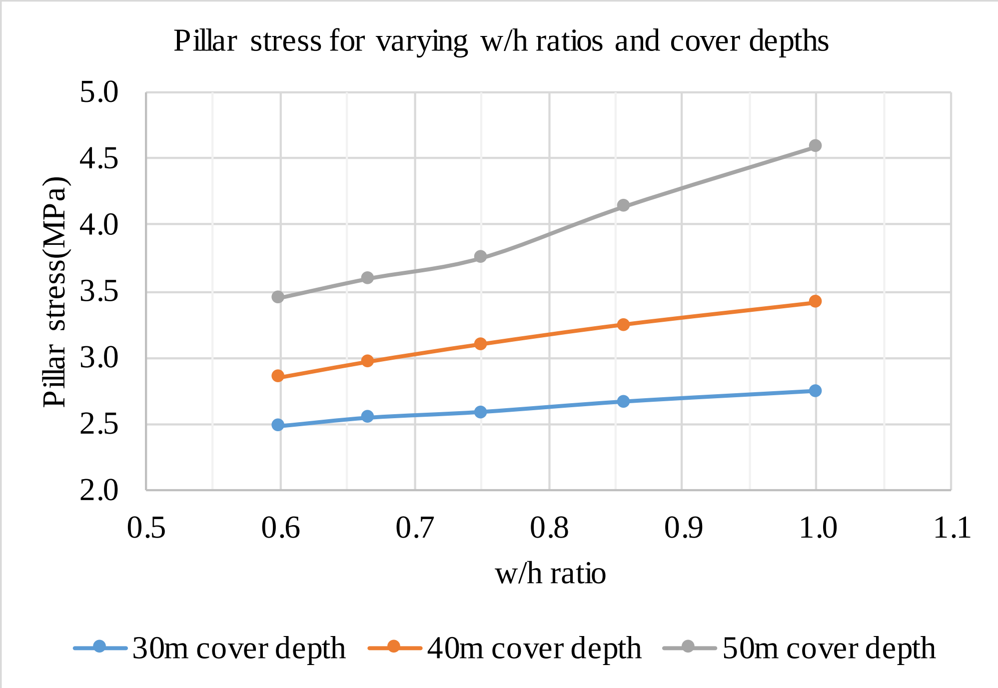

Figure 4-30: Pillar stress for varying w/h ratios and cover depths for a 47m wide panel width

4.3.3. 1.6m Web Pillar Width

Figure 4-31 presents graphs which indicate the web pillar behaviour at varying w/h ratios and cover depths at a 30m panel width. For visual purposes, the UDEC outputs are also included on the relevant point on the plot to indicate the actual stress distribution. In general, the core of the pillar is not significantly affected by yielding emanating from the sidewalls throughout all of the cover depths. At the maximum cover depth of 50m, the change in pillar behaviour occurs at the w/h ratio of 1, where the core of the pillar is under high stress. Although some significant yielding occurs with a decrease in the w/h ratio, the core can still sustain the stress imposed on the pillar. At the cover depths of 30m and 40m, the core of the web pillars is characterized by high stress, indicative of the ability to sustain the stress.

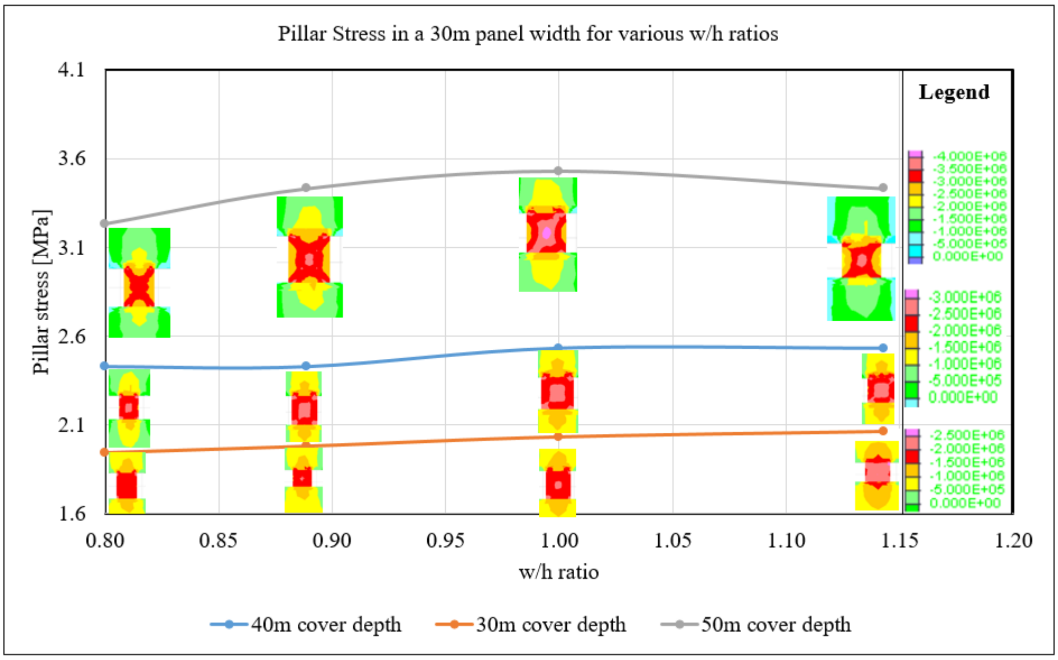

Figure 4-31: Progression of the stress distribution for decreasing w/h ratio at varying cover depths and a 30m panel width

The plots in Figure 4-32 indicate the influence of an increased panel width on the web pillar behaviour showing no signs of yielding on the core at the cover depth of 30m and 40m. Where the stress exceeds the pillar strength, the mode of failure will be shear. Shear failure is associated with the presence of confinement within the core of the pillar. At 50m cover depth, the stress relief is observed below w/h ratio of 1. This is associated with yielding of the sidewall which extends deeper into the core of the pillar with a decrease in the w/h ratio. This behaviour is replicated at the panel width of 50m (Figure 4-33).

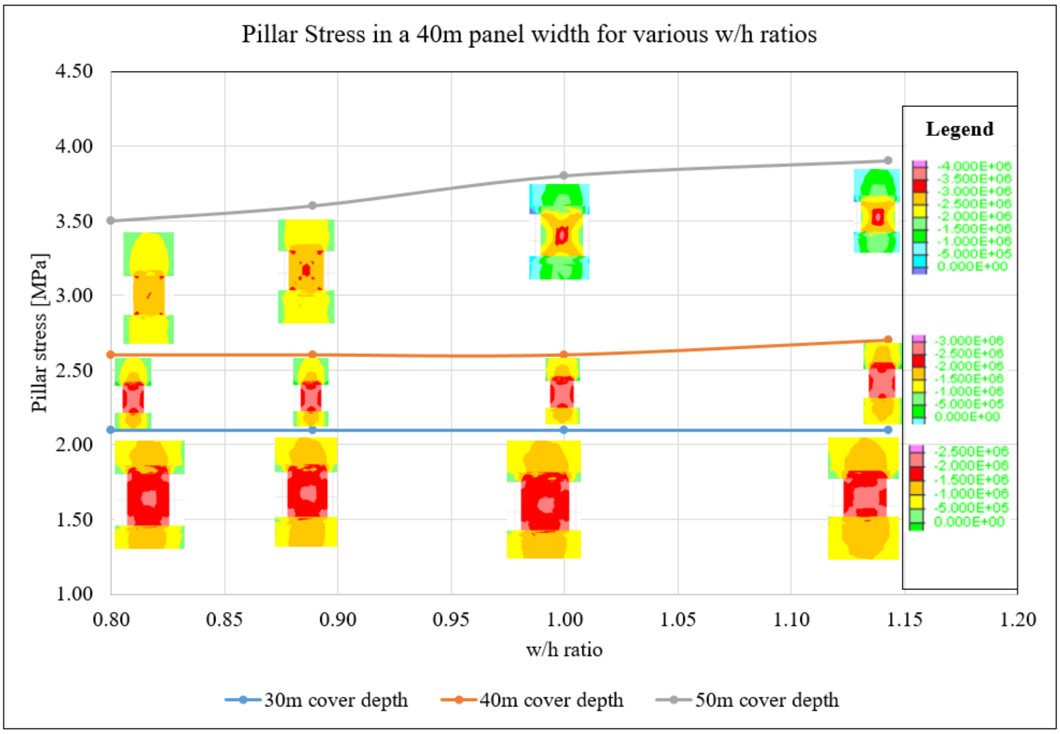

Figure 4-32: Progression of the stress distribution for decreasing w/h ratio at varying cover depths and a 40m panel width

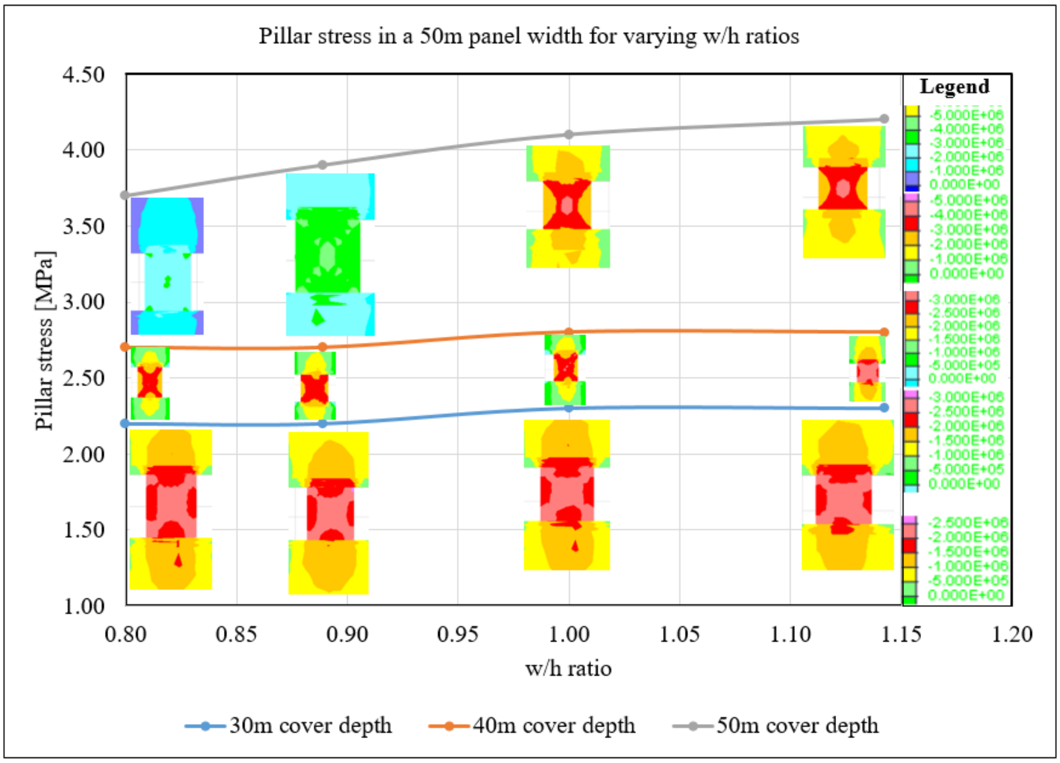

Figure 4-33: Progression of the stress distribution for decreasing w/h ratio at varying cover depths and a 50m panel width

4.3.4. 2m Web Pillar Width

The pillar stress distribution for a 2m wide web pillar at various w/h ratios and cover depth is presented in Figure 4-34. The core of the web pillar generally indicates high stress, which diminishes with an increase in w/h ratio at the cover depth of 50m. At the cover depth of 30m and 40m, the stress distribution within the core is generally consistent throughout all the w/h ratios. No yielding of the core is observed and hence, web pillar is expected to remain stable under these conditions. Where pillar stress exceeds its strength, the stress distribution within the pillar indicates that they will likely fail in shear.

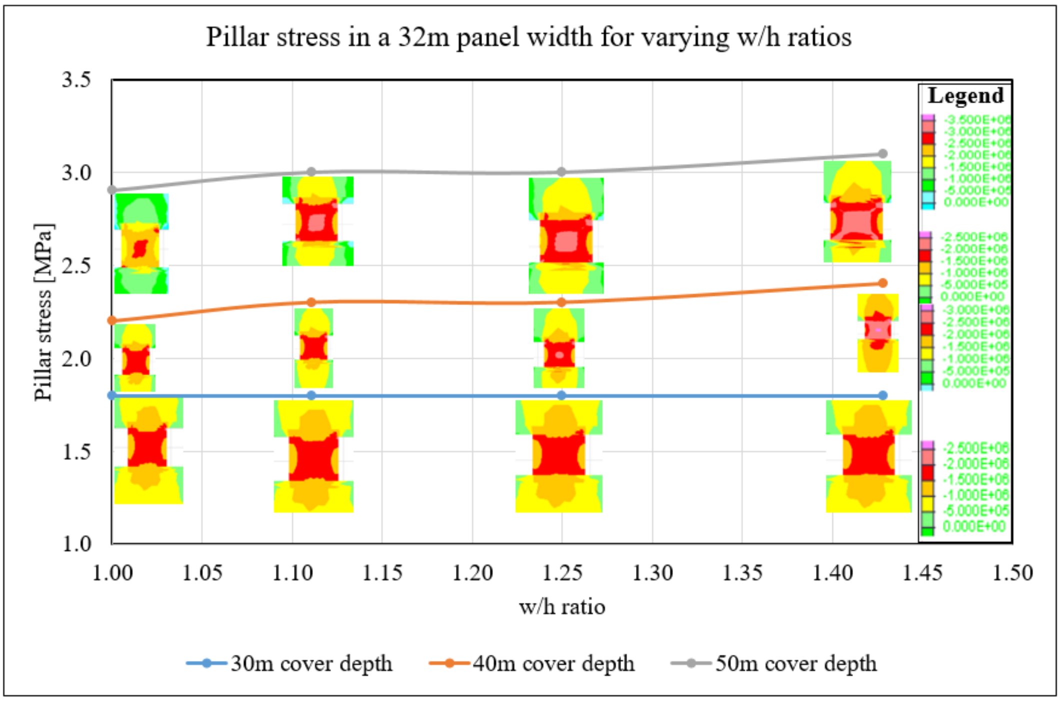

Figure 4-34: Progression of the stress distribution for decreasing w/h ratio at varying cover depths and a 32m panel width

Figure 4-35 and Figure 4-36 depict the web pillar behaviour and stress distribution output for 43m and 54m panel widths. As discussed earlier, potential shear failure is well demonstrated within the core of the pillar despite the edges having yielded.

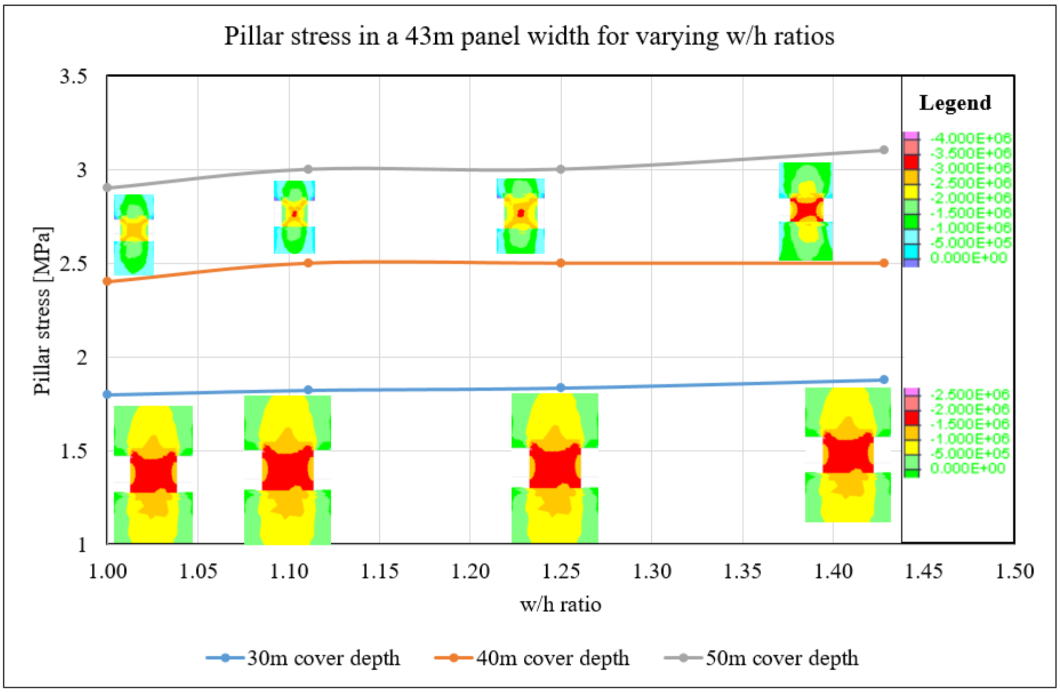

Figure 4-35: Progression of the stress distribution for decreasing w/h ratio at varying cover depths and 43m panel width

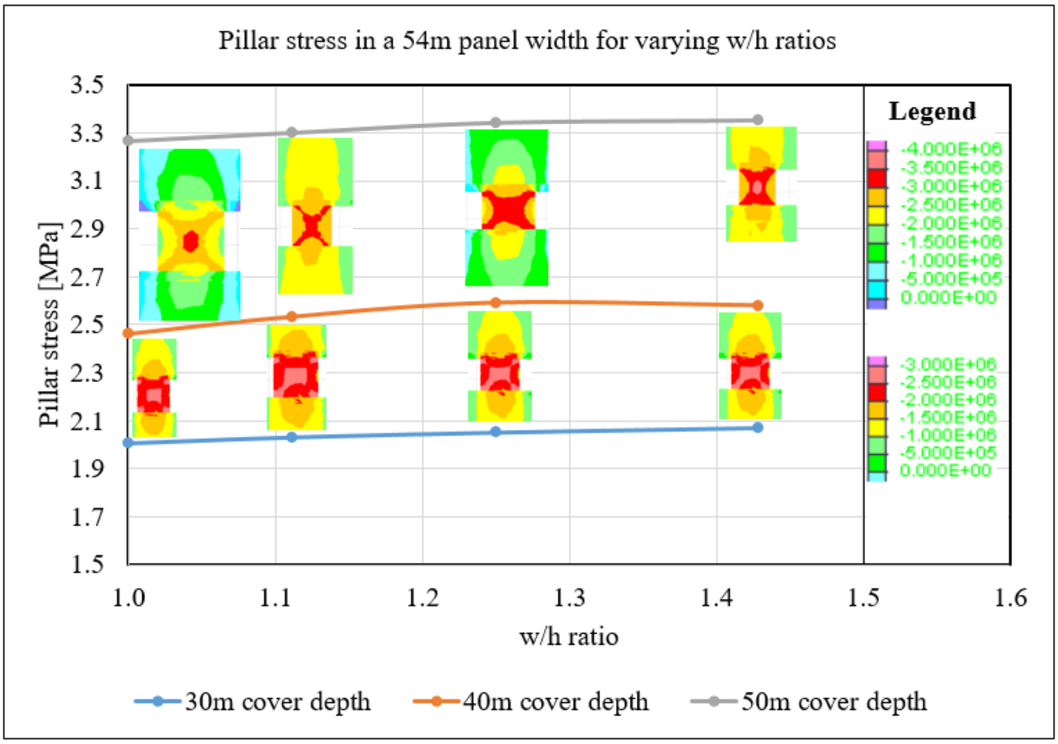

Figure 4-36: Progression of the stress distribution for decreasing w/h ratio at varying cover depths and 54m panel width

4.4. Chapter Summary

The UDEC modelling stress distribution results were presented and analysed in this chapter. Four (4) web pillar sizes were assessed at various w/h ratios, cover depths and panel widths. The numbers of web pillars were varied from five (5) to nine (9) in order to assess the influence of panel width on the web pillar stability. These parameters were combined with a variation in the cover depths from 30m to 50m. The assessment of the stress distribution on the web and barrier pillars depicted two potential pillar failure modes, tension or splitting and shear failure. The former occurs at the lower w/h ratios whilst the latter occurs at higher w/h ratio, due to the presence of confinement at the core.

A 0.8m web pillar width exhibits tensile / splitting failure below a w/h ratio of 0.5 and shear failure beyond this w/h ratio. With an increase in cover depth and panel width, further yielding is observed which results in stress transfer onto the barrier pillar, due to the reduced load carrying capacity of the web pillars. The stress distribution on a 1.2m wide web pillar width indicates that despite the sidewalls yielding, the core of the pillar still possesses a load carrying capacity. The influence of increased panel width is more pronounced with the lower w/h ratio, where the web pillar core loses its load carrying capacity. The 1.6m and 2m wide web pillars generally indicate a potential shear failure which exhibits the presence of confinement. However, a 1.2m wide web pillar indicates some potential yielding for a cover depth below 50m for a w/h ratio of 1. With a decrease in w/h ratio, cover depth and panel width, the stress is transferred onto the barrier pillars. This results in a yield surface which increases with a decrease in w/h ratio. However, the elastic portion of the barrier pillar is significant and reduces the potential of a cascading web pillar failure. Based on the assessment above, a 26m panel width comprising of 5 x 1.2m wide web pillars was selected for the initial pillar design layout and for instrumentation. The mining height of 1.8m was used based on the thickness of the coal seam and cover depth ranging from 40m to 45m.

Chapter 5
Pillar Stress Monitoring

5.1. Introduction

In order to fully evaluate and validate the final design layout, a remote monitoring program was planned and implemented. This was aimed at monitoring the loading cycle of the web and barrier pillar during the highwall mining process. This was conducted by means of recording any strain changes in the rock mass perpendicular to the direction of load. This will assist with assessing the actual pillar stresses for future optimization of the pillar extraction ratios and provide a measure of continuous risk monitoring for workers and equipment.

The Geokon model 4350 vibrating wire biaxial stressmeter (Figure 5-1) was used, which is designed to measure compressive stress changes in rock, salt, concrete or ice as well as other elastic and viscoelastic material (GEOKON, 2018). The principal stress changes are then measured by the vibrating wire sensors which are orientated at 60° intervals. The stressmeter measures the changes in resonant frequency brought about by any changes in the stress. This frequency is then related to the stress by using factory supplied calibration sheets. For this project, it was used for measuring the changes in compressive stresses within the pillars as mining progresses.

Figure 5-1: Geokon model 4350 vibrating wire biaxial stressmeter (GEOKON, 2018)

5.2. Sensor Layout

Multiple sensors were used to ensure that a correlation over a number of pillars and their location within the panel could be assessed. Five (5) Geokon 4350 sensors were selected for the purpose of pillar stress change monitoring. Panel 21 was selected for the drilling and installation of these sensors, where two (2) were installed on the barrier pillars and three (3) were installed in web pillars (Figures 5-2 and 5-3). This panel was selected due to the fact that its mining coincided with the arrival of the monitoring instruments.

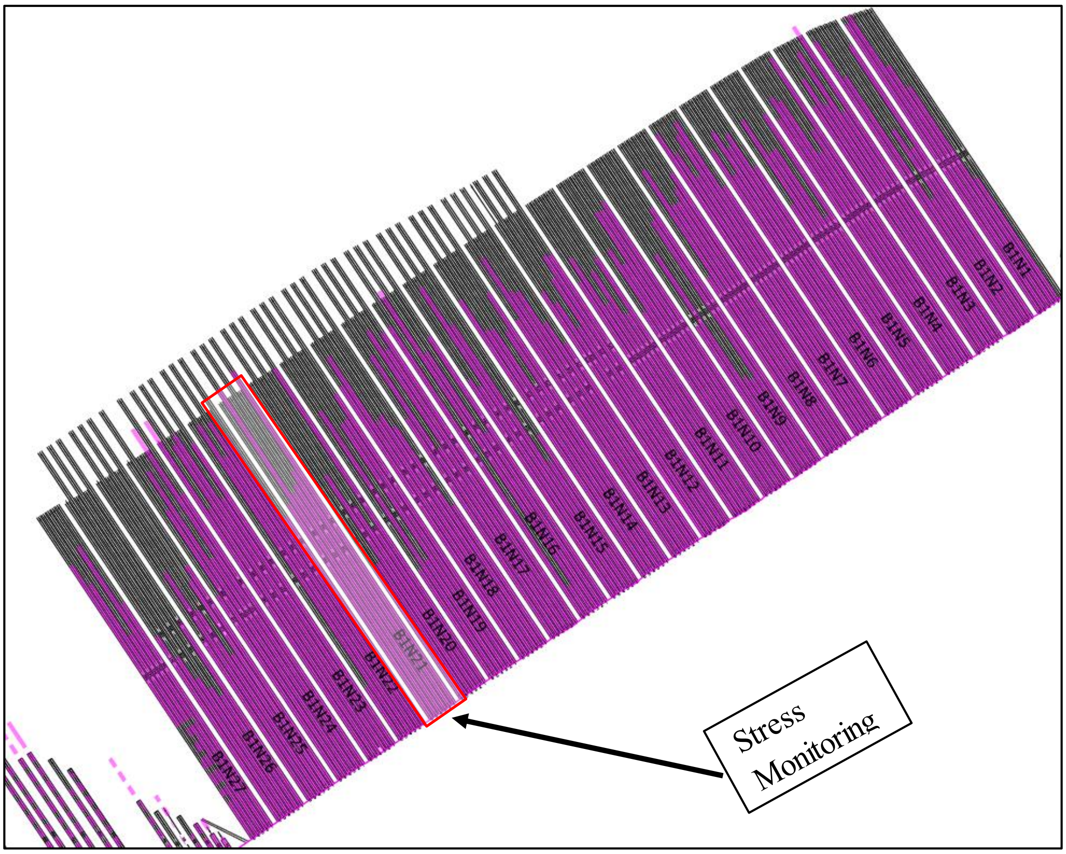

Figure 5-2: Plan view showing the position of panel 21, where the sensors were installed

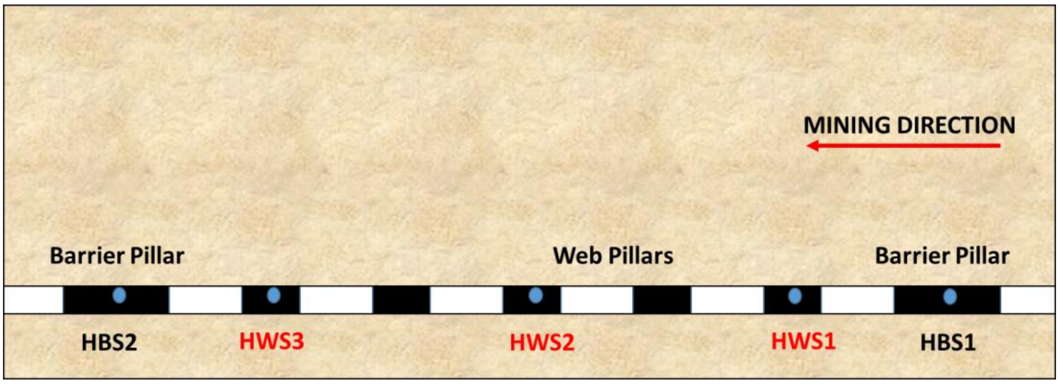

Figure 5-3: Section view of the array layout and sensor ID in panel 21

5.3. Drilling and Installation of Sensors

Site selection for the sensor drilling positions required regular consultation between various stakeholders, taking into consideration the issues pertaining to safety, security and accessibility. The identified locations and drilling collar locations were then demarcated on site by the Survey department using GPS enabled survey instruments. This allowed all sites to be accurately located and pre-drilled in the correct position prior to the arrival of the mechanised mining cut (Figure 5-4). The holes were drilled for a distance of 15m horizontally into the coal seam at predetermined pillar positions, due to the length of the available cabling.

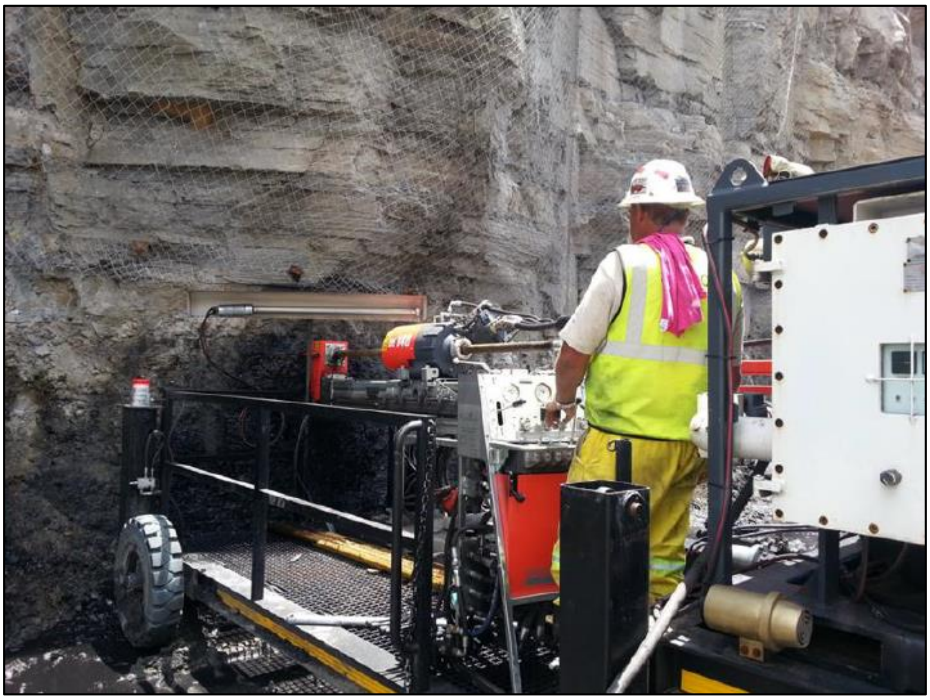

Figure 5-4: 15m length horizontal hole pre-drilling using a trailer mounted Atlas Copco Rotary drilling machine

The drilled holes were first filled with about 1m of a quick setting non-shrinking pumpable grout with the sensors being inserted into the grout. The installation of sensors was conducted as soon as possible after drilling was completed, so as to ensure that no decoupling occurred between the sensors and the rock (Figure 5-5).

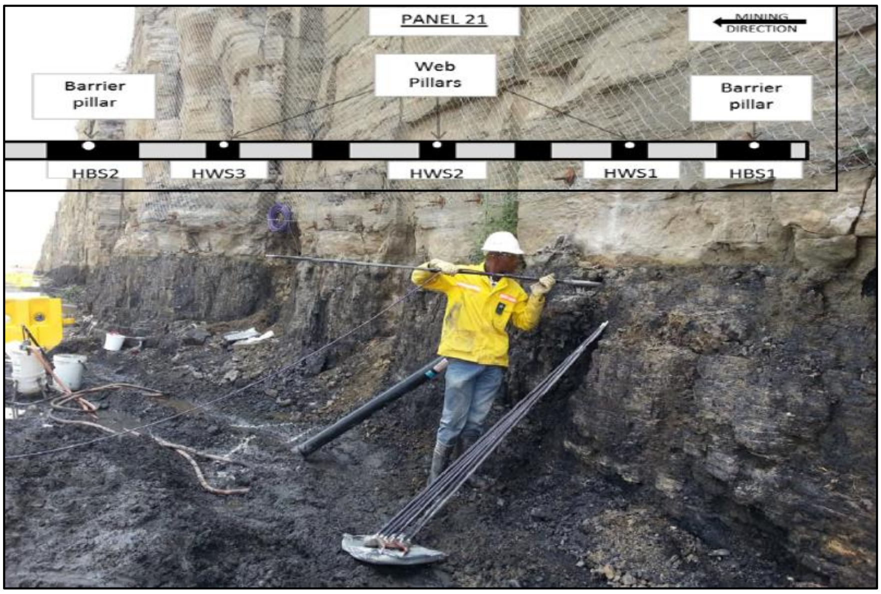

Figure 5-5: Installation of the sensors and relative positions in panel 21

5.4. Data Collection

The required sensor cables were routed up the highwall to the bench position where a multi-channel readout unit was installed. The data was manually collected from the sensors using a Geokon vibrating wire frequency analyser GK-404 (Figure 5-6). It is a portable, low-power, hand-held unit that is capable of running for more than 20 hours continuously on two AA batteries (GEOKON, 2018).

Figure 5-6: Geokon model GK-404 vibrating wire readout box (GEOKON, 2018)

Each sensor has 4 readout channels, with one of these being for temperature which was measured to be constant around 17˚C. For stress reduction purposes, temperature adjustments were thus ignored.

5.5. Data Interpretation

The raw data collected from the sensors is a frequency value and the values and corresponding sensor calibration sheets provided by Geokon were used to calculate the radial deformation of each gauge using Equation 5-1. This is easily recognizable when displayed as a relative magnitude diagram as shown in Figure 5-7. The gauge comprises of three (3) sensors, viz. Sensor 1, Sensor 2 and Sensor 3. Sensor 1 is located on the back end of the gauge, with Sensor 2 located 60˚ clockwise looking down the borehole and Sensor 3 is at 120˚ clockwise (GEOKON, 2018).

For the stress reduction and transformation, Equation 5-2 was applied to calculate the compressive stress and its direction (indicated by red arrows) which is acting on the sensor cylinder.

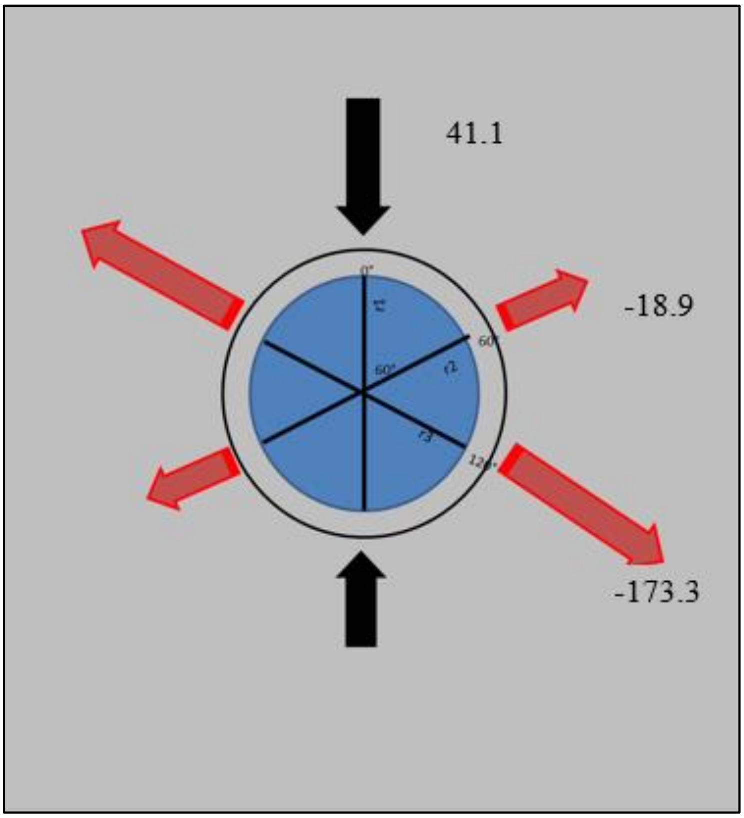

Figure 5-7: Relative magnitude of measured change in diameter

$$V_r = G(R_0 - R_t) \times 10^{-6} \text{ (Radial deformation measured in inches)} \tag{5-1}$$

$$p = \frac{1}{2}\left[\frac{1}{3B}\left((2V_{r1}-V_{r2}-V_{r3})^2+3(V_{r2}-V_{r3})^2\right)^{\frac{1}{2}}+\frac{1}{3A}(V_{r1}+V_{r2}+V_{r3})\right] \tag{5-2}$$

Where: G = Gauge correction factor (supplied with the sensor) as $r_1 = 0.3522$, $r_2 = 0.3542$ and $r_3 = 0.3502$)

R_0 = Initial reading

R_t = Reading at time, T, after application of stress

V_{rn} = Radial deformation on sensor n (where, n = 1, 2 and 3)

p = Compressive pressure

A & B = Coefficients determined from Figures 5-8 and 5-9, respectively. These depend upon the geometry and mechanical properties of the sensor and the surrounding rockmass.

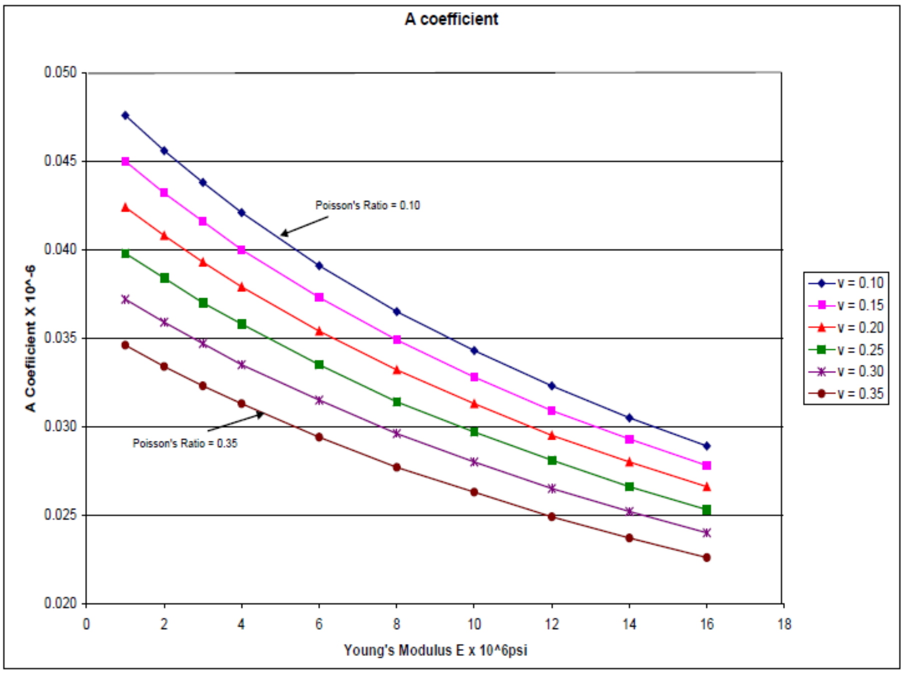

Figure 5-8: Coefficient 'A' plotted against rockmass Poisson's ratio (GEOKON, 2018)

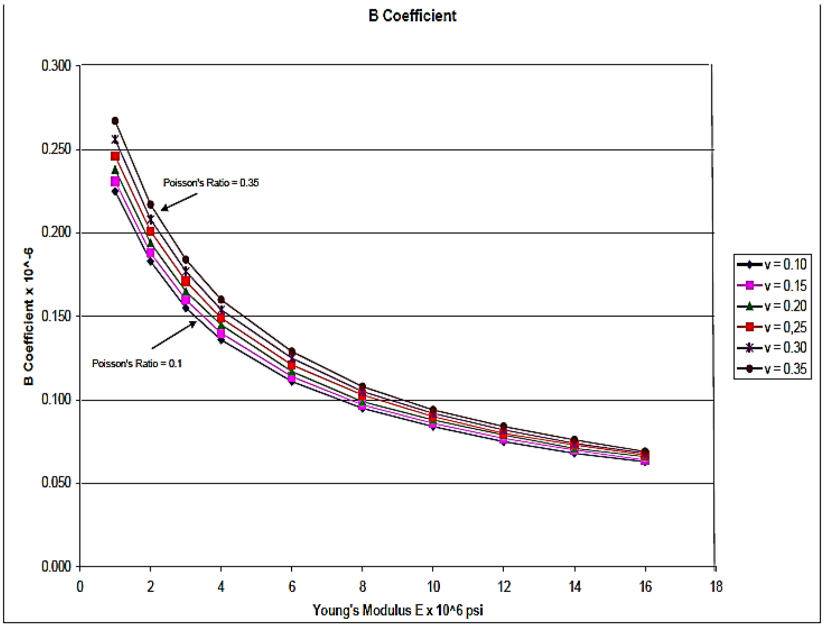

Figure 5-9: Coefficient 'B' plotted against rockmass Poisson's ratio (GEOKON, 2018)

A total number of 55 measurements were taken across the 5 sensors installed on the web pillars and barrier pillars, during the life of the operation. The raw data (in *frequency*^{2}x*10*$^{-3}$) recorded on various dates is presented in Table 5-1.

Table 5-1: Raw data (*in frequency*^{2}x*10*$^{-3}$*)* from the various sensors on various dates

Date	Axis	HBS1		HWS1		HWS2		HWS3		HBS2	
		R0	*Rt*	*R0*	*Rt*	*R0*	*Rt*	*R0*	*Rt*	*R0*	*Rt*
19-Feb	r1	6764.1	6764.1	6818.1	6818.1	6774.1	6774.1	6563.7	6563.7	6756.8	6756.8
	r2	6794.0	6794.0	7083.6	7083.6	6799.8	6799.8	6785.4	6785.4	6785.5	6785.5
	r3	6819.7	6819.7	6818.2	6818.2	6731.3	6731.3	6838.2	6838.2	6793.5	6793.5
5-Mar	r1	6764.1	6755.1	6818.1	6817.8	6774.1	6776.3	6563.7	6505.2	6756.8	6759.2
	r2	6794.0	6778.0	7083.6	7078.0	6799.8	6797.1	6785.4	6785.4	6785.5	6785.5
	r3	6819.7	6841.6	6818.2	6965.1	6731.3	6732.1	6838.2	6838.3	6793.5	6790.4
7-Mar	r1	6764.1	6714.4	6818.1	6803.7	6774.1	6773.1	6563.7	6505.9	6756.8	6760.5
	r2	6794.0	6754.5	7083.6	7063.7	6799.8	6791.4	6785.4	6783.1	6785.5	6785.5
	r3	6819.7	6892.2	6818.2	6989.9	6731.3	6738.7	6838.2	6839.5	6793.5	6790.0
8-Mar	r1	6764.1	6709.1	6818.1	6804.0	6774.1	6772.5	6563.7	6506.5	6756.8	6760.7
	r2	6794.0	6762.9	7083.6	7057.6	6799.8	6790.6	6785.4	6782.5	6785.5	6785.5
	r3	6819.7	6892.2	6818.2	6991.1	6731.3	6740.0	6838.2	6839.3	6793.5	6790.5
9-Mar	r1	6764.1	6708.5	6818.1	6801.7	6774.1	6764.8	6563.7	6507.8	6756.8	6762.2
	r2	6794.0	6757.5	7083.6	7075.1	6799.8	6790.5	6785.4	6779.0	6785.5	6783.1
	r3	6819.7	6892.2	6818.2	6984.5	6731.3	6748.9	6838.2	6840.9	6793.5	6790.4
10-Mar	r1	6764.1	6701.9	6818.1	6798.6	6774.1	6760.7	6563.7	6506.9	6756.8	6769.3
	r2	6794.0	6754.5	7083.6	7075.1	6799.8	6798.5	6785.4	6777.1	6785.5	6775.1
	r3	6819.7	6892.2	6818.2	6987.0	6731.3	6747.6	6838.2	6850.5	6793.5	6790.4
11-Mar	r1	6764.1	6698.4	6818.1	6790.8	6774.1	6750.4	6563.7	6505.2	6756.8	6773.5
	r2	6794.0	6754.6	7083.6	7075.2	6799.8	6815.3	6785.4	6759.4	6785.5	6767.5
	r3	6819.7	6892.2	6818.2	6988.6	6731.3	6739.1	6838.2	6854.4	6793.5	6790.1
12-Mar	r1	6764.1	6699.2	6818.1	6790.5	6774.1	6753.8	6563.7	6506.1	6756.8	6774.5
	r2	6794.0	6754.5	7083.6	7077.5	6799.8	6817.0	6785.4	6759.0	6785.5	6767.4
	r3	6819.7	6892.2	6818.2	6988.7	6731.3	6736.8	6838.2	6855.0	6793.5	6790.0
14-Mar	r1	6764.1	6691.9	6818.1	6781.2	6774.1	6753.8	6563.7	6474.0	6756.8	6774.5
	r2	6794.0	6749.6	7083.6	7102.0	6799.8	6817.0	6785.4	6752.0	6785.5	6767.4
	r3	6819.7	6892.2	6818.2	6995.0	6731.3	6736.8	6838.2	6880.1	6793.5	6790.0
15-Mar	r1	6764.1	6692.0	6818.1	6779.8	6774.1	6753.8	6563.7	6471.0	6756.8	6770.8
	r2	6794.0	6750.1	7083.6	7103.4	6799.8	6817.0	6785.4	6748.9	6785.5	6742.3
	r3	6819.7	6892.2	6818.2	6995.3	6731.3	6736.8	6838.2	6885.0	6793.5	6808.1
26-Mar	r1	6764.1	6693.0	6818.1	6777.0	6774.1	6738.0	6563.7	6466.5	6756.8	6752.5
	r2	6794.0	6746.0	7083.6	7102.5	6799.8	6821.5	6785.4	6740.5	6785.5	6728.5
	r3	6819.7	6892.2	6818.2	6991.5	6731.3	6735.0	6838.2	6892.5	6793.5	6825.0

5.6. Stress Data and Analysis

The change in stress from each sensor calculated from the above equations and frequency data are presented in this section. The barrier pillar stress change profile over time is presented in Figure 5-10. The plot indicates the maximum barrier pillar stress is 2.4MPa. The influence of mining in the vicinity of the installed gauges is evident on the graphs characterized by cycles of sudden increase and constant stress change.

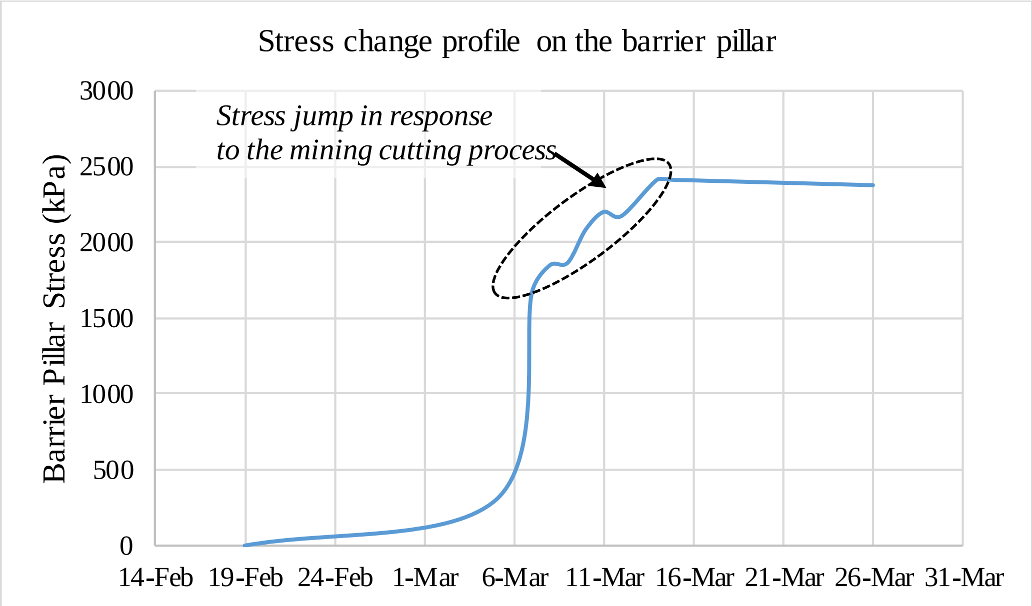

Figure 5-10: Barrier pillar stress change distribution over time

The web pillar stress change distribution profile is presented in Figure 5-11 and shows a pillar maximum stress of 3.14MPa at the time of taking the last measurement. The sudden increase in stress as a result of cutting process is more pronounced on the web pillar as compared to the barrier pillar.

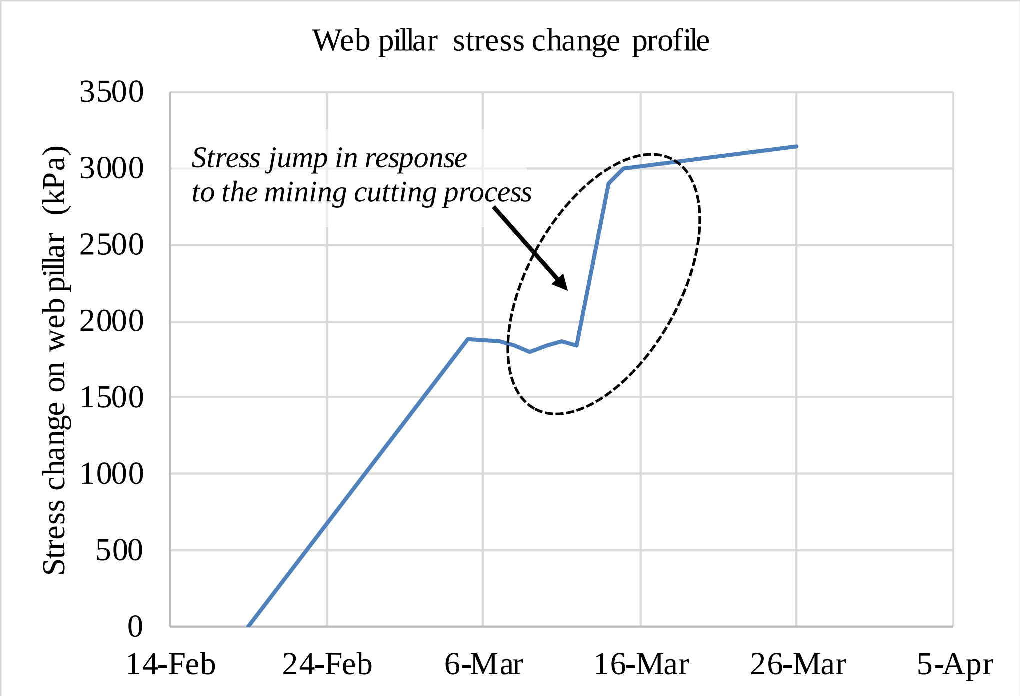

Figure 5-11: Web pillar stress distribution over time

For stability assessment, the above stresses were compared with the UCS data of the No. 5 coal seam as obtained from the previous laboratory tests (Glencore Coal Geotechnical Database, 2012). A plot of the No. 5 coal seam laboratory test results has been presented in Figure 3-4, where the UCS values were obtained at 0MPa confinement stress. The UCS values were observed to be ranging from a minimum of 14.05MPa to a maximum of 60.2MPa. The average UCS was found to be 25.2MPa based on the test results of the No.5 coal seam samples that are available in the database.

In order to assess the potential failure, the pillar stresses for both barrier and web pillars were plotted with the average sample UCS and the rule of thumb for fracture initiation (Figure 5-12). This rule of thumb indicates that fracture will initiate in a rock when the stress approaches one-third (1/3) of the UCS. In order to fulfil the crack initiation rule, the stress must be at least 8.33MPa, using the average UCS value of 25.2MPa.

The maximum web pillar and barrier pillar stresses are only 13% and 10% of the average UCS and no fracturing/failure was thus anticipated.

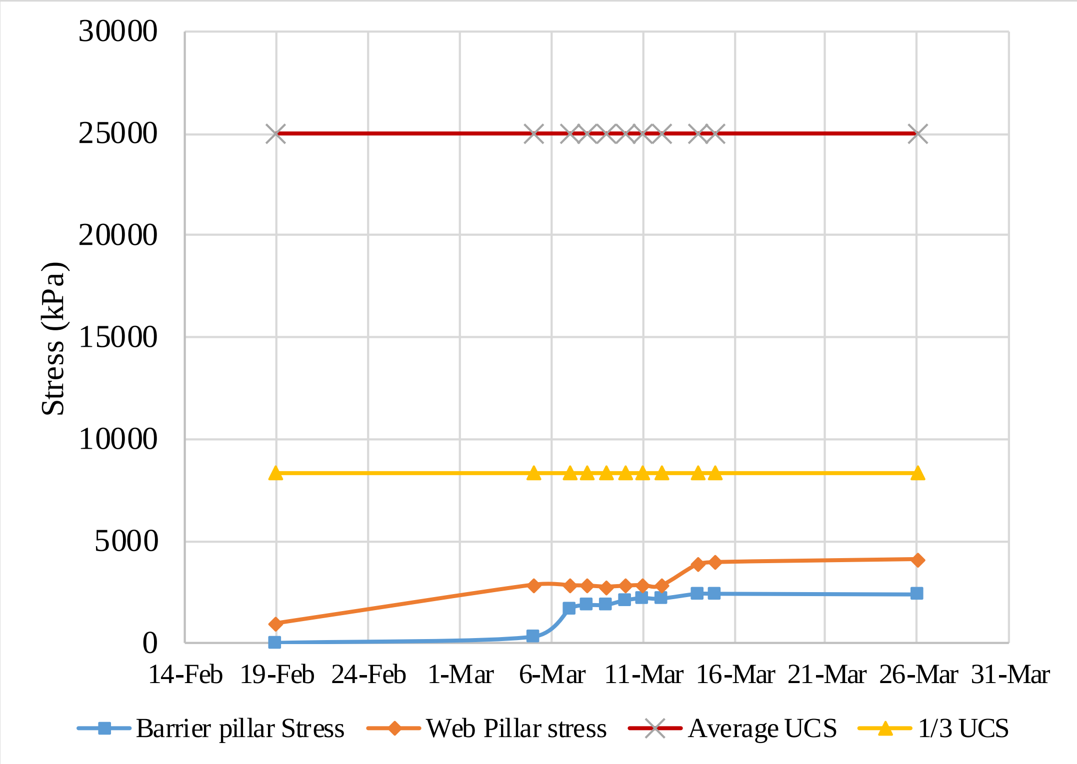

Figure 5-12: Pillar stress measurement plotted against the average UCS and crack initiation criterion

5.7. Chapter Summary

The stress measurements were conducted in order to monitor the loading cycle of the web and barrier pillars during the highwall mining process. Five (5) Geokon 4350 sensors were installed for the purpose of pillar stress change monitoring. Two (2) sensors were also installed on the barrier pillars and three (3) were installed in the web pillars. Due to this project coming to an abrupt stop, this stress measurement program could not be repeated for various panel geometries or locations. Hence, the measurements presented in this report are for a 28m wide panel comprising of 5 x 1.2m wide web pillars between barrier pillars. The maximum stress measured until the end of the project was found to be 2.4MPa on the barrier pillar and 3.14MPa on the web pillars. This is way below the average UCS of 25.2MPa of the No. 5 coal seam. Using the rule of thumb for crack initiation occurring at 0.3xUCS (8.33MPa), no failure or crack initiation was expected on the pillars, since the measured stresses are well below this criterion.

Chapter 6

Conclusions and Recommendations

The main aim of this project was to design the highwall mining layout for extracting the coal reserves that could not be safely and economically mined out using the conventional underground mining method. This was achieved by employing a hybrid approach, which comprises of empirical pillar strength estimation and numerical modelling to determine the pillar stresses for varying panel layouts. The Universal Discrete Element Code (UDEC) was used to determine the web and barrier pillar stresses at varying cover depths and extraction heights. The width of the excavations was kept constant (3.6m) throughout the analysis in line with the width of the cutting drum of the equipment. The pillar safety factor was then determined as the ratio of pillar strength and vertical stress and a threshold of 1.3 was utilized in line with the ARMPS-HWM minimum safety factor guidelines (Mark, 2006) for a panel width of less than 60m. The conclusions and recommendations made are discussed below.

6.1. Conclusions

The following conclusions can be drawn from the study, using the methodology described above:

- A 0.8m web pillar attains the threshold safety factor with the panel widths of 34m and 43m at the highest w/h ratio of 0.67. These correspond with the cover depths of 36m and 41.5m, respectively.
- The numerical modelling results indicates that a 0.8m web pillar width exhibits tensile/splitting failure below w/h ratio of 0.5 and shear failure beyond this w/h ratio. However, with an increase in cover depth and panel width, further yielding is observed, which results in stress transfer onto the barrier pillar whilst the web pillar stress decreases and then remains constant. This behaviour of stress change will result in a higher safety factor but in reality, this pillar will be undergoing splitting or tensile failure.
- A 1.2m web pillar attains the threshold safety factor at the cover depths of 45m and 43m corresponding with 37m and 47m panel widths, respectively.

At the panel width of 28m, this pillar width plots above the threshold safety factor across all of the cover depths.

- The stress distribution on a 1.2m web pillar width indicates that despite yielding of the sidewalls in some cases, the core of the pillar still possesses the load bearing capacity. The influence of an increased panel width is more pronounced with the lower w/h ratio, where the indications are that the core has also yielded.
- Increasing the web pillar size to 1.6m results in a threshold safety factor being attained across all panel widths up to the cover depth of 40m. As expected, due to the increased pillar size, the core of the pillar is wider and not significantly affected by yielding zones emanating from the pillar edges.
- A 2m web pillar safety factor plots above the threshold for all of the cover depths and panel widths.
- The stress measurements were conducted in order to monitor the loading cycle of the web and barrier pillars during the highwall mining process. Although this was conducted for one panel geometry, the maximum stress measured until the end of the project was found to be 2.4MPa on the barrier pillar and 3.14MPa on the web pillars. This is far below the average UCS of 25MPa and the minimum UCS of 14MPa of the No.5 coal seam. Using the rule of thumb for crack initiation at 0.3xUCS (8.33MPa), no failure or crack initiation was expected on the pillars, since the measured stresses are all well below this criterion.

6.2. Recommendations

Based on the above safety factor assessment, a minimum web pillar width at which the threshold safety factor is attained is 1.2m. This is achieved at a panel width of 28m (6 cuts / 5 pillars per panel) up to the maximum cover depth of 50m, which corresponds with the cover depth obtained from the geological information. This also correlates with the numerical modelling results which indicate that the core of the pillar remains stable for a number of geometric combinations.

In order to optimize percentage extraction, the layout should be reviewed in light of the stress measurements and this exercise should be repeated for a combination of panel widths, w/h ratios and cover depths. The use of extensometers to monitor displacements across the excavations could also assist with optimizing the width for different roof compositions. With the understanding of stress and pillar behaviour, the design matrix could be compiled for various variables for a quick design guideline.

References

ADDCAR Systems LLC, 2018. ADDCAR systems. [Online] Available at: www.addcarsystems.com [Accessed 12 February 2018].

Adhikary, D., Shen, B. & Duncan Fama, M.E, 2002. A study of highwall mining panel stability. International Journal of Rock Mechanics & Mining Sciences,Volume 39, Issue 5, pp. 643-659.

Barton, N., Lien, R. and Lunde, J., 1974. Engineering classification of rock masses for the design of tunnel support. Rock Mechanics, Volume 6, Issue 4, pp. 183–236
Buddery, P. & Oldroyd, D., 1992. Development of a Roof and Floor classification applicable to Collieries. Thomas Telford, London, Eurock'92.

Bieniawski, Z.T., 1979. The Geomechanics Classification in rock engineering classifications. Montreux,Rotterdam, A.A. Balkema, pp. 41-48.

Bieniawski, Z. T., 1989. Engineering rock mass classifications: a complete manual. New York, John Wiley & Sons.

Duncan Fama, M.E., Shen, B., Craig, M.S., Kelly, M., Follington, I.L. and Leisemann, B.E., 1999. Layout Design and Case Study for Highwall Mining of Coal. In: Proceedings of the 9th International Congress of Rock Mechanics, Balkema, Rotterdam.

Follington, L., Deeter, R., Share, D. & Moolman, C., 2001. A new underground auger mining system. The Journal of the Southern African Institute of Mining and Metallurgy,Volume 101, Issue 1, pp. 25-32.

GEOKON, 2018. GEOKON. [Online] Available at: https://www.geokon.com/content/manuals/4350BX_Biaxial_Stressmeter.pdf [Accessed 30 July 2018].

Glencore Coal Geotechnical Database, 2012. Geotechnical Database of all the Rock Types at Glencore Coal SA, Witbank.

Glencore Coal SA Production report, 2010. Production reports 2008 - 2010, eMalahleni: Internal report.

Glencore Coal SA Southstock Geology department, 2012. Geological borehole logs of 5 Seam operation, Internal database.

Glencore Coal SA, 2012. Mining complexes and resources.

Google Maps, 2018. Google maps. [Online] Available at: https://www.google.co.za/maps/@-26.0578478,29.1546202,44974m/data=!3m1!1e3
[Accessed 27 2019 2018].

Hoek, E. & Brown, E., 1997. Practical estimates of rock mass strength. International Journal of Rock Mechanics & Mining Sciences, Volume 34, pp. 1165-1186.

Hoek, E., 2012. Evolution of the Hoek-Brown criterion and the associated Geological Strength Index (GSI) Evolution of HB criterion and GSI classification. Second draft, pp. 1-52.

Hoelle, J., 2003. Analysis of unsupported roof spans highwall mining at Moura coal mine.,In: Proceedings Coal Operators' Conference, University of Wollongong & the Australasian Institute of Mining and Metallurgy, New South Wales.

Houghton, D. & Stacey, T., 1980. Application of probability techniques to underground situations. In: Proccedings of the 7th Regional Conference for Africa on Soil mechanics and Foundation Engineering , Accra,Volume 1, Balkema, pp. 879-883.

Hutchinson, D. & Diederichs, M., 1996. Cablebolting in underground mines. Canada: B-Technical Publishers.

Itasca Consulting Group, Inc., 2014. UDEC - Universal Distinct Eelement Code version 6.0 online user's Manual, Minneapolis, Minnesota: Itasca Consulting Group,Inc..

Latilla, J., van Wijk, J., Wevell, E. & Neal, D., 2002. Evaluation of the impact splitting technique used for predicting geotechnical conditions in underground coal mines. Maccauvlei. SANIRE 2002 Symposium "Re-defining the boundaries".

Lightfoot, N., 1999. Rock Engineering Practice For Tabular Hard Rock Mines. In: A. Jager & J. Ryder, eds. Numerical Modelling. Braamfontein, Johannesburg: The Safety in Mines Research Advisory Committee (SIMRAC), pp. 329-345.

Luo, Y., 2014. Highwall Mining:Design Methodology, Safety and Sustainability, West Virginia: West Virginia University: CERB Final Report No. 2014-004.

Madden, B., 2002. Preliminary geotechnical assessment of Strata Conditions in Trial Area, No. 5 Seam, South Witbank: Internal report reference RES 190-02.

Marinos, P. & Hoek, E., 2000. GSI: a geologically friendly tool for rock mass strength estimation. Melbourne, Technomic publishers, pp. 1422-1446.

Mark, C., 1999. Empirical Methods for Coal Pillar Design.Proceedings of the Second International Workshop on Coal Pillar Mechanics and Design. West Virginia, U.S.Department of Health and Human Services, National Institute for Occupational Safety and Health (NIOSH).

Mark, C., 2006. The evolution of intelligent coal pillar design: 1986-2006. Morgantown, WV, National Institute for Occupational Safety and Health, Washington, DC, pp. 325-334.

Mark, C., Chase, F. & Campoli, A., 1995. Analysis of retreat mining pillars stability. In: Proceedings of the 14th international conference on ground control in mining. Morgantown, WV: Dept. of Mining Engineering, College of Mineral and Energy Resources, West Virginia University, pp. 63-71.

Medhurst, T., 1999. Highwall mining: practical estimates of coal-seam strength and the design of slender pillars, Trans Inst Min Metall,Section A: Min Industry, 108: pp.161-171.

Middindi Consulting, 2012. Feasibility study on the 5 seam ADDCAR mining, eMalahleni: Xstrata Coal SA Internal report.

Mohan, G., Sheorey, P. & Kushwaha, A., 2001. Numerical estimation of pillar strength in Coal mines. International Journal of Rock Mechanics & Mining Sciences,Volume 38, Issue 8, pp. 1185-1192.

Mo, S., Zhang, C., Canbulat, I. & Hagan, P., 2016. A Review of Highwall Mining Experience and Practice.In: Proceedings of the 16th Coal Operators' Conference, Mining Engineering,University of Wollongong. Sydney, Australia.

NIOSH, 1998. LAMODEL user's guide, Pittsburgh, PA,USA: NIOSH Pittsburgh Research Laboratories.

Porathur, J., Karekal, S. and Palroy, P., 2013. Web Pillar design approach for Highwall Mining extraction. International Journal of Rock Mechanics & Mining Sciences,Volume 64, pp. 73-83.

Porathur, J., Roy, P., Shen, B. and Karekal, S., 2017. Highwall Mining: Applicability, Design & Safety. 1st ed. London: CRC Press/Balkema.

Prakash, A., Kumar, A. and Singh, K., 2015. Highwall Mining: A critical appraisal. MineTech, Volume 36, Issue 3, pp. 17-30.

Roberts, D., Ryder, J. and van der Merwe, J., 2005. Development of design procedures for long slender pillars Task 2.14, Johanesburg: COALTECH 2020.

Rocscience Inc., 2018. RocData version 5.0 online user Manual.

Ross, C., Conover, David, P. and Bain, J., 2017. Highwall Mining of Thick, Steeply Dipping Coal: A Case Study in Geotechnical Design and Recovery Optimization. Proceedings of the 36th International Conference on Ground Control in Mining.

Salamon, M. & Munro, A., 1967. A study of the strength of coal pillars. Journal of the South African Institute of Mining and Metallurgy, Volume 68, Issue 2, pp. 55-67.

Shen, B., 2014. Highwall Mining Stability - Project on Mine disaster prevention and Control, Pullenvale, Brisbane, Australia: Atlantis Press.

Shen, B. & Duncan Fama, M. D., 2001. Review of highwall mining experience in Australia and a case study, Brisbane: Australian Geomechanics.

Sheorey, P., 1992. Pillar Strength Considering in situ stress.In: Proceedings of the Workshop on Coal Pillar Mechanics and Design, Santa Fe., US Bureau of Mines IC 9315.

Sheorey, P., Das, M., Barat, D. & Singh, B., 1987. Coal pillar strength estimation from failed and stable cases. International Journal of Rock Mechanics, Mining Sciences and Geomechannics, Volume 24, Issue 6, pp. 347-355.

Tweefontein Survey Department, 2010. Mine layout plans, Internal Report.

Ulusay, R., 2015. The ISRM Suggested Methods for Rock Characterization,Testing and Monitoring. New York: Springer International Publishing.

Van der Merwe, J., 2003. New pillar strength formula for South African coal. The Journal of the Southern African Institute of Mining and Metallurgy,Volume 103, Issue 5, pp. 281-292.

van der Merwe, J. & Madden, B., 2010. Rock Engineering for underground coal mines. 2nd ed. Johannesburg: SAIMM.

van der Merwe, J. & Mathey, M., 2013. Probability of failure of South African Coal pillars. The Journal of the Southern African Institute of Mining and Metallurgy, Volume 113, Issue 11, pp. 849-857.

Vandergrift, T. & Garcia, J., 2005. Highwall Mining in a Multiple Seam, West United States Setting Design and Peformance. In: Proceedings of the 24th International Conference on Ground Control in Mining, West Virginia.

Verma, C., Porathur, J.L; Thote, N.R; Roy, P.P; Karekal, S., 2014. Empirical Approaches for Design of Web Pillars in Highwall Mining: Review and Analyis:Technical note. Journal of Geotechnical and Geological Engineering, Volume 32, Issue 2, pp. 587-599.

Wagner, H., 1974. Determination of the complete load deformation characteristics of coal pillars. Proc. 3rd International Congress on Rock Mechanics, International Society for Rock Mechanics (ISRM), Denver, pp. 1076–1086.

Zipf, R., 2005. Ground Control For Highwall Mining. Salt Lake City,Utah, The National Institute for Occupational Safety and Health (NIOSH), pp. 82-94.

Zipf, R. & Bhatt, S., 2004. Analysis of Practical Ground Control Issues in Highwall Mining. In: Proceedings of the 23rd International Conference on Ground Control in Mining.Morgantown, West Virginia: NIOSH Pittsburgh Research Laboratories, pp. 210-219.